PERFORMANCE ENHANCEMENT OF A SQUARE-CHANNEL HEAT EXCHANGER WITH BAFFLE VORTEX GENERATORS

SUPATTARACHAI SUWANNAPAN

A THESIS SUBMITTED IN PARTIAL FULFILLMENT
OF THE REQUIREMENT FOR THE DEGREE OF
DOCTOR OF ENGINEERING IN MECHANICAL ENGINEERING
FACULTY OF ENGINEERING
KING MONGKUT'S INSTITUTE OF TECHNOLOGY LADKRABANG
2014

KMITL-2014-EN-D-058-188

การเพิ่มสมรรถนะของเครื่องแลกเปลี่ยนความร้อนแบบท่อสี่เหลี่ยมจัตุรัสด้วยตัวสร้างการหมุนควงแบบครีบบาง

PERFORMANCE ENHANCEMENT OF A SQUARE-CHANNEL HEAT EXCHANGER WITH BAFFLE VORTEX GENERATORS

สุภัทรชัย สุวรรณพันธุ์
SUPATTARACHAI SUWANNAPAN

วิทยานิพนธ์นี้เป็นส่วนหนึ่งของการศึกษาตามหลักสูตรปริญญาวิศวกรรมศาสตรดุษฎีบัณฑิต
สาขาวิชาวิศวกรรมเครื่องกล
คณะวิศวกรรมศาสตร์
สถาบันเทคโนโลยีพระจอมเกล้าเจ้าคุณทหารลาดกระบัง
พ.ศ. 2557
KMITL-2014-EN-D-058-188

PERFORMANCE ENHANCEMENT OF A SQUARE-CHANNEL HEAT EXCHANGER WITH BAFFLE VORTEX GENERATORS

SUPATTARACHAI SUWANNAPAN

A THESIS SUBMITTED IN PARTIAL FULFILLMENT
OF THE REQUIREMENT FOR THE DEGREE OF
DOCTOR OF ENGINEERING IN MECHANICAL ENGINEERING
FACULTY OF ENGINEERING
KING MONGKUT'S INSTITUTE OF TECHNOLOGY LADKRABANG
2014

KMITL-2014-EN-D-058-188

หัวข้อวิทยานิพนธ์	การเพิ่มสมรรถนะของเครื่องแลกเปลี่ยนความร้อนแบบท่อสี่เหลี่ยมจัตุรัสด้วยตัวสร้างการหมุนควงแบบครีบบาง
นักศึกษา	นายสุภัทรชัย สุวรรณพันธุ์
รหัสนักศึกษา	53610207
ปริญญา	วิศวกรรมศาสตรดุษฎีบัณฑิต
สาขาวิชา	วิศวกรรมเครื่องกล
พ.ศ.	2557
อาจารย์ที่ปรึกษาวิทยานิพนธ์	รศ.ดร.พงษ์เจต พรหมวงศ์

บทคัดย่อ

วิทยานิพนธ์นี้ได้ทำการศึกษาเชิงทดลองการเพิ่มการถ่ายเทความร้อนและการเพิ่มสมรรถนะความร้อนในท่อสี่เหลี่ยมจัตุรัส ด้วยการสอดใส่ตัวสร้างการหมุนควงแบบต่าง ๆ ที่สภาวะฟลักซ์ความร้อนที่ผิวท่อคงที่ โดยใช้อากาศเป็นของไหลทดสอบ ทำการทดลองในช่วงการไหลแบบปั่นป่วนมีค่าตัวเลขเรย์โนลดส์ ตั้งแต่ 4000 ถึง 30,000 ในศึกษานี้ค่าการถ่ายเทความร้อนจะแสดงอยู่ในพจน์ของตัวเลขนัสเซิลท์ (Nu) และค่าความดันตกคร่อมจะแสดงอยู่ในพจน์ของตัวประกอบเสียดทาน (*f*) ในการศึกษานี้ จะทำการประยุกต์ใช้ตัวสร้างการหมุนควงชนิดต่าง ๆ กัน ซึ่งสามารถแบ่งออกเป็น 3 ส่วนหลัก ๆ ดังนี้

ส่วนที่ 1 จะเป็นการศึกษาพฤติกรรมการถ่ายเทความร้อนและการสูญเสียความดันภายในท่อจัตุรัสด้วยการสอดใส่ตัวสร้างการหมุนควงแบบผสมระหว่างใบบิดและแผ่นบางรูปตัววีที่ทำจากแผ่นบางรูปสี่เหลี่ยมผืนผ้าสองแผ่น (combined twisted-tape and V-baffles) ใบบิดที่ใช้การทดลองจะมีค่าอัตราส่วนการบิดสองค่า (y/w = Y = 4 และ 5) แผ่นบางรูปตัววีมีค่าอัตราส่วนการปิดกั้นการไหลสี่ค่า (R_B = e/H = 0.075, 0.1, 0.15 และ 0.2), มีค่าอัตราส่วนระยะพิตช์เจ็ดค่า (R_P = P/w = 2, 2.5, 4, 5, 8, 12 และ 16) และที่มุมปะทะการไหลเพียงหนึ่งค่า (α=30°)

ส่วนที่ 2 จะเป็นการศึกษาคุณลักษณะของการถ่ายเทความร้อนและการสูญเสียความดันภายในท่อจัตุรัสด้วยการสอดใส่ตัวสร้างการหมุนควงแบบแผ่นบางรูปตัววีแยกตัวและแผ่นบางสี่เหลี่ยมคางหมูจัดวางรูปตัววี (discrete and trapezoidal V-baffles) ซึ่งจะติดบนผิวทั้งสองข้างของแผ่นบางยาว และใส่เข้าไปตามแนวทแยงมุมของท่อกึ่งกลางการไหล ในการทดลองนี้แผ่นบางรูปตัววีแยกตัวจะมีค่าอัตราส่วนการปิดกั้นการไหลสี่ค่า (R_B = e/H = 0.075, 0.1, 0.15 และ 0.2), มีค่าอัตราส่วนระยะพิตช์สี่ค่า (R_P = P/H = 0.5, 1, 1.5 และ 2) และมีมุมปะทะการไหลสามค่า (α = 30°, 45° and 60°) จากนั้นในส่วนของตัวสร้างการหมุนควงแบบแผ่นบางสี่เหลี่ยมคางหมูวางรูปตัววีจะมีค่าอัตราส่วนการปิดกั้นการไหลและอัตราส่วนระยะพิตช์เหมือนกันกับตัวแผ่นบางรูปตัววีแยกตัวแต่ที่มุมปะทะเพียงหนึ่งค่าเท่านั้น (α=30°)

ส่วนที่ 3 จะเป็นการศึกษาพฤติกรรมการถ่ายเทความร้อนและการสูญเสียความดันภายในท่อจัตุรัสด้วยการสอดใส่ตัวสร้างการหมุนควงแบบแผ่นบางวางเอียงทำมุมและแผ่นบางสี่เหลี่ยมผืนผ้าวางรูปตัววี (angled and V-shaped baffles) โดยตัวสร้างการหมุนควงทั้งสองแบบนี้จะติดอยู่ที่ขอบทั้งสองข้างของแผ่นบางยาวและสอดใส่เข้าไปในแนวระนาบของท่อ ซึ่งจะทำให้ตัวสร้างการหมุนควงทั้งสองแบบนี้อยู่ชิดติดกับผิวท่อแต่ตรงข้ามกัน ในการทดลองจะมีการปรับเปลี่ยนตัวแปรต่าง ๆ เหมือนกันกับในส่วนก่อนหน้านี้ การหาค่าสมการความสัมพันธ์ของตัวแปรต่าง ๆ เช่น อัตราส่วนการ

ปิดกั้นการไหล อัตราส่วนระยะพิตช์และมุมปะทะการไหล เพื่อนำไปสู่การหาค่าสมรรถนะความร้อนที่เหมาะสมที่สุดของการทดลองนี้เหมือนที่แสดงในส่วนที่ 2

ผลการทดลองแสดงให้เห็นว่าอัตราการถ่ายเทความร้อนและการสูญเสียความดันจะมีค่าเพิ่มมากขึ้นเมื่อค่าอัตราส่วนการปิดกั้นและมุมปะทะการไหลเพิ่มขึ้น แต่จะให้ผลในทางตรงกันข้ามเมื่ออัตราส่วนระยะพิตช์มีค่าเพิ่มขึ้น พบว่าในกรณีที่ใช้ตัวสร้างการหมุนควงแบบแผ่นบางรูปตัววีวางชิดผิวท่อตรงข้ามกัน จะให้ค่าสมรรถนะความร้อนสูงสุดซึ่งมีค่าอยู่ระหว่าง 1.9-2.0 ที่มุมปะทะการไหล (α = 20°), อัตราส่วนการปิดกั้นการไหล (R_B = 0.075) และ อัตราส่วนระยะพิตช์ (R_P = 0.5). เมื่อทำการเปรียบเทียบค่าสมรรถนะความร้อนพบว่าแผ่นบางรูปตัววีวางชิดผิวท่อจะให้ค่าสูงกว่าแผ่นบางเอียงทำมุมวางชิดผิวท่อ, แผ่นบางสี่เหลี่ยมคางหมูวางรูปตัววี, แผ่นบางรูปตัววีแยกตัว,ใบบิดสี่ใบร่วมกับแผ่นบางรูปตัววี และใบบิดใบเดียวร่วมกับแผ่นบางรูปตัววี มีค่าประมาณ 7, 9, 12, 13 และ 19% ตามลำดับ

Thesis Title	Performance Enhancement of a Square-Channel Heat Exchanger with Baffle Vortex Generators
Student	Mr. Supattarachai Suwannapan
Student ID.	53610207
Degree	Doctor of Engineering
Program	Mechanical Engineering
Year	2014
Thesis Advisor	Assoc.Prof.Dr. Pongjet Promvonge

ABSTRACT

The thesis presents an experimental study on the heat transfer and thermal performance enhancement in a constant heat-fluxed square-duct inserted with different turbulators or swirl/vortex flow generators. Air is used as the test fluid with the mass flow rate range in the form of Reynolds number from 4000 to 30,000. The heat transfer rate and the pressure drop characteristics in the test duct are presented in terms of Nusselt number (Nu) and friction factor (*f*), respectively. The investigation on the application of various turbulator or vortex generator configurations is classified into three parts as follows:

Part I deals with the heat transfer and pressure loss behaviors in a square duct with combined twisted-tape and V-baffle inserts. The characteristics of the combined devices are as follows. For twisted-tapes, two twist ratios of twisted tapes (y/w = Y = 4 and 5) are introduced. For V-baffles, parametric variables are four baffle-to duct-height ratios (called blockage ratio; R_B = e/H = 0.075, 0.1, 0.15 and 0.2), seven baffle-pitch to tape-width ratios (called pitch ratio: R_P = P/w = 2, 2.5, 4, 5, 8, 12 and 16) and a single attack angle or V-tip half-angle, α = 30°.

Part II is relevant to the heat transfer and friction loss characteristics in a square duct inserted with discrete and trapezoidal V-baffles placed in the central core flow. The V-baffles were placed repeatedly on a double-sided thin sheet or straight tape before diagonal insertion. The V-baffles mounted on the tape are arranged in the form of discrete/broken and trapezoidal V-shaped baffles. The baffle characteristics include four blockage ratios (R_B=e/H=0.075, 0.1, 0.15 and 0.2), four pitch ratios (R_P=P/H=0.5, 1, 1.5 and 2) and three attack angles (α=30°, 45° and 60°), except for the trapezoidal V-baffles having α=30°, only.

Part III is concerned with the heat transfer, pressure loss and thermal performance behaviors in a square duct fitted with angled and V-shaped baffles placed on two opposite duct walls. To keep the baffles close tightly to the duct wall, the V-baffles are attached repeatedly on both edges of a straight-tape having its width approximately equal to the duct height. Then, the baffle-edged tape is inserted

horizontally into the duct to let the baffles place on the opposite walls. The pertinent baffle parameters are also the blockage ratio, pitch ratio and angle of attack. The optimum values of those parameters are obtained as suggested in Part II and then, the optimization is performed to find out the optimal thermal performance and baffle configurations.

The experimental results show that the heat transfer rate and friction factor values are found to increase with the increment of R_B and α but the decrease of R_P. The optimization reveals that the use of V-baffles placed on two opposite walls yields the highest thermal enhancement factor, η, in the range of 1.9-2.0 at α=20°, R_B=0.075 and R_P=0.5. In comparison, the V-baffle-edged tape provides the η higher than the angled-baffle-edged tape, V-trapezoidal baffles, discrete V-baffles, four V-baffled twisted-tape and single V-baffled twisted-tape at about 7, 9, 12, 13 and 19%, respectively.

ACKNOWLEDGMENTS

I would like to express my profound gratitude to my advisor, Assoc.Prof.Dr. Pongjet Promvonge, and staffs of department of mechanical engineering for the kindness to guidance and suggestion, encouragement, and patience during the supervision of this research.

The financial support from Energy Policy and Planning Office (EPPO) Energy Policy and Planning Office, Ministry of Energy, Thailand is also gratefully acknowledged.

Moreover, I wish to give special thanks to the number of thermo-fluid and CFD students in the department of mechanical engineering at King Mongkut's Institute of Technology Ladkrabang for helping and sharing of their discussions.

Finally, I really appreciate my family for their moral support and encouragement all along.

CONTENTS

CONTENTS (continued)

CONTENTS (continued)

CONTENTS (continued)

LIST OF TABLES

LIST OF FIGURES

LIST OF FIGURES (continued)

LIST OF FIGURES (continued)

NOMENCLATURE

A	convection heat transfer area of duct, m^2
A_c	cross-sectional area, m^2
C_p	specific heat capacity, J/kgK
D_h	hydraulic diameter of duct (=H), m
e	baffle height, m
f	friction factor
H	duct height, m
h	average heat transfer coefficient, W/m^2K
k	thermal conductivity, W/mK
L	length of test duct, m
$\dot{m}$	mass flow rate, kg/s
Nu	Nusselt number
P	baffle pitch spacing, m
P_w	wetted perimeter of cross-section, m
ΔP	pressure drop, Pa
Pr	Prandtl number
R_B	baffle blockage ratio, e/H
Re	Reynolds number
R_P	baffle pitch ratio, P/w
Q	heat transfer, W
T	temperature, K
t	thickness of baffle, m
V_m	mean velocity, m/s
w	tape width, m
Y	twist ratio, y/w
y	pitch length of twisted tape (180° rotation), m

Greek symbols

α	attack angle of baffle, °
η	thermal enhancement factor, $(Nu/Nu_0)/(f/f_0)^{1/3}$
ν	kinematics viscosity, m^2/s
ρ	density of air, kg/m^3

Subscripts

b	bulk
0	smooth duct
conv	convection
i	inlet
e	exit
bp	blowing power
s	duct surface

CHAPTER 1
INTRODUCTION

1.1 Statement of the problems

Heat exchangers have been widely used in both small and large scale industries, including household compliances such as refrigeration, condenser and evaporator etc. The heat exchanger industry is also a highly competitive market. The design of the equipment or system with high thermal efficiency must consider other requirements such as heat transfer rate, pressure penalty, structure, size, lifetime, maintenance, reliability and security. Nowadays, there are many types of heat exchangers available in the market. For example, double pipe heat exchangers, shell and tube heat exchangers, plate heat exchangers, plate and shell heat exchangers, plate fin heat exchangers and so on.

Originally, heat exchangers were introduced using plain or smooth surface. Then, the improvement has developed using several heat transfer enhancement techniques. The improvement techniques can be classified into two major groups which are passive and active techniques. The passive technique uses particularly designed surface characteristics of the tube or duct and special fluids to enhance the heat transfer rate. This technique has no external power involved. The examples are coated surfaces, rough surfaces, extended surfaces, displaced inserts, coiled tubes, surface tension and additive liquids or gases. The active technique requires external power source to stimulate the vibration of the surface or fluid which can increase the heat transfer rate.

The present research focuses on the passive technique to increase the heat transfer rate. In the present study, devices were inserted into the heat exchanger tube. These devices acted as a vortex generator to create a turbulent/swirl/vortex flow inside the tube. The result could lead to an increase in heat transfer rate. However, the pressure loss would be increased. Therefore, in order to yield the optimum thermal performance, the designed parameters which are shape, size, height, angle and pitch of the vortex generator are studied to investigate their effects on the heat transfer and flow friction.

1.2 Objectives of the research

The main aims of the research are:

1.2.1 To study the design parameters of turbulators or swirl/vortex generators that have major influence on the heat transfer and pressure loss in the square duct.

1.2.2 To explain the behaviors of heat transfer and pressure loss and compare the experimental results between the square duct with turbulators or swirl/vortex generators with the smooth duct.

1.2.3 To establish a mathematical relationship of design parameters that has major influence on the heat transfer and pressure loss.

1.3 Scope and conditions of the research

1.3.1 The test fluid is air.

1.3.2 Reynolds number is ranging from 4,000 to 30,000.

1.3.3 The surface heat flux is uniform.

1.3.4 The flow distribution in the duct is fully developed.

1.3.5 The experiments consist of different turbulators or swirl/vortex generators as follows: the modified twisted-tape combined with V-baffles, the discrete V-baffles placed on a tape, the trapezoidal V-baffles mounted on a tape, the angled baffles on two opposite walls and the V-baffles on two opposite walls with different V-tip directions.

1.3.6 The performance indexes are presented in terms of Nusselt number and friction factor for the heat transfer rate and pressure loss, respectively. The comparison among these configurations is done in terms of thermal performance factor.

Table 1.1 Scope and conditions of the research.

Turbulator or swirl/vortex generator	**Blockage ratio (R_B)**	**Pitch ratio (R_P)**	**Twist ratio (Y)**	**V-tip direction**	**Angle of attack (α)**
Single twisted-tape & V-baffles	0.1, 0.15, 0.2	2, 2.5, 4, 5	4, 5	V-upstream	30°
Four twisted-tapes & V-baffles	0.075, 0.1, 0.15, 0.2	4, 8, 12, 16			
Discrete V-baffles	0.075, 0.1, 0.15, 0.2	0.5, 1, 1.5, 2	-	V-upstream, V-downstream	30°, 45°, 60°
Trapezoidal V-baffles	0.075, 0.1, 0.15, 0.2	0.5, 1, 1.5, 2	-	V-upstream	30°
Angled baffles on two opposite walls	0.1, 0.2	0.5, 1, 2	-	-	30°
V-baffles on two opposite walls	0.075, 0.1, 0.15, 0.2	0.5, 1, 1.5, 2	-	V-upstream	20°, 30°, 45°

1.4 Conceptual and hypothesis

The present research focuses on the experimental investigation of a square-duct heat exchanger inserted with different turbulators or swirl/vortex generators. The turbulators or swirl/vortex generators are devices usually used to prolong the flow and create the turbulent vortex flow in the heat exchangers. When air flows into the duct of heat exchangers, there is a layer of air called the boundary-layer between the duct's surfaces where the air is undisturbed. The thickness of this boundary layer can be broken or reduced by using the turbulators or swirl/vortex generators inserted in the duct. These devices create and increase the turbulence intensity leading to the reduction of boundary-layer's thickness. This phenomenon provides higher heat transfer rate. Therefore, these concepts are applied in the present research.

1.5 Benefits of the research

1.5.1 Can improve the thermal performance of a square-duct heat exchanger with the new development and design turbulator or swirl/vortex generator and applying into both industry and in agriculture.

1.5.2 Able to reduce the use of energy, size and materials of heat exchangers that lead to lower production cost and provide higher thermal performance.

1.6 Thesis outline

The thesis entitled "Performance Enhancement of a Square-Channel Heat Exchanger with Baffle Vortex Generators" consists of 8 chapters. The background of problem, objectives, scope and expected benefits were introduced in Chapter 1. Chapter 2 surveyed and reviewed the other interested research works related to the present research.

Chapters 3 and 4 described the associate basis convection heat transfer fundamentals in the present research and the design of equipment of a square-duct heat exchanger including the design parameters of each turbulators and the experimental procedure. The experimental results for using combined twisted-tape and V-baffles, discrete/trapezoidal V-baffles in central core flow and angled/V-shaped baffles on two opposite walls were presented in Chapters 5, 6 and 7, respectively. The effects of turbulator or swirl/vortex generator geometries on the heat transfer augmentation, pressure drop and thermal performance were discussed too. Chapter 8 summarized the main conclusions, the suggestions of the present research and the recommendation for future work.

CHAPTER 2
LITERATURE REVIEW

This chapter presents the previous works related to current research. In the past, many researchers have studied the effects of turbulators or swirl/vortex generators on heat transfer, pressure drop and thermal performance behaviors in pipe/duct heat exchanger. Several techniques have been carried out focusing on an enhancement of heat transfer rate and trying to reduce the pressure penalty. The literatures related to current research are divided into two groups depending on heat exchanger's geometries. The first group is using of turbulators or swirl/vortex generators such as twisted-tapes, wire coils, ribs, fins, baffles winglets, etc. in a circular tube. The second group is using of those turbulators or swirl/vortex generators in a square duct/rectangular channel.

2.1 The effect of turbulator or swirl/vortex generator on heat transfer, pressure drop and thermal performance behaviors in a circular pipe

This section presents the broad uses of typical twisted-tapes and their modifications. Then, the combinations of twisted-tapes with other vortex generators and also with the geometrical modified tubes are presented. Finally, the using of nanofluids is also introduced.

2.1.1 Typical twisted-tapes

The most extensive turbulators used in circular tube are twisted-tapes. There are many researchers studied the heat transfer enhancement using the typical twisted-tapes. For example, Eiamsa-ard et al. [1] compared the typical twisted tapes with uniform and non-uniform alternate lengths. The experimental results showed that the uniform and non-uniform alternate twist lengths yielded higher Nusselt number than the typical twisted tapes. Bas and Ozceyhan [2] experimentally investigated the flow friction and heat transfer behaviors using a twisted tape as swirl generator inserted in a tube. The using of twisted tapes considerably increased the heat transfer rate and also pressure drop compared with the plain tube.

Eiamsa-ard and Seemawute [3] presented both experimental and numerical results of the local heat transfer coefficient and flow characteristics of decaying turbulent swirl flow generated by short-length twisted tapes. Again, Eiamsa-ard et al. [4] reported the heat transfer enhancement attributed to helically twisted tapes.

Ferroni et al. [5] evaluated the pressure drop in round tubes provided with physically separated, multiple, short-length twisted tapes. They reported that

adoption of multiple short-lengths could decrease pressure drop at least 50% lower than typical full-length twisted-tape.

Wongcharee and Eiamsa-ard [6] investigated the effects of twisted tapes with alternate-axes and wings on heat transfer, flow friction and thermal performance characteristics in a round tube. The Nusselt number, friction factor as well as thermal performance factor given by the tape with alternate-axes and trapezoidal wings are higher than those given by the others. Again, Wongcharee and Eiamsa-ard [7] reported the thermohydraulic characteristics of the circular tubes equipped with alternate clockwise and counterclockwise twisted-tapes.

Hejazi et al. [8] conducted an experimental investigation on the augmentation of heat transfer coefficients and pressure drop during condensation of HFC-134a in a horizontal tube with different twisted tape inserts. Eiamsa-ard et al. [9] studied the influences of twin-counter/co-twisted tapes on heat transfer rate, friction factor and thermal enhancement index. They reported that the counter twisted tapes had more thermal efficiency than co-twisted tapes.

Eiamsa-ard et al. [10] experimentally investigated heat transfer, flow friction and thermal performance factor characteristics in a tube fitted with delta-winglet twisted tape, using water as working fluid. They presented that the oblique delta-winglet twisted tape had more thermal efficiency than the straight delta-winglet twisted tape. Eiamsa-ard and Promvonge [11] presented an experimental study of turbulent heat transfer and flow friction characteristics in a circular tube equipped with typical twisted tapes and alternate clockwise and counterclockwise twisted tapes.

Eiamsa-ard et al. [12] presented a comparative investigation of enhanced heat transfer and pressure loss by insertion of single twisted tape, full-length dual and regularly-spaced dual twisted tapes as swirl generators, in a round tube under axially uniform wall heat flux conditions. Eiamsa-ard et al. [13] presented an experimental study on the mean Nusselt number, friction factor and enhancement efficiency characteristics in a round tube with short-length twisted tape insert. The enhancement efficiency of the tube with the short-length tape insert was lower than the full-length one.

2.1.2 Modified twisted-tapes

Beyond the typical twisted-tapes, other researchers have modified the twisted-tapes to enhance the heat transfer rate and reduce the pressure drop. For examples, Nanan et al. [14, 15] studied the influence of perforated and non-perforated helical twisted-tapes on the heat transfer, friction loss and thermal performance characteristics in a circular pipe under a uniform heat flux condition.

The perforated helical twisted-tapes were designed to reduce the friction loss of fluid flow.

Bhuiya et al. [16-18] conducted a number of experiments to study the effects of double counter twisted tapes, perforated twisted tapes and triple twisted tapes on heat transfer and fluid friction characteristics in a circular heat exchanger tube. The experimental results demonstrated that the thermal performance factor in the tube with those twisted tape inserts were higher than the plain tube. The Nusselt number and thermal enhancement efficiency were increased with decreasing of twist ratio.

Chang and Guo [19] experimentally studied the heat transfer enhancement in the developing and developed flow regimes. They used the continuous and spiky twist tapes combined with perforated, jagged and notched winglets. They found that the V-notched spiky twisted tape offered the highest thermal performance.

Murugesan et al. [20] experimentally investigated heat transfer, friction factor and thermal enhancement factor characteristics of a double pipe heat exchanger fitted with square-cut twisted tapes and plain twisted tapes. They used water as working fluid. They reported that heat transfer rate, friction factor and thermal enhancement factor in the tube equipped with square-cut twisted tapes were significantly higher than plain twisted tapes. Murugesan et al. [21] experimentally investigated the Nusselt number, friction factor and thermal enhancement factor of a double pipe heat exchanger equipped with twisted tape consisting wire nails and plain twisted tapes. They found that Nusselt number, friction factor and thermal enhancement factor in the tube equipped with wire nails twisted tapes were higher than plain twisted tapes.

Seemawute and Eiamsa-ard [22] studied the effect of peripherally-cut twisted tape with alternate axis on the fluid flow and heat transfer characteristics in a uniform heat flux circular tube.

Eiamsa-ard and Promvonge [23] presented the effect of twisted tape with serrated-edge inserted in a constant heat-fluxed tube. They reported that heat transfer rate increased with the increment of depth ratio but decreased with increasing width ratio. Eiamsa-ard et al. [24] studied the effects of peripherally-cut twisted tape inserts on heat transfer, friction loss and thermal performance factor characteristics in a round tube.

Chang et al. [25] presented an experimental study on compound heat transfer enhancement in a tube fitted with serrated twisted tape. Chang et al. [26] reported the axial heat transfer distributions and the pressure drop coefficients of the tube fitted with a broken twisted tape. The local Nusselt numbers and mean Fanning

friction factors in the tube fitted with the broken twisted tape increased as the twist ratio decreased.

For better understanding of the twisted tapes and their modifications, the various twisted tapes mentioned in this section are presented in table 2.1.

Table 2.1 Twisted tapes and its modifications [19].

Schematic of twisted tape	Re range	f/f_∞	Nu/Nu_∞	TPF
Multiple twisted tapes				
Chang (2005) 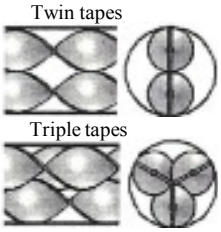 y/w=1.67	3000-14,000	**Twin twisted tapes**		
		15.76-12.61	2.45-1.73	0.97-0.74
		Triple twisted tapes		
		19.21-14.36	3.03-2.58	1.13-1.06
Eiamsa-ard (2010)  Twin tape, y/w=2.5,3,3.5,4	3700-21000	26.6-11.2	2.07-1.22	1.10-0.92
Eiamsa-ard (2010)  Twin tape, y/w=2.5,3,3.5,4	3700-21000	36.30-13.90	2.85-1.46	1.40-1.01
Notched twisted tape				
Rahimia (2009)  y/w=2.94	2950-11800	7.17-4.62	1.86-1.52	0.96-0.90
Eiamsa-ard (2010) 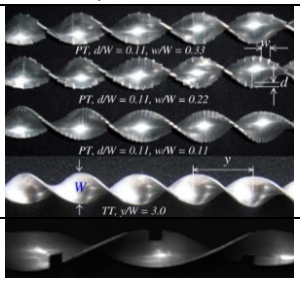	3000-20000	12.5-3.7	3.3-1.35	1.44-0.87
Murugesan (2010) y/w=2.2,4.4,6.6	2000-12000	5.20-2.50	1.92-1.49	1.27-1.09
Murugesan (2011) 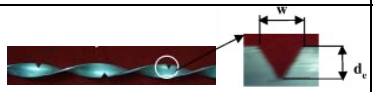 y/w=2,4.4,6; d/W=w/W=0.34	3000-11000	26.70-10.3	3.17-1.79	1.18-1.02
Seemawute, Eiamsa-ard (2010) 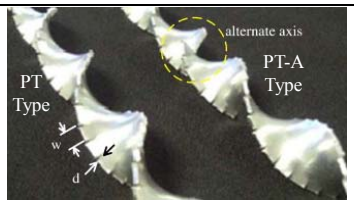 y/w=3; d/W=0.11; w/W=0.11,0.22,0.33	5000-20000	**PT**		
		26.90-14.20	1.08-0.86	1.13-0.87
		PT-A		
		49.60-24.50	2.80-1.70	1.25-0.85

Table 2.1 (continued)

Schematic of twisted tape	Re range	f/f_∞	Nu/Nu_∞	TPF
Jagged and winglet twisted tapes				
Rahimia (2009)  y/w=2.94	2950-11800	8.70-6.51	2.49-1.96	1.21-1.05
Wongcharee, Eiamsa-ard (2011) 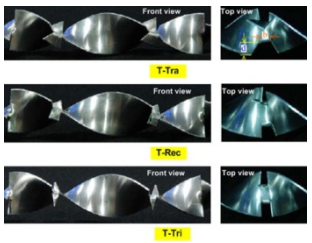 y/w=4; d/W=0.1,0.2,0.3; w/W=0.2	5500-20200	**Trapezoid edged winglets**		
		35.40-18.50	2.68-1.70	1.43-1.09
		Rectangular edged winglets		
		30.20-16.5	2.50-1.60	1.40-1.06
		Triangular edged winglets		
		27.20-15.20	1.90-1.20	1.35-1.06
Murugesan (2010) 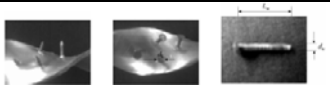 y/w=2,4,6; $L_w/W=0.6$; $d_w/W=0.085$	2000-12000	1.33-1.06	1.75-1.08	1.33-1.28
Perforated twisted tapes				
Rahimia (2009)  y/w=2.94	2950-11800	6.65-4.40	1.60-1.33	0.85-0.81
Spiky twisted tapes				
Chang (2007) 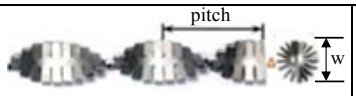 y/w=1,1.5,2,2.5,∞	3000-40000	2.5-30	3.5-1.3	1.40-0.76
Compound twisted tapes and other HTE devices				
Promvonge (2008) 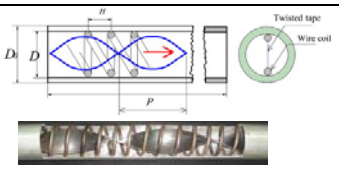 y/w=4,6	3000-27000	75-15	6.50-2.1	1.55-0.80

2.1.3 Twisted-tapes combined with other devices

The twisted-tapes have also been used in combination with other devices. For examples, Eiamsa-ard and Wongcharee [27] experimentally studied the influence of double twisted-tape inserts combined with micro-fin on heat transfer, friction factor and thermal performance factor in a tube. Eiamsa-ard et al. [28] studied the influence of circular-ring turbulators and twisted tapes on the heat transfer enhancement, pressure drop and thermal performance factor characteristics in a

round tube. The experimental results revealed that the thermal performance factor of the combined circular-ring turbulators with twisted tapes were considerably higher than circular-ring turbulator alone.

Nagarajan et al. [29] experimentally investigated the heat transfer and friction factor characteristics of micro-finned tube fitted with full-length twisted tape and left–right twisted tape inserts. Eiamsa-ard et al. [30] experimentally investigated heat transfer, friction factor and thermal performance behaviors in a tube equipped with the combined devices between the twisted tape and constant/periodically varying wire coil pitch ratio.

Promvonge [31] studied the influences of insertion of wire coils in conjunction with twisted tapes on heat transfer and turbulent flow friction characteristics in a circular tube using air as the test fluid. They reported that the combined twisted tape and wire coil with smaller twist and coil pitch ratios provided higher heat transfer rate than larger twist and coil pitch ratios under the same conditions. Promvonge and Eiamsa-ard [32] experimentally investigated heat transfer, friction factor and enhancement efficiency characteristics in a circular tube fitted with conical-ring turbulators and a twisted-tape swirl generator.

2.1.4 Twisted-tapes with modified tubes

The twisted-tapes have also been adopted with geometrically modified tubes to increase the thermal efficiency. For examples, Promvonge et al. [33] experimentally investigated turbulent convective heat transfer characteristics in a helical-ribbed tube fitted with twin twisted tapes. The experiment was carried out in a double tube heat exchanger using the helical-ribbed tube having a single rib-height to tube-diameter ratio. The experimental results revealed that the co-swirling inserted tube performed much better than the ribbed/smooth tube alone at similar operating condition.

Thianpong et al. [34] experimentally investigated friction and compound heat transfer behaviors in a dimpled tube fitted with a twisted tape swirl generator using air as working fluid. The result showed that both heat transfer coefficient and friction factor in the dimpled tube fitted with the twisted tape were higher than the dimple tube acting alone. Bharadwaj et al. [35] experimentally studied pressure drop and heat transfer characteristics of flow of water in a 75-start spirally grooved tube with twisted tape insert. Laminar to fully turbulent ranges of Reynolds numbers have been considered. They reported that, for spirally grooved tube with and without twisted tape, heat transfer increased considerably in laminar and moderately in turbulent regimes. Mengna et al. [36] experimentally investigated the pressure drop and compound heat transfer characteristics of a converging-diverging tube with evenly spaced twisted-tapes.

2.1.5 Twisted-tapes with nanofluids

Recently, the using of twisted-tapes has expanded to other working fluids such as nanofluids. For examples, Naik et al. [37] presented the effect of twisted tape and wire coil inserts on heat transfer and friction factor behaviors in circular pipe. They used CuO/water nanofluid with volume concentrations of 0.1% and 0.3% as working fluid. The experimental results revealed that the thermal performance factor associated with nanofluid in a tube using wire coil inserts were higher than the twisted tape inserts.

Azmi et al. [38] determined the heat transfer coefficients and friction factor of TiO_2/water nanofluid in tubes with twisted tapes having different twist ratios. By using of twisted tapes, the heat transfer coefficient increased with decreasing in twist ratio. Esmaeilzadeh et al. [39] carried out an experimental investigation on heat transfer and friction factor characteristics of γ-Al_2O_3/water nanofluid through circular tube with various thickness of twisted tape inserts. The experiments were performed in laminar flow regime. The results showed that twisted tape inserts enhanced the average convective heat transfer coefficient. The highest enhancement was achieved at maximum volume concentration.

Wongcharee and Eiamsa-ard [40] presented heat transfer enhancement by using CuO/water nanofluid in corrugated tube equipped with twisted tape. They reported that heat transfer rate increased with increasing CuO/water nanofluid concentration and decreasing twist ratio. The twisted tape coupled with corrugated tube in counter pattern offered higher thermal performances than parallel pattern. Eiamsa-ard and Wongcharee [41] experimentally investigated the combined effects of CuO/water nanofluids, dual twisted-tapes and a micro-fin tube on the heat transfer rate, friction factor and thermal performance factor characteristics.

2.1.6 Other devices in circular tubes

Apart from twisted-tape, other vortex generators have also been introduced to enhance the thermal performance in circular tubes. For examples, Promvonge et al. [42] studied the influence of 30° inclined vortex rings on heat transfer augmentation in a uniform heat-fluxed tube. Thianpong et al. [43] experimentally investigated heat transfer, friction factor and thermal performance characteristics in a tube equipped with twisted-rings. They reported that most twisted-rings gave lower Nusselt number and friction factor than typical circular rings. Eiamsa-ard and Promvonge [44] studied the convective heat transfer and friction behaviors of turbulent tube flow through a straight tape with double-sided delta wings. Eiamsa-ard and Promvonge [45] experimentally investigated the heat transfer and friction factor characteristics in a tube fitted with diamond-shaped turbulators.

2.2 The effect of turbulator or swirl/vortex generator on heat transfer, pressure drop and thermal performance behaviors in a duct/channel

This section presents the using of ribs, fins, baffles and winglets as vortex generator. The combinations of ribs with winglets and also with the grooved surfaces are reviewed. Then, the other turbulators used in the channels are presented. Finally, the using of nanofluids is also introduced.

2.2.1 Ribs, fins and baffles

Ribs, fins, and baffles have been widely used as vortex generators to enhance the heat transfer rate in the channel. For example, Lee et al. [46] investigated the heat transfer and friction factors characteristics in the stationary rectangular divergent channel with parallel angled ribs. They reported that the two opposite 45° parallel rib angled wall channel had the greatest thermal performance. Liu et al. [47] experimentally studied on heat transfer characteristics in steam-cooled rectangular channels with two opposite rib-roughened walls. They reported that the average Nusselt number for the channel with $\alpha=45^{\circ}$ was higher than $\alpha=60^{\circ}$.

Tang and Zhu [48] numerically investigated the turbulent flow and heat transfer behavior in rectangular channel with inclined broken ribs. They reported that the V-type ribbed array gave the best thermal performance factor.

Shui et al. [49] conducted experimental and numerical investigation to study the effect of duct aspect ratio on heat transfer and friction characteristics. The optimum thermal enhancement factor was found at aspect ratio of 0.5. Xie et al. [50] presented numerical study of square cross-section ribbed channels with different arrangements of downstream half-size ribs. Using of downstream ribs was a suitable way to decrease the pressure loss and improve the flow structure while kept comparable enhancement in heat transfer as expected.

Karwa and Chitoshiya [51] experimentally studied the thermo-hydraulic performance of a solar air heater with 60° v-down discrete rib roughness on the airflow side of the absorber plate. Sriromreun et al. [52] investigated the influence of baffle turbulators on heat transfer augmentation in a rectangular channel. In the experiment, the Nusselt number, friction factor and thermal performance enhancement factor for in-phase 45° Z-baffles were found to be considerably higher than the out-phase 45° Z-baffle.

Promvonge et al. [53, 54] studied the turbulent flow and heat transfer characteristics in a square duct fitted diagonally with 30° angle-finned tapes. Promvonge et al. [55] numerically investigated on laminar flow and heat transfer characteristics in a three-dimensional isothermal wall square-channel fitted with inline 45° V-shaped baffles on two opposite walls. The baffled channel flow showed a fully developed periodic flow and heat transfer profile for $x/D\approx8$ down-stream of

the inlet. It was apparent that the longitudinal counter-rotating vortex flows created by the V-baffle can induce impingement/attachment flows over the walls resulting in greater increase in heat transfer over the test channel.

Promvonge et al. [56] numerically studied of heat transfer characteristics in a three dimensional square-duct with inline 60° V-shaped discrete thin ribs placed on two opposite heated walls. The computation revealed that the ribbed duct flow was fully developed periodic flow and heat transfer profiles at about x/D=7–11 downstream of the inlet. It was found that a pair of counter-rotating vortices (P-vortex) caused by the rib can induce impingement/attachment flows on the walls leading to greater increase in heat transfer over the test duct.

Jedsadaratanachai et al. [57] presented a numerical analysis of laminar periodic flow and heat transfer characteristics in a square channel mounted with 30° angled baffles of various pitches. They reported that decreasing in pitch ratio led to the rise of friction factor only. Peng et al. [58] studied experimentally and numerically convection heat transfer in a channel with 90° ribs and V-shaped ribs. The results showed that both the 90° ribs and V-shaped ribs enhanced the convection heat transfer compared with a flat wall without ribs, but the pressure drop also increased.

Singh et al. [59] experimentally investigated the heat and fluid flow characteristics of rectangular duct having one broad wall heated and roughened with periodic discrete V-down rib. Lanjewar et al. [60] presented experimental investigation on heat transfer and friction factor characteristics of rectangular duct roughened with W-shaped ribs. The maximum of thermo-hydraulic performance occurs at angle of attack of 60°.

Tanda [61] experimentally investigated the forced convection heat transfer in a rectangular channel with inclined 45° angled rib turbulators. Promvonge [62] presented the turbulent forced convection heat transfer and friction loss behaviors for airflow through a channel fitted with a multiple 60° V-baffle turbulator. Hans et al. [63] experimentally investigated the effect of multiple v-rib roughness on heat transfer coefficient and friction factor in an artificially roughened solar air heater duct.

Song et al. [64] numerically studied the flow and heat transfer in a finned flat tube heat exchanger with crossed discrete double inclined rib. The heat transfer is enhanced by secondary flows around the ribs and a series of vortices generated downstream of the ribs, including the main vortices, induced vortices and corner vortices. The Nusselt number for the attack angle of $\alpha=45^{\circ}$ was larger than for $\alpha=30^{\circ}$ and $\alpha= 60^{\circ}$. The friction factor increased with the attack angle.

Promvonge and Kwankaomeng [65] numerically investigated on periodic laminar flow and heat transfer characteristics in a three-dimensional isothermal wall

channel with 45° staggered V-baffles. Kwankaomeng and Promvonge [66] numerically investigated on periodic laminar flow and heat transfer behaviors in a three-dimensional isothermal wall square duct fitted with 30° angled baffles on lower duct wall. Promvonge et al. [67-69] numerically investigated on laminar periodic flow and heat transfer in a three-dimensional isothermal-wall square channel fitted with 30° and 45° inclined baffles on one channel wall and on two opposite walls. The increase in the blockage ratio and the attack angle resulted in considerable increased in the Nusselt number and friction factor values.

Thianpong et al. [70] experimentally investigated on turbulent heat transfer and friction loss behaviors in a channel fitted with different heights of triangular ribs. Two rib arrangements, namely, in-line and staggered arrays, were introduced. The uniform rib height performed better than the corresponding non-uniform one. The in-line rib arrangement provided higher heat transfer and friction loss than the staggered one. In comparison, the largest e/H rib with inline array yielded the highest increase in both the Nusselt number and the friction factor values while the lowest e/H rib with staggered array provided the best thermal performance.

Aharwal et al. [71] presented an experimental investigation on heat transfer and friction characteristics of solar air heater ducts with integral repeated discrete square ribs on the absorber plate. Karwa and Maheshwari [72] presented results of an experimental study of heat transfer and friction in a rectangular section duct with fully perforated baffles or half perforated baffles at various relative roughness pitchs. In general, the half perforated baffles were thermo-hydraulically better to the fully perforated baffles at the same pitch.

Islam et al. [73] experimentally investigated the effect of duct height on heat transfer enhancement of a surface affixed with arrays of short rectangular plate fins of a co-rotating type pattern in the duct. An infrared imaging system was used to measure detailed distributions of the heat transfer at the endwall along with the fin base. They reported that heat transfer initially increased with duct height and then finally decreased with increasing the duct height. SriHarsha et al. [74] studied the effect of rib height to the hydraulic diameter ratio on the local heat transfer distributions in a double wall ribbed square channel with 90° continuous attached and 60° V-broken ribs. The enhancements from 60° V-broken ribs were higher than 90° continuous ribs. However, with an increase in the rib height, the enhancements were found to decrease in channel with broken ribs.

Sripattanapipat and Promvonge [75] numerically investigated on laminar periodic flow and heat transfer in a two dimensional horizontal channel with isothermal walls and with staggered diamond-shaped baffles. They reported that optimum thermal performance was at the baffle angle of 5°, baffle height and

spacing of 0.5H and 1H, respectively. Kamali and Binesh [76] studied the turbulent heat transfer and friction in a square duct with various-shaped ribs mounted on one wall. The simulations were performed for square, triangular, trapezoidal with decreasing height in the flow direction, and trapezoidal with increasing height in the flow direction.

Gupta et al. [77] studied the local heat transfer distributions in a double wall ribbed square channel with 90° continuous, 90° saw tooth profiled and 60° V-broken ribs. The enhancements using 60° V-broken ribs were higher than 90° continuous ribs. The effect of pitch to the rib height ratio was not significant. Aharwal et al. [78] presented the experimental investigation of heat transfer and friction factor characteristics of a rectangular duct roughened with repeated square cross-section split-rib with a gap, on one broad wall arranged at an inclination with respect to the flow direction. The thermo-hydraulic performance parameter is found to be the maximum for the relative gap width of 1.0 and the relative gap position of 0.25.

Promvonge and Thianpong [79] experimentally studied on heat transfer and friction loss behaviors in a constant heat flux channel fitted with triangular (isosceles), wedge (right-triangular) and rectangular shapes. The wedge rib pointing downstream yielded the highest Nusselt number and the friction factor. The triangular rib with staggered array showed better thermal performance. Khan et al. [80] experimentally studied the heat transfer augmentation in developing turbulent flow through a ribbed square duct.

Dutta and Hossain [81] experimentally investigated the local heat transfer characteristics and the associated frictional head loss in a rectangular channel with inclined solid and perforated baffles. The local Nusselt number distribution was strongly depended on the position, orientation, and geometry of the baffled plate. Chandra et al. [82] experimentally studied the surface heat transfer and friction characteristics of a fully developed turbulent air flow in a square channel with transverse ribs on one, two, three, and four walls. The heat transfer coefficient and friction factor results were enhanced with the increase in the number of ribbed walls.

Momin et al. [83] experimentally investigated the effect of geometrical parameters of V-shaped ribs on heat transfer and fluid flow characteristics of rectangular duct of solar air heater with absorber plate having V-shaped ribs on its underside. Murata and Mochizuki [84] numerically studied the heat transfer in a rib-roughened duct by using the second-order finite difference method in coordinates fitted to transverse or angled ribs for both laminar and turbulent regions. Tsia and Hwang [85] experimentally studied the heat transfer and friction in a rectangular duct roughened by arrays of alternate attached and detached ribs. They reported that the

entrance distance for the composite ribbed duct was longer than the fully-attached and detached ribbed ducts.

2.2.2 Winglets

The winglets have been introduced to improve the heat transfer rate. For examples, Skullong and Promvonge [86] presented an experimental study on the heat transfer and flow friction characteristics in a solar air heater channel fitted with delta-winglet. They reported that the 30° delta-winglet placed only on the upper wall yielded the best thermal performance. Zhou and Ye [87] experimentally investigated the performance of a pair of new vortex generators-curved trapezoidal winglet and compare with traditional vortex generators, rectangular winglet, trapezoidal winglet and delta winglet. The results showed that delta winglet pair was the best in laminar and transitional flow region, while curved trapezoidal winglet pair had the best thermohydraulic performance in fully turbulent region.

Min et al. [88] experimentally investigated the influence of a modified rectangular longitudinal vortex generator obtained by cutting off the four corners of a rectangular wing on fluid flow and heat transfer characteristics in a rectangular channel. Results showed that the modified rectangular wing pairs had better flow and heat transfer characteristics than rectangular wing pair.

2.2.3 Ribs combined with winglets

To further improve the thermal performance, the combinations of ribs and winglets are also introduced. For examples, Promvonge et al. [89] studied the effects of combined ribs and delta-winglet with attack angles (α) of 60°, 45° and 30° on forced convection heat transfer and friction loss behaviors for turbulent airflow through a solar air heater channel. Promvonge et al. [90] experimentally investigated the effects of combined ribs and winglet type vortex generators on forced convection heat transfer and friction loss behaviors for turbulent airflow through a constant heat flux channel. They reported that the in-line ribs gave the highest increment in both the Nusselt number and friction factor while the staggered ribs showed better thermal performance.

Chompookham et al. [91] experimentally investigated the effect of combined wedge ribs and winglet type vortex generators on heat transfer and friction loss behaviors in a channel, two types of wedge ribs are introduced: wedge ribs pointing downstream and pointing upstream. Alam et al. [92] reviewed the using of turbulators in different forms such as ribs, baffles, delta winglets, obstacles, vortex generator, rings and perforated blocks/baffles to improve the performance of heat exchangers and solar air heaters. They reported that perforation in ribs/baffles/blocks and combination of combined rib and delta winglet led to the better thermo-hydraulic performance.

For better understanding of the ribs, fins, baffles, winglets and their combinations, their characters and geometries are summarized in table 2.2 and 2.3.

Table 2.2 Summary of important turbulators used by various investigators [92].

Authors	Type of turbulators	Reynolds number (Re)	Relative height (e/D)	Relative height (p/e)	Remark
Hwang, Liou (1995)	Solid and perforated ribs on two opposite walls in staggered fashion	10000–50000	0.081 0.162	5, 10, 15, 20	Nu/Nu_s=1.0–1.55 for solid and 1.15 for perforated, f/f_s=6–9 for solid and 4–6 for perforated
Hwang (1998)	Perforated fences on two opposite walls	8000–50000	0.081	10	Perforated fences for small t/e give better performance
Sara (2001)	Perforated block attached to one wall	6670–40000	0.081	0.309–1.407	Nu/Nu_s=0.8–1.0 for solid and 1.0–1.4 for perforated, f/f_s=0.7–0.9 for solid and 0.3–0.8 for perforated
Liou, Chan (1998)	Solid and perforated ribs detached from wall	5000–50000	0.081, 0.106, 0.162	10	Detached solid and perforated ribs are better than detached perforated ribs
Moon, Lau (2003)	Perforation in middle, above mid-plane and below mid-plane in blockage of duct size	20000–30000	1	p=63.5, 76.2 mm	Nu=155.79–244.75, f=5.34–42.79 for Re 20000 Nu=320.08–501.39, f=5.08–47.26 for Re 30000
Tariq (2004)	Rib with slit perforation	32100	0.0624	0.0624	Rib have open area ratio 20% being optimum

Table 2.2 (continued)

Authors	Type of turbulators	Reynolds number (Re)	Relative height (e/D)	Relative height (p/e)	Remark
Sriromreun (2012)	Z-shaped baffles	4400–20,400	e/H 0.1–0.3	P/H 1.5–3	Nu_{max}=380 and f_{max}1.1 at e/H=0.3, P/H=1.5, in phase.
Chompookham (2010)	Winglet-type vortex generators	5000–22,000	e/H 0.2	P/H 1.33	Combination of staggered wedge rib and the WVGs performed efficiently.
Promvonge (2011)	Rib with delta winglet	5000–20,000	e/H 0.2	P/H 1.33	Nu/Nu_s=2.3–2.6, f/f_s=4.7–10.1.
Bekele (2011)	Delta shaped obstacles	3400-27600	e/H 0.25–0.75	P_l/e 3/2–11/2	Nu/Nu_s=3.6 at Re=7277, P_l/e=3/2 and e/H=0.75.
Thianpong (2012)	Twisted rings	4000–20,000	-	P/D 1–2	Maximum performance factor=1.24 at W/D=0.05, p/D=1.0 at Re=6000.

2.2.4 Ribs combined with groove

There is the using of ribs with groovy surfaces in the channels. For examples, Skullong et al. [93] presented an experimental study on turbulent flow and heat transfer characteristics in a solar air heater channel fitted with combined 45° wavy-rib and groove turbulators. They reported that the combined rib-groove on both the upper and lower walls provided the highest heat transfer rate and friction factor in comparison with ribbed wall. Mohammed et al. [94] numerically investigated the thermal and hydraulic characteristics of turbulent nanofluids flow in a rib–groove channel. They reported that the rectangular rib–triangular groove had highest Nusselt

number. The SiO_2 nanofluid gave highest Nusselt number compared with other nanofluids.

Eiamsa-ard and Promvonge [95] studied the effects of combined rib-grooved turbulators on heat transfer and friction characteristics in a rectangular duct. In the experiments, three types of rib-groove arrangements: rectangular-rib and triangular-groove, triangular-rib and rectangular-groove and triangular-rib with triangular-groove were introduced. They reported that the triangular-rib with triangular-groove gave the highest thermal performance for all pitch ratios studied. Eiamsa-ard and Promvonge [96] numerically investigated the turbulent forced convection in a two-dimensional channel with periodic transverse grooves on the lower channel wall.

2.2.5 Nanofluids

Recently, the using of nanofluids as working fluids is also introduced. For examples, Parsazadeh et al. [97] numerically investigated the effects of different types of nanoparticles with different nanoparticle parameters in a fully detached ribbed channel. The bottom wall of the channel was kept at a constant temperature while the upper wall was thermally insulated. They reported that the highest heat transfer enhancement was achieved with SiO_2 nanofluid and the friction factor did not considerably change when using different types of nanoparticles in the base fluid.

Nassan et al. [98] presented a comparison between heat transfer characteristics of Al_2O_3/water and CuO/water nanofluids through a square cross-section cupric duct in laminar flow under uniform heat flux. The results indicated that a considerable heat transfer enhancement has been achieved by both nanofluids compared with base fluid. CuO/water nanofluid gave better heat transfer augmentation compared with Al_2O_3/ water nanofluid.

2.2.6 Other turbulators

Other shapes of the vortex generators have also been studied. For examples, Bopche and Tandale [99] experimentally investigated on heat transfer coefficient and friction factor by using artificial roughness in the form of specially prepared inverted U-shaped turbulators on the absorber surface of an air heater duct. Eiamsa-ard et al. [100] experimentally investigated the effects of wire coil elements on heat transfer and flow friction characteristics in a square-duct. Apart from the full-length coil, 1D and 2D length coil elements placed in tandem inside the duct with various free-space lengths were introduced to reduce the friction loss. The experimental results showed that the use of wire coil inserts for the full-length coil, 1D and 2D coil elements with a short free-space length leads to a considerable increase in heat transfer and friction loss over the smooth duct with no insert. The full-length wire

coil provided higher heat transfer and friction factor than the tandem wire coil elements under the same operating conditions.

Saha [101] experimentally studied the heat transfer and the pressure drop characteristics of turbulent flow of air through rectangular and square ducts with internal transverse rib turbulators on two opposite surfaces of the ducts and with wire-coil inserts. The transverse ribs in combination with wire-coil inserts had been found to perform better than either ribs or wire-coil inserts acting alone. Ray and Date [102] presented numerical prediction of characteristics of laminar, as well as, turbulent flow and heat transfer in a square sectioned duct inserted with a twisted tape, whose width equals the length of the duct side.

2.3 Guidelines of research

In the literature survey above, the advantage of the twisted-tape vortex generator is low flow resistance and ease in manufacturing but the drawback is lower vortex strength while the benefit of the baffle vortex generator is the lowest penalty of pressure drop at a certain angle of attack. Therefore, in this work, a novel insert device (or vortex generating device) is developed and expected to provide higher swirl/vortex strength at the near-wall region from using the baffles and higher fluid mixing between the central-core and the near-wall regimes from using the twisted-tape, and thus, to improve the heat transfer rate in the wall region leading to greater increase in thermal performance.

The main aim of this research is to investigate the effect of geometric parameters of the proposed swirl/vortex generator on heat transfer rate, pressure loss and thermal performance in square-duct heat exchanger. The geometric parameters of the insert device considered with relative to duct's height are consisted of shape, size, angle, height and pitch. The results should be useful in the design of heat exchangers to achieve the maximum thermal performance while maintains low cost, energy saving, and reduces the environmental impact.

CHAPTER 3
CONVECTIVE HEAT TRANSFER FUNDAMENTALS

3.1 Introduction

This chapter explains the fundamental concepts of thermal-fluid sciences that will build on earlier understand in the current study, thermal performance enhancement techniques including mathematic and statistical methods for the model design and analysis of problem to achieve the optimal relevant parameters.

3.2 Fundamentals of thermal-fluid sciences

3.2.1 Definition of a fluid [103]

Fluid mechanics deals with the behavior of fluids at rest and in motion. It is logical to begin with a definition of a fluid: a fluid is a substance that deforms continuously under the application of a shear stress no matter how small the shear stress may be. Thus fluids comprise the liquid and gas phases of the physical forms in which matter exists. The distinction between a fluid and solid state of matter is clear if you compare fluid and solid behaviors. A solid deforms when a shear stress is applied, but its deformation does not continue to increase with time.

Figure 3.1a and b shows the deformation of solid and fluid under the action of a contact shear force respectively. In Fig. 3.1a, the shear force is applied to the solid through the upper plate to which the solid has been bended while in Fig. 3.1b when the shear force is applied to the upper plate, the deformation of fluid element continues to increase as long as the force is applied. The fluid in direct contact with the solid boundary has the same velocity as the boundary itself, there is no-slip at the boundary.

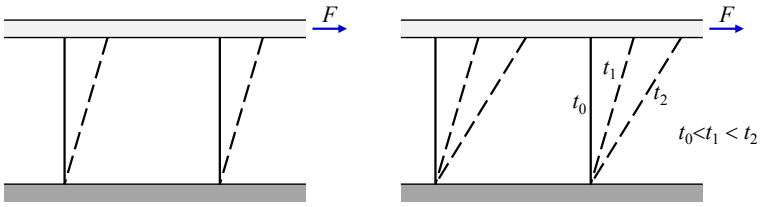

Figure 3.1 Behaviors of (a) solid and (b) fluid, under the action of a constant shear force.

3.2.2 The no-slip condition [104]

An experimental observation indicates that a fluid in motion comes to a complete stop at the surface and assumes a zero velocity relative to the surface.

The no-slip condition is responsible for the development of the velocity profile. Because of friction between the fluid layers, the layer that sticks to the wall slows the adjacent fluid layer, which slows the next layer, and so on. A fluid layer adjacent to a moving surface has the same velocity as the surface. A consequence of the no-slip condition is that all velocity profiles must have zero values with respect to the surface at the points of contact between a fluid and a solid surface (see Fig. 3.2). The only exception to the no-slip condition occurs in extremely rarefied gases.

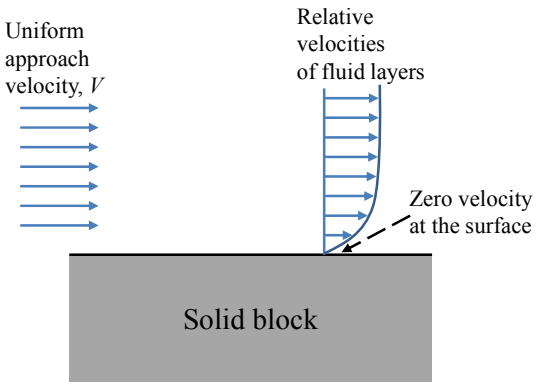

Figure 3.2 A zero velocity at the surface for a fluid flowing over a stationary surface due to the no-slip condition.

3.3 Flow in ducts [104]

Liquid or gas flow through ducts is commonly used in heating and cooling applications, and fluid distribution networks. The fluid in such applications is usually forced to flow by a fan or pump through a flow section. The friction is directly related to the pressure drop and head loss during flow through ducts and ducts. The pressure drop is then used to determine the pumping power requirement.

The fluid velocity in a duct changes from zero at the surface because of the no-slip condition to a maximum at the duct center. In fluid flow, it is convenient to work with an average or mean velocity V_m, which remains constant in incompressible flow when the cross-sectional area of the duct is constant. The mean velocity in heating and cooling applications may change somewhat because of changes in density with temperature. But, in practice, the fluid properties are evaluated at some average temperature and treated as constants.

The value of the mean velocity $\mathrm{V_m}$ is determined from the requirement that the conservation of mass principle be satisfied. That is,

$$\dot{m} = \rho V_m A_c \qquad (3.1)$$

where $\dot{m}$ is the mass flow rate, ρ is the density, $\mathrm{A_c}$ is the cross-sectional area.

3.3.1 Laminar and turbulent flows

The existence of these laminar, transitional, and turbulent flow regimes is verified by injecting some dye streaks into the flow in a glass duct, as the British scientist Osborne Reynolds did over a century ago. In observation, the dye streak forms a straight and smooth line at low velocities when the flow is laminar, has bursts of fluctuations in the transitional regime, and zigzags rapidly and randomly when the flow becomes fully turbulent.

The transition from laminar to turbulent flow depends on the geometry, surface roughness, flow velocity, surface temperature, and type of fluid, among other things. Osborne Reynolds discovered that the flow regime depends mainly on the ratio of the inertial forces to viscous forces in the fluid. This ratio is called the Reynolds number and is expressed for internal flow in a circular duct as

$$\mathrm{Re} = \frac{\mathrm{V_m D}}{\nu} = \frac{\rho \mathrm{V_m D}}{\mu} \tag{3.2}$$

where

$\mathrm{V_m}$ = mean flow velocity, m/s
D = characteristic length of the geometry (duct diameter), m
$\nu = \mu/\rho$ = kinematic viscosity of the fluid, $\mathrm{m^2/s}$.

For flow through noncircular ducts, the Reynolds number is based on the hydraulic diameter D_h defined as

$$\mathrm{D_h} = \frac{4\mathrm{A_c}}{\mathrm{P}} \tag{3.3}$$

where $\mathrm{A_c}$ is the cross-sectional area of the duct and P is its perimeter
Under most practical conditions, the flow in a circular duct is laminar for Re < 2300, turbulent for Re > 4000, and transitional in between. That is,

Re < 2300	laminar flow
2300 ≤ Re ≤ 4000	transitional flow
Re > 4000	turbulent flow

3.3.2 The entrance region

The region of the flow in which the effects of the viscous shearing forces caused by fluid viscosity are felt is called the velocity boundary layer or just the boundary layer. The hypothetical boundary surface divides the flow in a duct into

two regions: the boundary layer region, in which the viscous effects and the velocity changes are significant, and the inviscid flow region, in which the frictional effects are negligible and the velocity remains essentially constant in the radial direction.

The thickness of this boundary layer increases in the flow direction until the boundary layer reaches the duct center and thus fills the entire duct, as shown in Fig. 3.3. The region from the duct inlet to the point at which the boundary layer merges at the centerline is called the hydrodynamic entrance region, and the length of this region is called the hydrodynamic entry length L_h. Flow in the entrance region is called hydrodynamically developing flow since this is the region where the velocity profile develops. The region beyond the entrance region in which the velocity profile is fully developed and remains unchanged is called the hydrodynamically fully developed region. The flow is said to be fully developed when the normalized temperature profile also remains unchanged. Hydrodynamically developed flow is equivalent to fully developed flow when the fluid in the duct is not heated or cooled since the fluid temperature in this case remains essentially constant throughout. The velocity profile in the fully developed region is parabolic in laminar flow and somewhat flatter (or fuller) in turbulent flow due to eddy motion and more vigorous mixing in the radial direction.

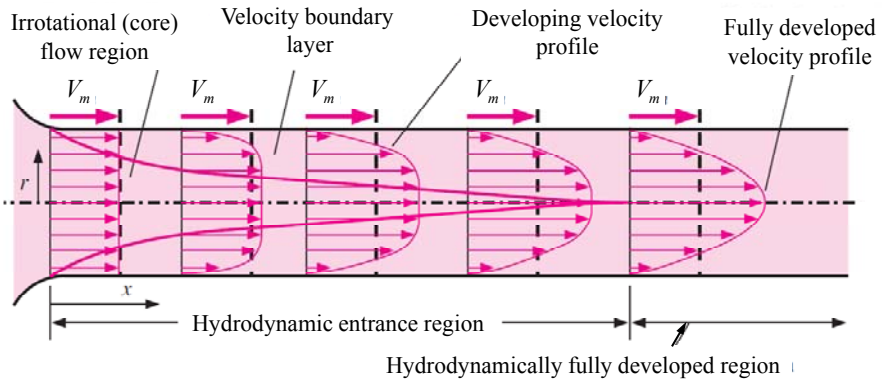

Figure 3.3 The development of the velocity boundary layer in a duct.

The hydrodynamic entry length is usually taken to be the distance from the duct entrance where the friction factor reaches within about 2 percent of the fully developed value.

In turbulent flow, the hydrodynamic entry length is approximately taken to be

$$L_{h,\,turbulent} \approx 10D \tag{3.4}$$

A quantity of interest in the analysis of duct flow is the pressure drop ΔP since it is directly related to the power requirements of the fan or pump to maintain flow. The

pressure loss (or head loss) is available, the required pumping power to overcome the pressure loss is determined from

$$\dot{W}_{pump,L} = \dot{V}\Delta P_L = \dot{V}\rho g h_L = \dot{m} g h_L \tag{3.5}$$

where $\dot{V}$ is the volume flow rate and $\dot{m}$ is the mass flow rate.
The pressure loss for all types of fully developed internal flows

Pressure loss $$\Delta P_L = f\frac{L}{D}\frac{\rho V_m^2}{2} \tag{3.6}$$

where $\rho V_m^2/2$ is the dynamic pressure and the dimensionless quantity f is the friction factor
The duct head loss is obtained by dividing ΔP_L by ρg to give

Head loss $$h_L = \frac{\Delta P_L}{\rho g} = f\frac{L}{D}\frac{V_m^2}{2g} \tag{3.7}$$

3.4 Forced convection [104]

In forced convection, the fluid is forced to flow over a surface or in a duct by external means such as a pump or a fan.

3.4.1 Physical mechanism of convection

The convection heat transfer relations to be rather complex because of the dependence of convection on so many variables. This is not surprising, since convection is the most complex mechanism of heat transfer. Despite the complexity of convection, the rate of convection heat transfer is observed to be proportional to the temperature difference and is conveniently expressed by Newton's law of cooling as

$$\dot{q}_{conv} = h_s(T_s - T_\infty) \tag{3.8}$$

or

$$\dot{Q}_{conv} = h_s A_s(T_s - T_\infty) \tag{3.9}$$

where

$\dot{Q}$ = the rate of heat transfer to or from the fluid, W

h = convection heat transfer coefficient, W/m^2 $^\circ$C

A_s = heat transfer surface area, m^2

T_s = temperature of the surface, $^\circ$C

T_∞ = temperature of the fluid sufficiently far from the surface, $^\circ$C

In convection studies, it is common practice to nondimensionalize the governing equations and combines the variables, which group together into dimensionless numbers in order to reduce the number of total variables. It is also common practice to nondimensionalize the heat transfer coefficient h with the Nusselt number, defined as

$$Nu = \frac{hD}{k} \tag{3.10}$$

where k is the thermal conductivity of the fluid and D is the tube/duct diameter. The Nusselt number made significant contributions to convective heat transfer and it is viewed as the dimensionless convection heat transfer coefficient.

3.5 General considerations for tube flow [104]

When a fluid is heated or cooled as it flows through a tube, the temperature of the fluid at any cross section changes from T_s at the surface of the wall to some maximum (or minimum in the case of heating) at the tube center. In fluid flow it is convenient to work with an average or mean temperature T_m that remains uniform at a cross section. Unlike the mean velocity, the mean temperature T_m will change in the flow direction whenever the fluid is heated or cooled.

The mean temperature T_m of a fluid changes during heating or cooling. Also, the fluid properties in internal flow are usually evaluated at the bulk mean fluid temperature, which is the arithmetic average of the mean temperatures at the inlet and the exit. That is,

$$T_b = (T_{m,i} + T_{m,e})/2 \tag{3.11}$$

where

T_b = bulk mean fluid temperature

$T_{m,i}$ = mean temperatures at the inlet

$T_{m,e}$ = mean temperatures at the exit

3.5.1 Thermal Entrance Region

The thickness of this boundary layer also increases in the flow direction until the boundary layer reaches the tube center and thus fills the entire tube, as shown in Fig. 3.4. The region of flow over which the thermal boundary layer develops and reaches the tube center is called the thermal entrance region, and the length of this region is called the thermal entry length L_t. Flow in the thermal entrance region is called thermally developing flow since this is the region where the temperature profile develops. The region beyond the thermal entrance region in which the dimensionless temperature profile expressed as $(T_s - T)/(T_s - T_m)$ remains unchanged is called the thermally fully developed region. The region in which the flow is both hydrodynamically and thermally developed and thus both the velocity and dimensionless temperature profiles remain unchanged is called fully developed flow.

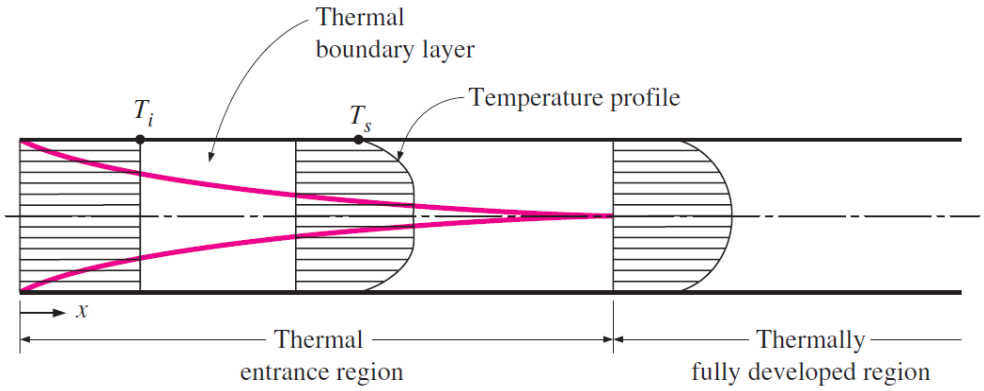

Figure 3.4 The development of the thermal boundary layer in a tube.

In turbulent flow, the thermal entry lengths are approximately taken to be

$$L_{t,\,turbulent} \approx 10D \tag{3.12}$$

3.5.2 General thermal analysis

The conservation of energy equation for the steady flow of a fluid in a tube can be expressed as (see Fig. 3.5)

$$\dot{Q} = \dot{m}C_p(T_e - T_i) \tag{3.13}$$

where T_i and T_e are the mean fluid temperatures at the inlet and exit of the tube, respectively, and $\dot{Q}$ is the rate of heat transfer to or from the fluid.

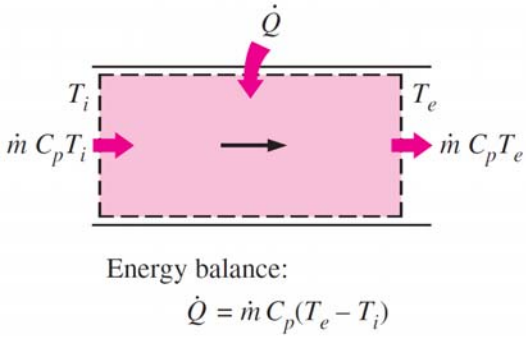

Figure 3.5 The heat transfer to a fluid flowing in a tube equal to the increase in the energy of the fluid.

The thermal conditions at the surface can usually be approximated with reasonable accuracy to be constant surface temperature (T_s = constant) or constant surface heat flux ($\dot{q}_s$ = constant). The constant surface heat flux condition is realized when the tube is subjected to radiation or electric resistance heating uniformly from all directions.

Surface heat flux is expressed as

$$\dot{q}_s = h_x(T_s - T_m) \tag{3.14}$$

where h_x is the local heat transfer coefficient and T_s and T_m are the surface and the mean fluid temperatures at that location.

In the case of $\dot{q}_s$ constant, the rate of heat transfer can also be expressed as

$$\dot{Q} = \dot{q}_s A_s = \dot{m} C_p(T_e - T_i) \tag{3.15}$$

In the fully developed region, the surface temperature T_s will also increase linearly in the flow direction since h is constant and thus $T_s - T_m$ = constant (see Fig. 3.6). Of course this is true when the fluid properties remain constant during flow.

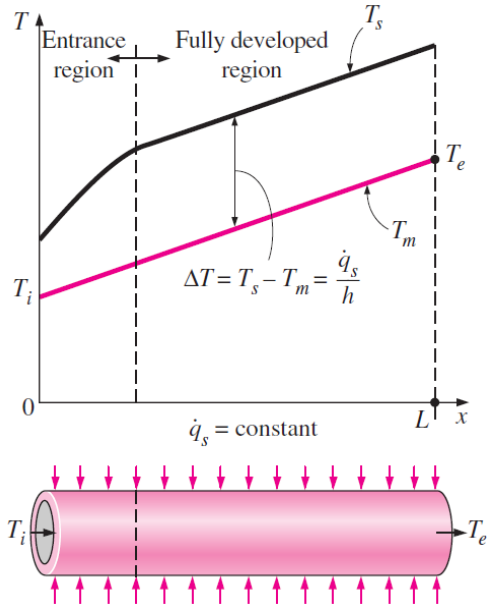

Figure 3.6 Variation of the tube surface and the mean fluid temperatures along the tube for the case of constant surface heat flux.

3.5.3 Turbulent flow in tubes

Turbulent flow is commonly utilized in practice because of the higher heat transfer coefficients associated with it. Most correlations for the friction and heat transfer coefficients in turbulent flow are based on experimental studies because of the difficulty in dealing with turbulent flow theoretically.

For smooth tubes, the friction factor in turbulent flow can be determined from the explicit first Petukhov equation given as

Smooth tubes:

$$f = (0.790 \ln \mathrm{Re} - 1.64)^{-2} \qquad 10^4 < \mathrm{Re} < 10^6 \tag{3.16}$$

Another equation of the friction factor in turbulent flow is the correlation of Blasius given as

$$f = 0.316 \mathrm{Re}^{-0.25} \qquad 3000 \le \mathrm{Re} \le 20{,}000 \tag{3.17}$$

For fully developed turbulent flow in smooth tubes, the Nusselt number can evaluate by Colburn equation as

$$\mathrm{Nu} = 0.023 \mathrm{Re}^{0.8} \mathrm{Pr}^{n} \tag{3.18}$$

where n = 0.4 for heating and 0.3 for cooling of the fluid flowing through the tube. This equation is known as the Dittus–Boelter equation.

The fluid properties are evaluated at the bulk mean fluid temperature $T_b = (T_i + T_e)/2$, when the temperature difference between the fluid and the wall is very large.

The Nusselt number relations above are fairly simple, but they may give errors as large. This error can be reduced by using more complex but accurate relations such as Gnielinski equation. The accuracy of this relation at lower Reynolds numbers expressed as

$$Nu = \frac{(f/8)(Re-1000)Pr}{1+12.7(f/8)^{0.5}(Pr^{2/3}-1)} \qquad 3\times10^3 < Re < 5\times10^6 \qquad (3.19)$$

where the friction factor, f, can be determined from an appropriate relation such as the first Petukhov equation.

3.5.4 Turbulent flow in noncircular tubes

The turbulent flow relations given above for circular tubes can also be used for noncircular tubes with reasonable accuracy by replacing the diameter D in the evaluation of the Reynolds number by the hydraulic diameter, D_h. (Fig. 3.7)

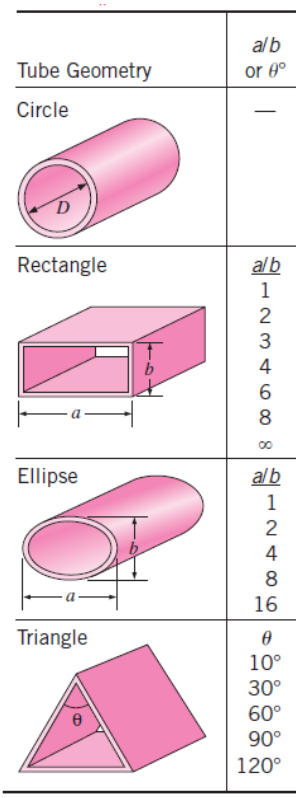

Figure 3.7 Nusselt number for fully developed flow in tubes of various cross sections ($D_h = 4A_c/P$, $Re = V_m D_h/\nu$, $Nu = hD_h/k$)

3.5.5 Heat transfer enhancement [104, 105]

Techniques to enhance the heat transfer can be organized into two major groups: first, is passive techniques to design the surface characteristics of specialty duct different from smooth or fluid or chemical work to be added for enhanced heat transfer rate, with no external power is involved, such as coated surfaces, rough surfaces, extended surfaces, displaced insert, swirl flow, coiled tubes, surface tension and additives liquids/gases. The second is the active techniques require external power source to help stimulate, such as electric or acoustic fields and surface vibration, result in the vibration of the surface or fluid which can increase the heat transfer.

For the passive techniques, tubes with rough surfaces have much higher heat transfer coefficients than tubes with smooth surfaces. Therefore, tube surfaces are often intentionally roughened, corrugated, or finned in order to enhance the convection heat transfer coefficient and thus the convection heat transfer rate (Fig. 3.8). Heat transfer in turbulent flow in a tube has been increased by roughening the surface. Roughening the surface, of course, also increases the friction factor and thus the power requirement for the pump or the fan. The convection heat transfer coefficient can also be increased by inducing pulsating flow by pulse generators, by inducing swirl by inserting a twisted tape into the tube, or by inducing secondary flows by coiling the tube.

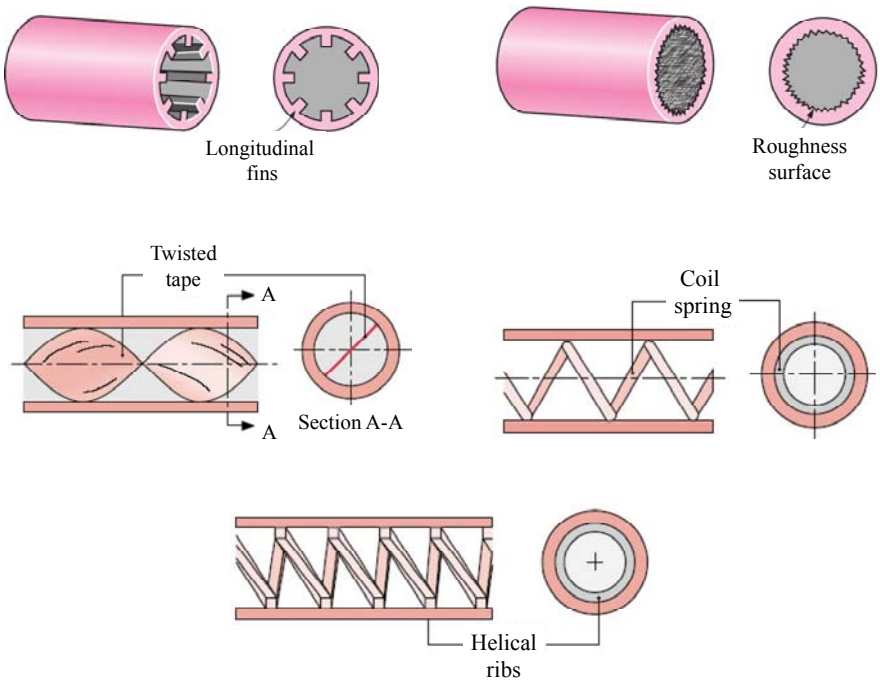

Figure 3.8 Internal flow heat transfer enhancement schemes: roughened surface, longitudinal fins, twisted-tape insert, coil spring wire insert and helical ribs.

3.5.6 Thermal performance

The thermal enhancement factor (η) defined as the ratio of the heat transfer coefficient of an augmented surface, h_b to that of a smooth surface, h_0 at a constant blowing power is suggested by Ralph L. Webb [105]

$$P_0 = P_b$$

$$(\Delta PQ)_0 = (\Delta PQ)_b$$

$$\left[\left(\frac{f\rho L\overline{V}^2}{2D_h}\right)(\overline{V}A)\right]_0 = \left[\left(\frac{f\rho L\overline{V}^2}{2D_h}\right)(\overline{V}A)\right]_b$$

$$\left(f\overline{V}^3\right)_0 = \left(f\overline{V}^3\right)_b$$

$$\left(f\,Re^3\right)_0 = \left(f\,Re^3\right)_b$$

$$\frac{f_0}{f_b} = \frac{Re_b^3}{Re_0^3}$$

$$\frac{Re_b}{Re_0} = \left(\frac{f_0}{f_b}\right)^{1/3}$$

$$\frac{Re_b}{Re_0} = \frac{1}{(f_b/f_0)^{1/3}}$$

$$Re_b = \frac{Re_0}{(f_b/f_0)^{1/3}} \tag{3.20}$$

So, the thermal enhancement factor (η) that is,

$$\eta = \left.\frac{h_b}{h_0}\right|_{bp} = \left.\frac{Nu_b}{Nu_0}\right|_{bp} = \left(\frac{Nu_b}{Nu_0}\right)\left(\frac{f_b}{f_0}\right)^{-1/3} \tag{3.21}$$

where subscripts are

b = tube with baffle

0 = smooth tube

bp = blowing power

3.6 Regression analysis

Regression analysis is a statistical tool for estimating the relationships between variables. It includes many techniques for modeling and analyzing several variables, when the focus is on the relationship between a dependent variable (Y) and one or more independent variables ($X_1, X_2, ..., X_n$). The estimation target is a function of the independent variables called the regression function that the relationship is shown in linear form [106, 107]

$$Y = a + bX \tag{3.22}$$

where

Y = dependent variable
X = independent variables
a = constant
b = slope

The general form of multiple exponential regressions expressed as

$$Y = a\, X_1^{c_1} X_2^{c_2} X_3^{c_3} ... X_n^{c_n} \tag{3.23}$$

and the multiple linear regress in logarithmic scale given as

$$\ln(Y) = \ln c_0 + c_1 \ln(X_1) + c_2 \ln(X_2) + c_3 \ln(X_3) ... + c_n \ln(X_n) \tag{3.24}$$

where

c_i = linear coefficient value of X_i

3.7 Response surface methodology

The response surface methodology is the mathematic and statistical methods for design the model and analysis of problem to achieve the optimal response parameters. The response surface methodology is relationships between variables, response variable (Y) and independent variables (X). The surface represented by $f(X_1, X_2)$ is called a response surface [108]

In general form of the estimate function for first order given as

$$Y = \beta_0 + \beta_1 X_1 + \beta_2 X_2 + \ldots + \beta_n X_n + \varepsilon \tag{3.25}$$

and the general form of the estimate function for second order given as

$$Y = \beta_0 + \sum_{i=1}^{n} \beta_i X_i + \sum_{i=1}^{n} \beta_{ii} X_i^2 + \sum_{i}^{n} \sum_{\substack{j \\ i<j}}^{k} \beta_{ji} X_i X_j + \varepsilon \tag{3.26}$$

where

β = intercept

β_i = the linear effect of X

β_{ii} = the quadratic effect of X

β_{ji} = the interaction effect of X_i, X_j

ε = error observed in the response Y

CHAPTER 4
EXPERIMENTAL SETUP AND SMOOTH DUCT VERIFICATION

This chapter describes the experimental setup, the installation of equipment in a square-duct heat-exchanger used in current research. Then, next section introduces the types of swirl/vortex generators and their geometries mounted in the test section. Finally, the research methodology and verification of smooth duct are presented.

4.1 Experimental set up

A schematic diagram of the experimental setup is presented in Fig. 4.1. The system consists of a high-pressure blower, an orifice flow meter, a settling tank, and a square duct test section. The overall length of the duct was 3000 mm comprised an entrance section of 2000 mm and a test section of 1000 mm. The test section in square duct was made of aluminum plate having thickness of 3 mm. The test section had a cross sectional area of 45×45 mm^2 (H×H) and a length of 1000 mm (L).

The AC power supply provided energy for heating four walls of the test section and maintaining a uniform surface heat flux condition. Air as the working fluid was forced through the system by a 1.45 kW high-pressure blower. An inverter was used to control the air flow rate. The flow rate was measured by using an orifice plate. The orifice plate was calibrated by hot wire and vane-type anemometers. The pressure drop across the orifice was measured using an inclined manometer. In Fig. 4.2 the axial temperature distributions along the test section were measured by twenty-eight thermocouples. Two thermocouples were positioned 80 mm at the entrance and 10 mm at the exit of the duct to measure the inlet and outlet temperatures. All thermocouples were type-K having 1.5 mm diameter wire. All measured temperature values were fed into a data logger (Fluke 2650A) and recorded via a personal computer. Two static pressure taps were located at the top walls to measure axial pressure drops across the test section. This pressure drop was determined to calculate the friction factor. They were located at the centre line of the duct. First pressure tap was located 30 mm from the entrance of the test section. And another pressure tap was located 50 mm at the exit of the test section. The pressure drop was measured by a digital differential pressure transducer.

The uncertainty analysis in the data calculation was based on [110]. The maximum uncertainties of non–dimensional parameters were ±5% for Reynolds number, ±7% for Nusselt number and ±9% for friction factor. The uncertainty in the

axial velocity measurement was estimated to be less than ±7%, and pressure drop had a corresponding uncertainty of ±5% whereas the uncertainty in temperature measurement at the duct walls was about ±0.5%.

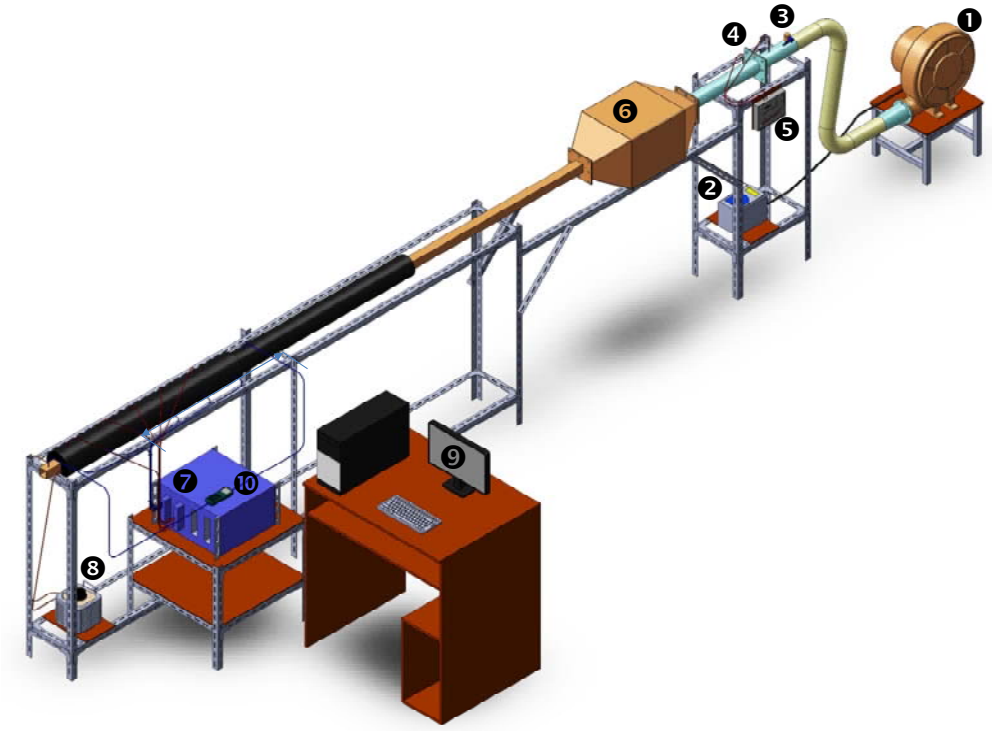

Figure 4.1 Schematic diagrams of experimental apparatus.

(1) high-pressure blower, (2) inverter, (3) control valve, (4) orifice plate, (5) inclined manometer, (6) settling tank, (7) data Logger FLUKE 2650A, (8) variac transformer, (9) personal computer, (10) digital differential pressure.

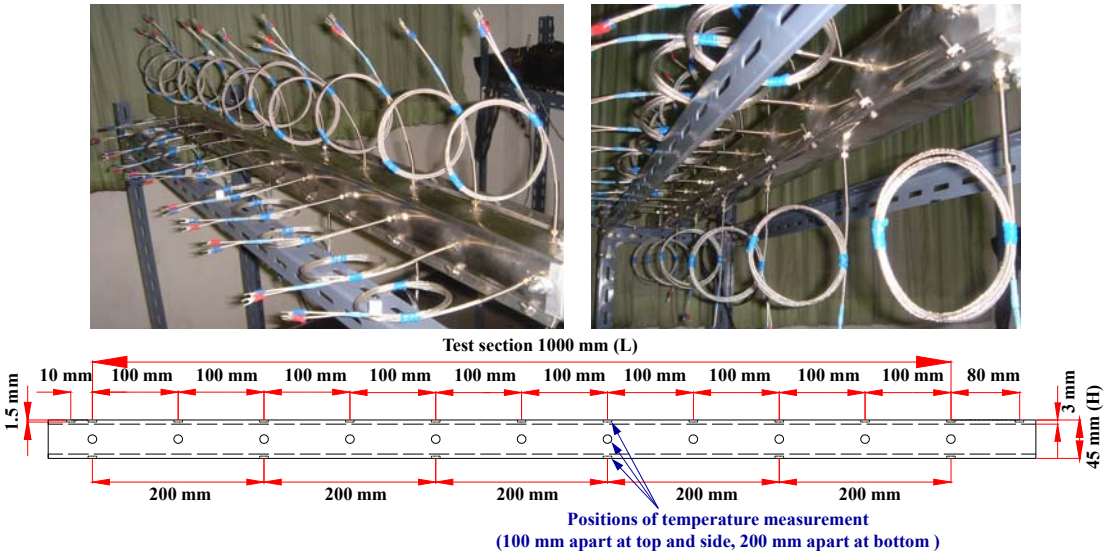

Figure 4.2 Test section and details of temperature measurement position.

4.2 The details of equipment

The equipment used for experimental investigation of square-duct heat exchanger can be divided into three groups; flow equipment, data recording equipment and other equipment as follows:

4.2.1 Flow equipment

4.2.1.1 An air high-pressure blower (model TB-150) is a centrifugal blower with rated power of 1.5 (2P) kW, rated voltage of 220/380 V, 3 phases, a maximum air flow rate of 3.4 m^3/minute and normal/maximum pressure of 185/190 mbar as presented in Fig. 4.3.

Figure 4.3 High-pressure blower

4.2.1.2 A motor was VENZ B3 foot mounted series. It is used to power steering blower with rated power of 1.5 kW (2P), rated voltage of 220/380 V, 3 phases, 50 Hz, 2900 rpm and 14.8 A as shown in Fig. 4.4

Figure 4.4 Motor

4.2.1.3 An inverter ND1 series was a frequency inverter with rated voltage of 380 V, 3 phases, output of 11 A , rated power of 5.5 HP. It was used to control speed of the motor as displayed in Fig. 4.5

Figure 4.5 Inverter

4.2.1.4 An orifice meter was a device that used to measure air flow rate. The orifice plate was positioned between blower and settling tank as depicted in Fig. 4.6. The orifice plate was made from steel sheet having a thickness of 5 mm, a front side diameter of 47 mm and a rear side diameter of 51 mm.

Figure 4.6 Orifice meter

4.2.1.5 An inclined manometer was Dwyer mark II model 25 (3" WC). It was used to measure differential pressure across an orifice plate. This pressure drop was used to calculate air flow rate. The manometer had an accuracy of ±3% full-scale range 0 to 3" H_2O, a maximum pressure of 10 psi using red oil with 0.826 specific gravity as shown in Fig. 4.7.

Figure 4.7 Inclined manometers

4.2.1.6 A Settling tank was used to arrange and adjust the air flow to become a steady flow before entering the square-duct. The cross sectional area of the settling tank was 450x450 mm^2 as portrayed in Fig. 4.8.

Figure 4.8 Settling tank

4.2.2 Data recording equipment

4.2.2.1 A data logger Fluke 2650A was used to record the temperatures. It had channel capacity 20 to 120 channels per chassis (6 analog input modules of 20 channels each). The data logger was linked with a personal computer as exhibited in Fig. 4.9.

Figure 4.9 Data logger Fluke 2650A

4.2.2.2 Thermocouples were used to measure inlet/outlet temperatures and also the surface temperatures along the test section as illustrated in Fig. 4.10. All of thermocouples are type K. They were positioned 11 points on the top and side walls, 6 points on the bottom wall and 2 points on the entrance and exit sections.

Figure 4.10 Thermocouple, type K

4.2.3 Other equipment

4.2.3.1 A variac transformer was an AC voltage controller It can provide a variable AC voltage that supplied to the heater plate. The variac transformer was TDGC2-3 kVA model, single-phase, 50 Hz. 12 A, input voltage 220 VAC and output voltage 0-250 VAC as shown in Fig. 4.11

Figure 4.11 Variac transformer

4.2.3.2 A digital differential pressure Dwyer series 475 Mark III model

ranging from 0-10" WC. This manometer was used to measure differential pressure across the test section. Its measurement accuracy was ±5% as displayed in Fig. 4.12.

Figure 4.12 Dwyer 475 Mark III Digital Manometers

4.2.3.3 A vane-type anemometer TESTO 445 model was used to measure air velocity in the duct. It had a measuring range of 0-60 m/s. This anemometer was used for calibrating the air flow as showed in Fig. 4.13.

Figure 4.13 Vane-type anemometers, TESTO 445

4.3 Swirl/Vortex generators

This section presents six different types of swirl/vortex generators as inserted in a square-duct.

4.3.1 Combined single twisted tape and baffle

Figure 4.14a, b and c shows twisted-tape alone, combined single twisted-tape and V-baffle (two walls, 2W) and combined single twisted-tape and V-baffle (four walls, 4W), respectively. The combined single twisted-tape and V-baffle geometries were twist length to tape width ratio or twist ratio (Y=y/w=4 and 5), baffle- to duct-height ratio, (R_B=e/H=0.1, 0.15 and 0.2), baffle-pitch to duct-height ratio, (R_P=P/w=2, 2.5, 4 and 5) at a single baffle attack angle, α=30°, V-upstream.

(a)

(b)

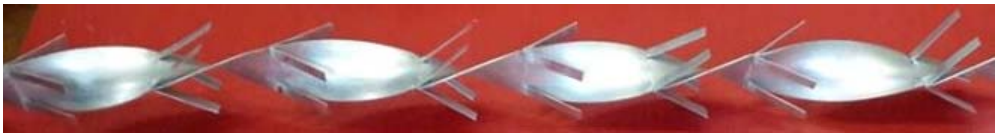

(c)

Figure 4.14 (a) Twisted-tape alone, (b) combined single twisted-tape and V-baffle (two walls, 2W) and (c) combined single twisted-tape and V-baffles (four walls, 4W).

4.3.2 Combined four twisted tapes and V-baffles

Figure 4.15a and b displays twisted-tape alone; and combined four twisted-tapes and V-baffles (four walls, 4W), respectively. The combined four twisted-tapes and V-baffle's geometries were twist length to tape width ratio or twist ratio (Y=y/w=4), baffle- to duct-height ratio, (R_B=e/H=0.075, 0.1, 0.15 and 0.2), baffle-pitch to duct-height ratio, (R_P=P/w=4, 8 12 and 16) at a single baffle attack angle, α=30°, V-upstream.

(a)

(b)

Figure 4.15 (a) Twisted-tape alone and (b) combined four twisted-tapes and V-baffles (four wall, 4W)

4.3.3 Discrete V-baffles

Figure 4.16 shows the discrete V-baffles placed on a double-sided straight tape. The discrete V-baffle's geometries were baffle- to duct-height ratio or blockage ratio, (R_B=e/H=0.075, 0.1, 0.15 and 0.2), baffle pitch to duct height ratio, (R_P=P/H=0.5, 1.0, 1.5 and 2.0) and three baffle attack angle, α=30°, 45° and 60°.

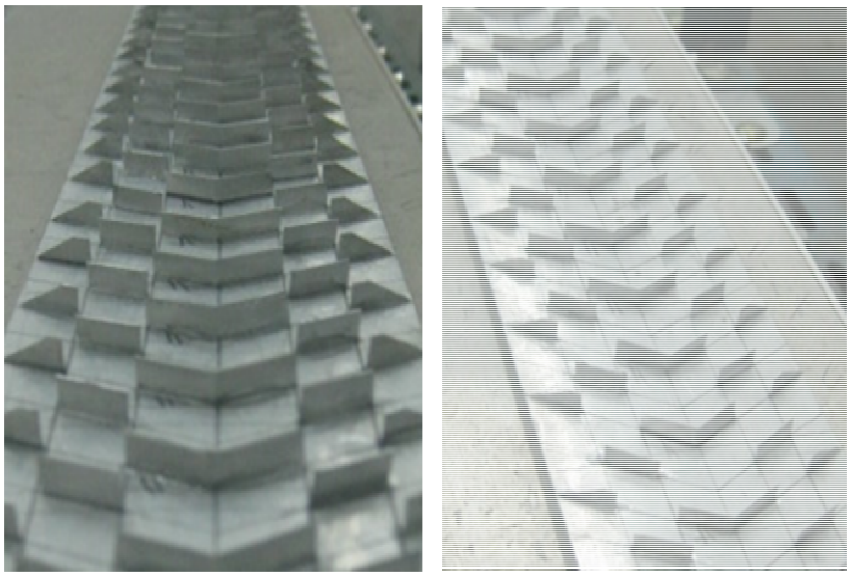

Figure 4.16 Discrete V-baffles tape

4.3.4 Trapezoidal V-baffles

Figure 4.17 shows the trapezoidal V-baffles placed on a double-sided straight tape. The trapezoidal V-baffle's geometries were baffle- to duct-height ratio or blockage ratio, (R_B=e/H=0.075, 0.1, 0.15 and 0.2), baffle pitch to duct height ratio, (R_P=P/H=0.5, 1.0, 1.5 and 2.0) and a single baffle attack angle, α=30°, V-upstream.

Figure 4.17 Trapezoidal V-baffles attached on a straight tape.

4.3.5 Angled baffles on two opposite walls

Figure 4.18 shows the angled baffles attached on both edges of a straight tape. The angled-baffle's geometries were baffle- to duct-height ratio or blockage ratio, (R_B=e/H=0.1 and 0.2), baffle pitch to duct height ratio, (R_P=P/H=0.5, 1.0 and 2.0) and a single baffle attack angle, α=30°.

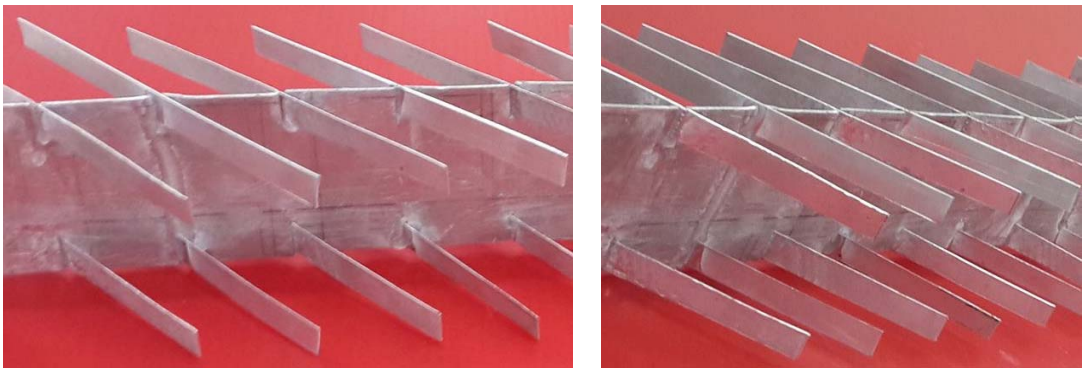

Figure 4.18 Angled baffles attached on a straight tape.

4.3.6 V-baffles on two opposite walls

Figure 4.19 shows the V-baffles mounted on both edges of a straight tape before insertion. The V-baffle geometries were baffle-to duct-height ratio or blockage ratio, (R_B=e/H=0.075, 0.1, 0.15 and 0.2), baffle pitch to duct height ratio, (R_P=P/H=0.5, 1.0, 1.5 and 2.0) and three baffle attack angle, α=20°, 30° and 45°.

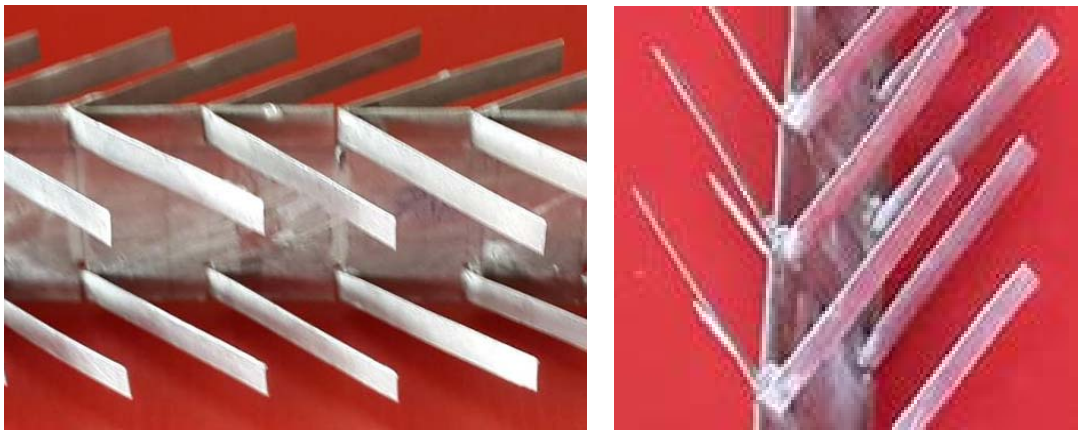

Figure 4.19 V-baffles attached on a straight tape.

4.4 Procedure of the research

4.4.1 First, installing the swirl/vortex generator into the square-duct test section.

4.4.2 Second, turning on the fan switch for the air flow through the test section and then adjusting the inverter to control the required fan speed.

4.4.3 Third, measuring the pressure drop across the test section.

4.4.4 Fourth, opening the variac transformer and adjusting the voltage that supply AC power to the heater plate.

4.4.5 Fifth, turning on the data logger Fluke 2650A program.

4.4.6 Sixth, observing the inlet/outlet and the surface temperatures and waiting until the surface temperatures were stable, then recording the temperature values.

4.4.7 Finally, analyzing the heat transfer in form of Nusselt number and the pressure loss in form of friction factor and the thermal enhancement factor.

4.5 Validation of smooth square duct

The Nusselt number (Nu) and friction factor (*f*) obtained from the smooth duct were compared with the correlations of Dittus-Boelter, Gnielinski, Blasius and Petukhov. These correlations are suggested for first validation of turbulent flow in ducts [109].

Correlation of Dittus-Boelter

$$\mathrm{Nu} = 0.023\mathrm{Re}^{0.8}\mathrm{Pr}^{0.4} \qquad \text{for heating} \qquad (4.1)$$

Correlation of Gnielinski

$$\mathrm{Nu} = \frac{(f/8)(\mathrm{Re}-1000)\mathrm{Pr}}{1+12.7(f/8)^{1/2}\left(\mathrm{Pr}^{2/3}-1\right)} \qquad 3000 < \mathrm{Re} < 5\times10^{6} \qquad (4.2)$$

Correlation of Blasius

$$f = 0.316\mathrm{Re}^{-0.25} \qquad 3000 \le \mathrm{Re} \le 20{,}000 \qquad (4.3)$$

Correlation of Petukhov

$$f = (0.79\ln\mathrm{Re} - 1.64)^{-2} \qquad 3000 \le \mathrm{Re} \le 5\times10^{6} \qquad (4.4)$$

Figure 4.20 shows a comparison of Nusselt number and friction factor obtained from the smooth duct with those from the correlations of Eqs. (4.1) - (4.4). Both results showed reasonably well agreements within ±5% with the correlations.

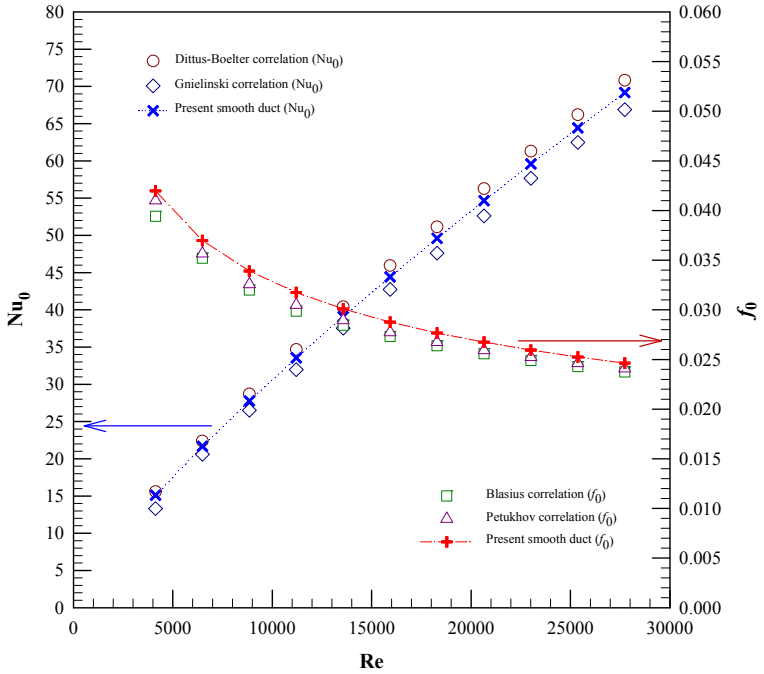

Figure 4.20 Validation of Nu_0 and f_0 for present smooth duct.

CHAPTER 5
TWISTED-TAPES WITH V-BAFFLES

This chapter deals with the experimental results of heat transfer enhancement, friction factor including thermal performance in a square-duct heat exchanger inserted with combined twisted-tapes and V-baffle vortex generators. In the literature survey from previous chapter, the twisted-tape vortex generator generally has a low flow resistance and ease in manufacturing but lower vortex strength while the rectangular V-baffle vortex generator yields the lowest penalty of pressure drop if its attack angle is sufficiently small. Therefore, considering the merits of both the vortex generator devices, a newly designed enhancement device using the combined twisted-tapes and V-baffles is proposed. In this new vortex flow device, the V-baffles are integrated into the twisted-tapes by attaching the V-tip of baffles on both edges of the tape to keep the baffles as close as possible to the duct walls after insertion. This new device is expected to provide higher swirl/vortex strength at the near-wall region from the V-baffles and higher fluid mixing between the central-core and the near-wall regimes from the twisted-tape, and thus improve the heat transfer rate in the wall region leading to greater increase in thermal performance. The applications of the combined twisted-tapes and V-baffles (called "V-baffled twisted tape") are divided into 2 sections as follows:

Section 1 is concerned with the insertion of the combination of a single twisted tape and V-baffles into a heat exchanger square-duct. The V-baffles were incorporated into both edges of the tape by letting the V-baffles attach only to the duct walls.

Section 2 is related to the application of combined quadruple twisted tapes and V-baffles. The quadruple twisted tapes were attached together using superglue while the V-baffles were mounted on the tape edges close to the duct wall only. This means that the V-baffles are placed only on the duct walls. This new device in this section is called "multiple V-baffled twisted tapes".

5.1 Single twisted-tape with V-baffles

In Fig. 5.1a below, the twisted tape was made of aluminum sheet with its dimension of 42×1200×0.8 mm^3. The twisted tapes were formed with two different twist ratios, Y=y/w=4 and 5 where twist ratio is defined as twist length (y) in 180° rotation to tape width (w). The rectangular baffle made of 0.3 mm aluminum strip was formed in V-shape to become a V-baffle with a V-tip half angle (α) of 30° and attached on the two opposite edges of the twisted-tape by putting the V-tip of the

baffle on the cut edge of the tape as seen in Figs. 5.1b and c. This arrangement would let the V-baffles place on the two opposite duct walls (2W) for the case of P=y or the four walls (4W) for P=y/2. The three V-baffles were 4.5, 6.75 and 9.0 mm high (e), equivalent to three baffle- to duct-height ratios, R_B =e/H=0.1, 0.15 and 0.2, respectively and were mounted on the tape edges with four baffle-pitch to tape–width ratios (R_P=P/w=2, 4 for Y=4; and 2.5, 5 for Y=5) at α=30°.

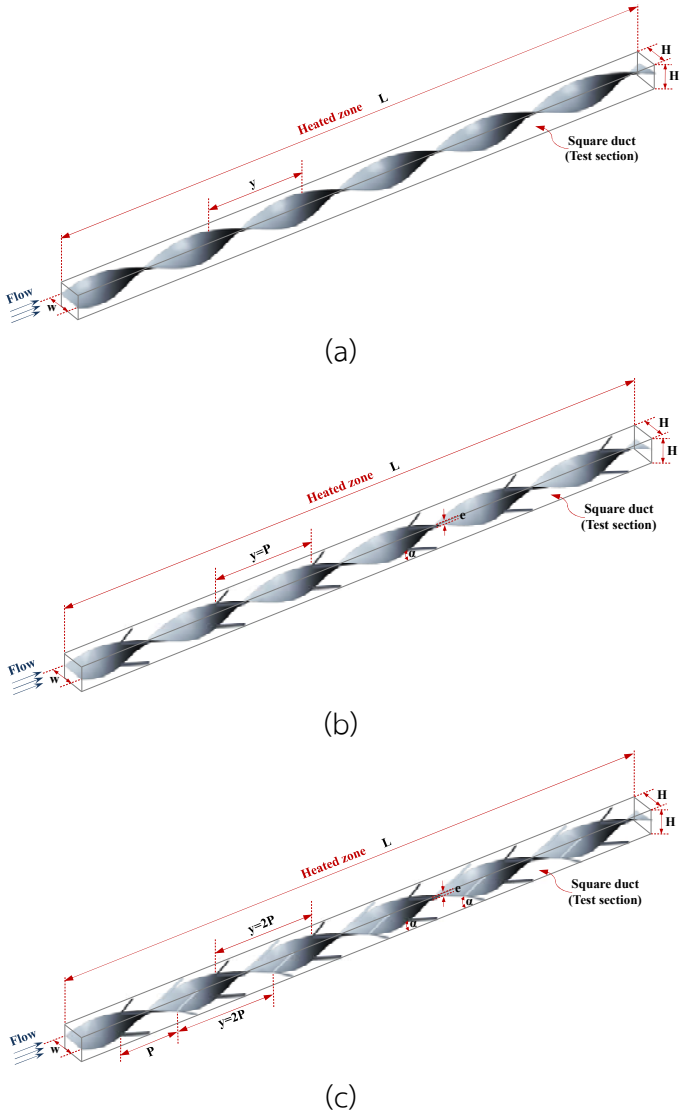

Figure 5.1 Vortex generators: (a) twisted tape alone, TT; (b) combined twisted-tape and V-baffles on two walls (TT-2W) and (c) combined twisted-tape and V-baffles on four walls (TT-4W).

The present results on heat transfer and pressure drop characteristics in a uniform heat-fluxed square-duct with combined twisted-tape and V-baffle inserts are presented in terms of Nusselt number (Nu) and friction factor (*f*). The variations of Nu and *f* obtained under a turbulent regime are presented in the Fig. 5.2a and b, respectively. In Fig. 5.2a, the inserted duct yields considerable heat transfer

enhancement with similar trend patterns in comparison with the smooth duct and the Nu increases with the rise of Reynolds number (Re). In Fig. 5.2b, it is visible that the use of the combined vortex generators leads to substantial increase in friction factor above the smooth duct and the friction factor shows a decrease tendency with the increment of Reynolds number.

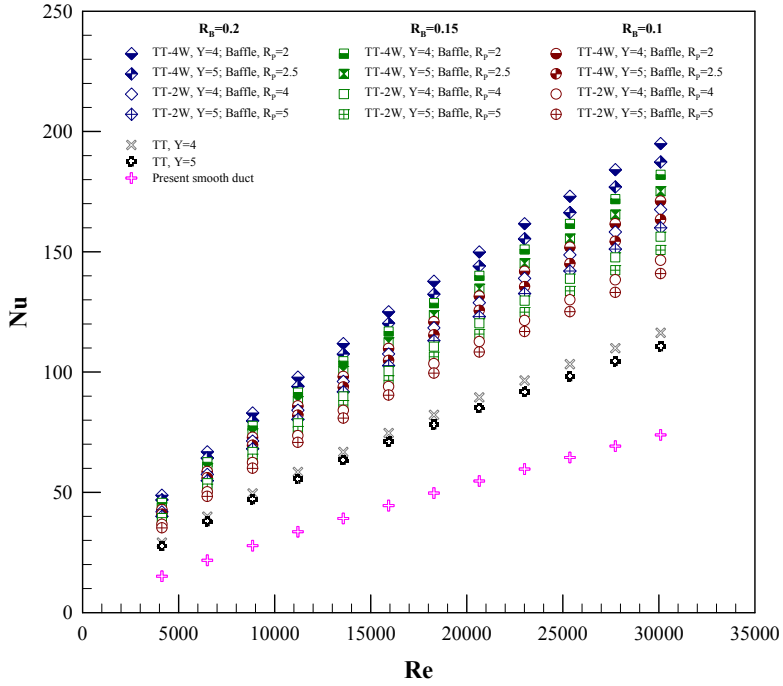

(a)

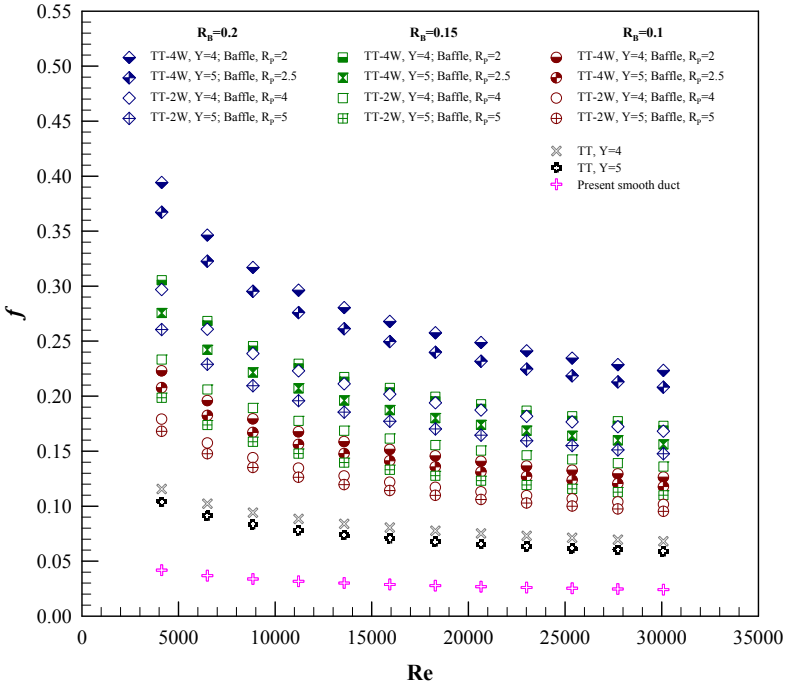

(b)

Figure 5.2 Variations of (a) Nu and (b) *f* with Re.

5.1.1 Effect of R_B and R_P

The variations of the Nusselt number ratio with Re and R_B values is displayed in Fig. 5.3a and b, respectively, where the Nusselt number ratio, Nu/Nu_0, defined as a ratio of the augmented Nusselt number to Nusselt number of smooth duct. It is visible in the figure that the increment of R_B results in the increase in Nu/Nu_0 while the rise of R_P provides the reversing trend of Nu/Nu_0. This is because the effect of the vortex flows from the combined devices can help increase the turbulence intensity and transport fluid from the central core to the near-wall regions. Also, the vortex flows can wash up the flow trapped in the duct corner regions normally act as ineffectively heat transfer areas, leading to higher heat transfer rate in the duct. The combination of twisted-tape and V-baffle provides the Nu/Nu_0 at about 2.16-3.22, 2.01-3.03, 1.91-2.82 times for R_B=0.2, 0.15 and 0.1, respectively. The twisted tapes alone with Y=4 and 5 yield the Nu/Nu_0 at about 1.56-1.90 and 1.49-1.82, respectively.

This indicates that the combined twisted-tape and baffle-pair yields higher heat transfer rate at about 40-44% than the twisted-tape alone. It is worth noting that, at R_P=2, the combined twisted tape at Y=4 and V-baffle with R_B=0.2 gives the highest Nu/Nu_0 around 5.9% and 12.2% above that with R_B=0.15 and 0.1, respectively and about 3.9% higher than that with Y=5 and R_P=2.5. This is caused by higher flow blockage of using R_B=0.2 and R_P=2 including twisted-tape at Y=4 leading to stronger vortex strength of the flow and thus promoting high levels of mixing over the others.

The effect of Re and R_B on pressure drop in terms of friction factor ratio, f/f_0 is, respectively, presented in the Figs. 5.4a and b for various R_P. It is observed in the figure that the inserted duct provides a considerable increase in f/f_0 with increasing R_B but with decreasing R_P. However, the f/f_0 is found to slightly decrease with the increment in Re or nearly independent of Re. The inserted duct at R_B=0.2, R_P=2 and Y=4 provides the highest f/f_0 and the f/f_0 of the R_B=0.15 is higher than that of the R_B=0.1. This is because the use of R_B=0.2, R_P=2 and Y=4, caused higher flow blockage, larger surface area and the act caused by the vortex flow leading to substantial increase in pressure drop. The f/f_0 for the combined twisted-tape at Y=4 and V-baffles is about 6.11-9.44, 4.80-7.31, 3.94-5.34 at R_B=0.2, 0.15 and 0.1, respectively, while that for the twisted tape alone at Y=4 and 5, is in the range of 2.57-2.62 and 2.44-2.48. This means that the use of the combined devices gives the f/f_0 at about 73.6% higher than that of the twisted-tape alone. It is noted that the f/f_0 for Y=4; R_P=2 and R_B=0.2 is maximum around 22.5% and 43.4% higher than that for R_B=0.15 and 0.1, respectively and about 6.9% above that for Y=5 and R_P=2.5.

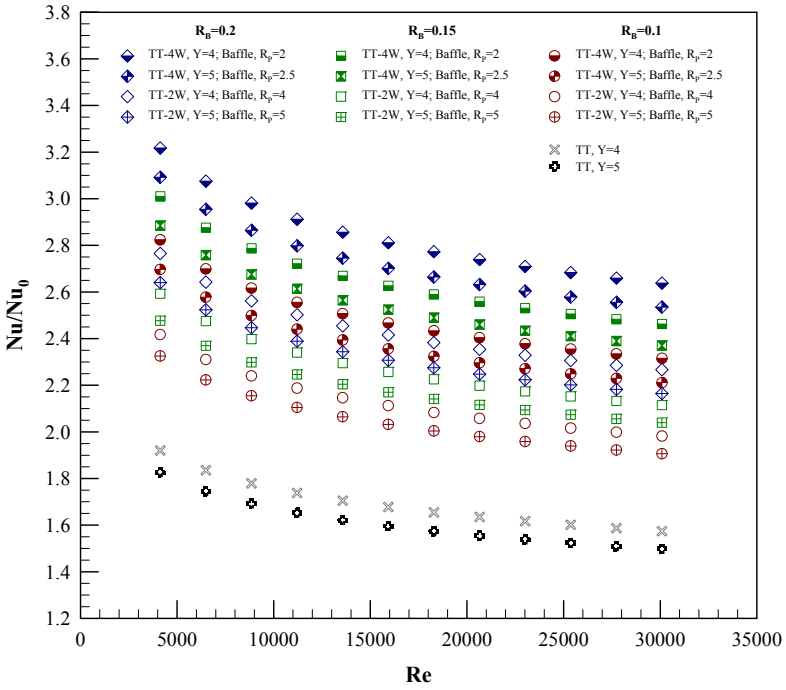

(a)

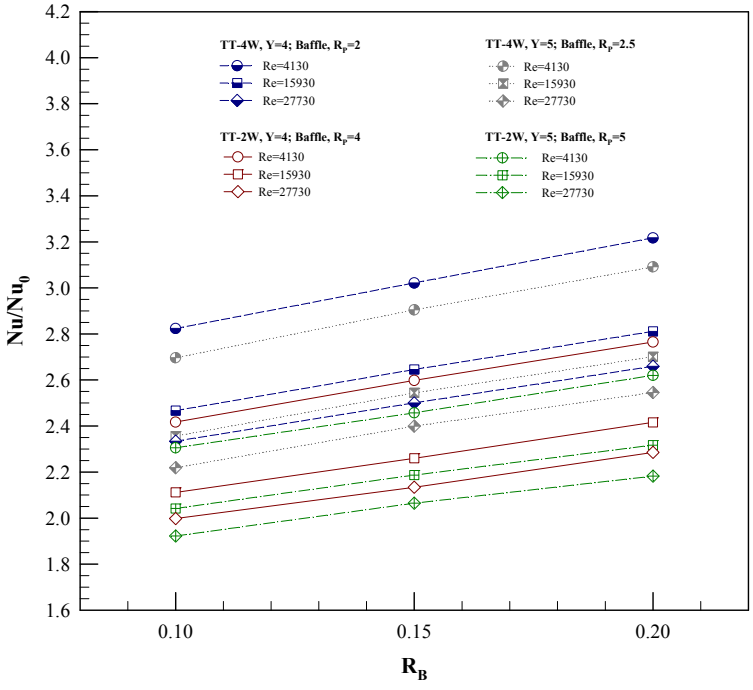

(b)

Figure 5.3 Variations of Nu/Nu_0 with (a) Re and (b) R_B.

5.1.2 Effect on thermal performance

Figure 5.5 presents the variation of the thermal enhancement factor (η) with Re for various R_B and R_P values. The data of Nu/Nu_0 and f/f_0 are compared at a similar blowing power. In the figure, the η tends to decrease with the increment in Re for all the cases investigated. The use of the newly designed vortex generator

leads to much higher η than that of twisted tape alone indicating the advantage of the compound vortex-flow devices. It is visible that the maximum η is achieved for the combined twisted-tape with Y=4 and V-baffles at R_B=0.1 and R_P=2. These R_P and R_B are considered to be the best operating condition in this investigation. The highest η is about 1.62 at the lowest Re and much higher than the others around 2–17%.

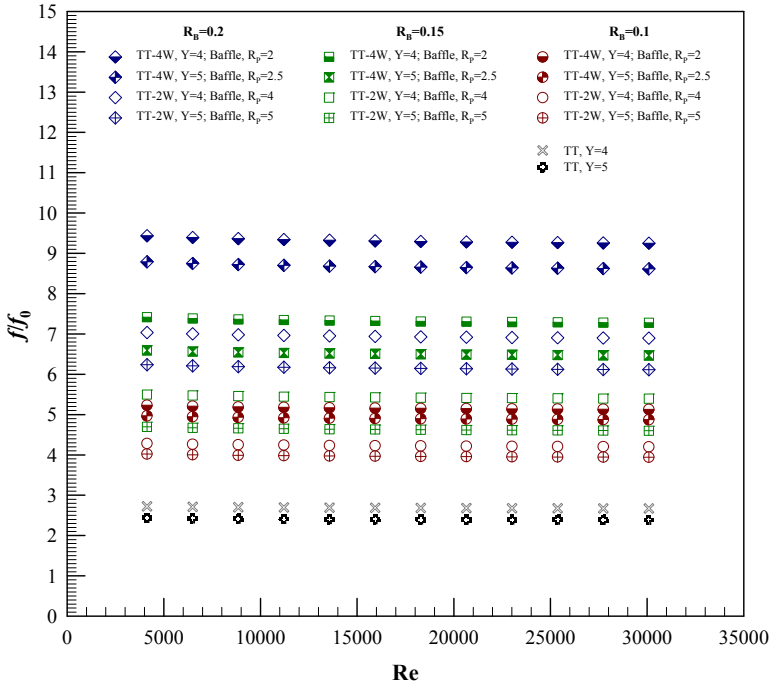

(a)

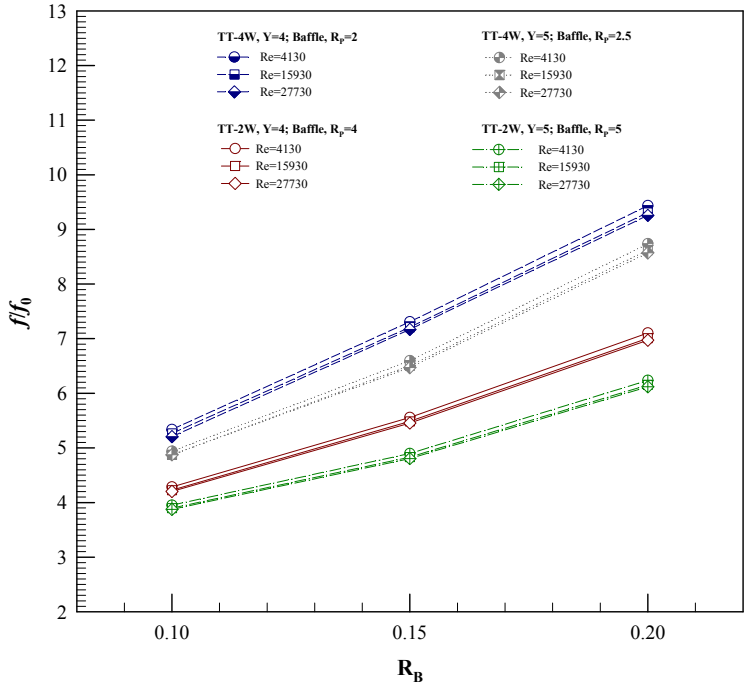

(b)

Figure 5.4 Variations of f/f_0 with (a) Re and (b) R_B.

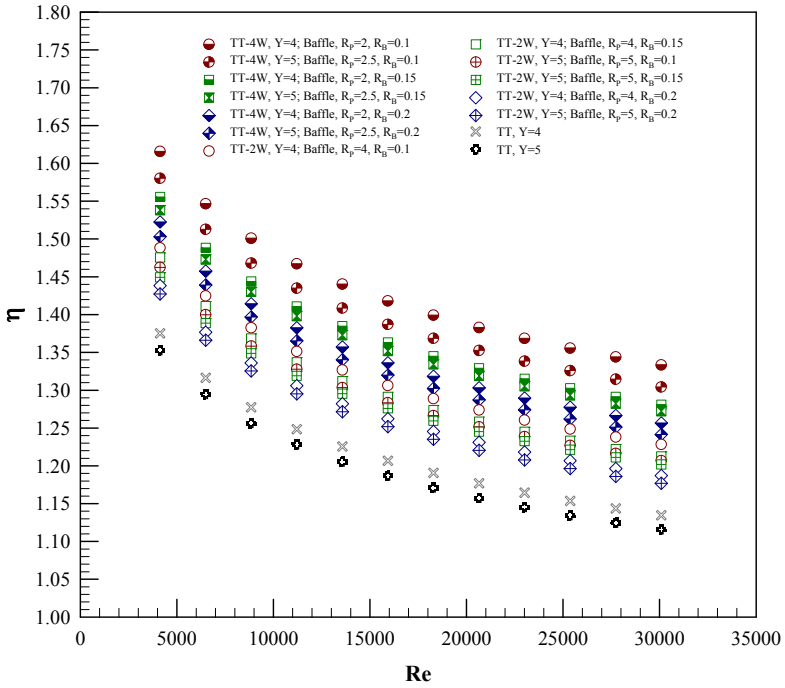

Figure 5.5 Variation of η with Re.

The Nu and f values for the combined twisted-tape and V-baffles are correlated as functions of Reynolds number (Re), Prandtl number (Pr), baffle blockage ratio (R_B), pitch ratio (R_P) and twist ratio (Y). These correlations for the combined twisted-tape and V-baffle insert valid for R_B=0.10, 0.15 and 0.20; R_P=2, 2.5, 4 and 5; and Y=4 and 5 in the Re range of 4000 to 30,000 are written as:

(a) Nu and f correlations of twisted-tape alone

$$Nu = 0.1368\,Re^{0.6976}Pr^{0.4}Y^{-0.2237} \tag{5.1}$$

$$f = 1.6585\,Re^{-0.2860}Y^{-0.2423} \tag{5.2}$$

(b) Nu and f correlations of combined twisted-tapes and V-baffles on two walls

$$Nu = 0.2691\,Re^{0.6976}Pr^{0.4}Y^{-0.2310}R_B^{\,0.1861} \tag{5.3}$$

$$f = 16.3586\,Re^{-0.2860}Y^{-0.4263}R_B^{\,0.6710} \tag{5.4}$$

(c) Nu and f correlations of combined twisted-tapes and V-baffles on four walls

$$Nu = 0.3084\,Re^{0.6976}Pr^{0.4}Y^{-0.2101}R_B^{\,0.1920} \tag{5.5}$$

$$f = 26.1677\,Re^{-0.2860}Y^{-0.3661}R_B^{\,0.8168} \tag{5.6}$$

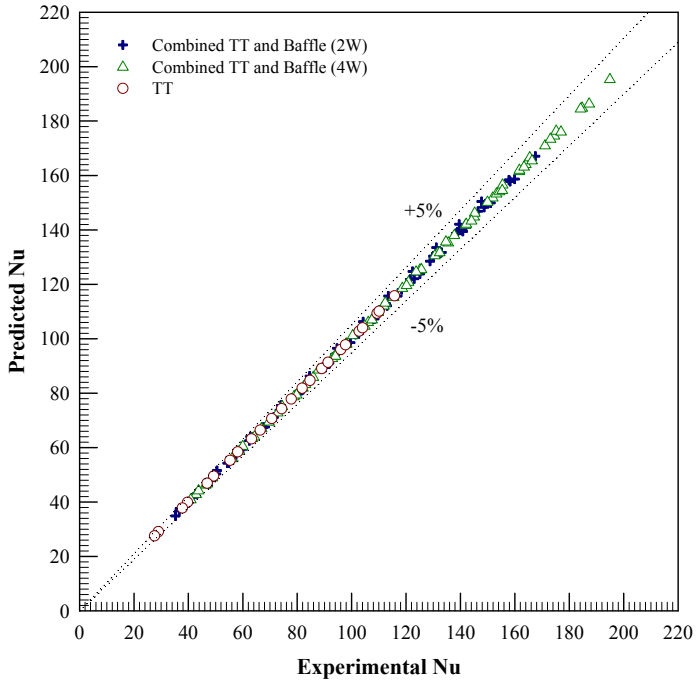

(a)

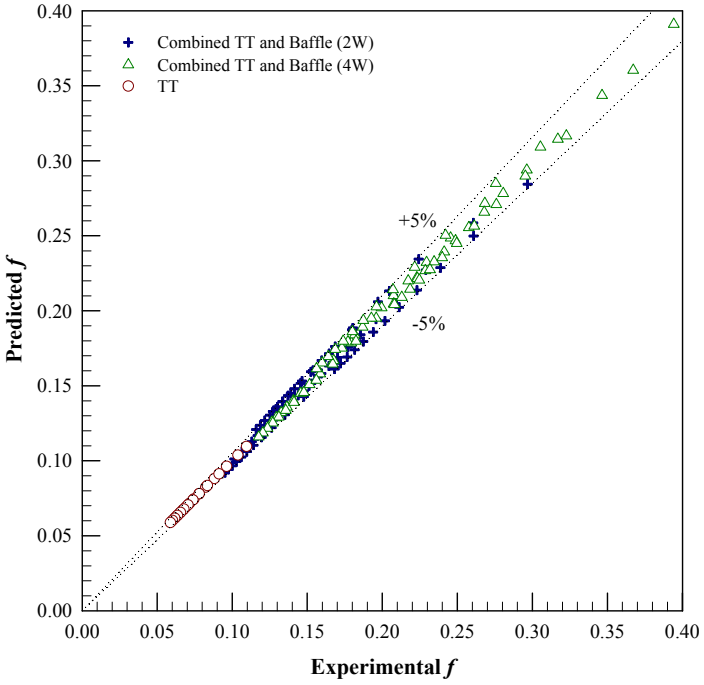

(b)

Figure 5.6 Predicted data of (a) Nu and (b) *f* versus experimental data.

5.2 Quadruple twisted-tapes with V-baffles

This section is a continuation from the previous section in order that the improvement is required by using multiple twisted-tapes where the tape width is reduced by a half of that in the previous section. Figure 5.7a and b shows respectively, the four twisted-tapes alone and the combined four twisted-tapes and

V-baffles on four walls (4W). Each of the twisted-tape has dimension of 21×1200×0.8 mm^3. The twisted-tapes with a single twist ratio, Y=y/w=4 were formed with two twist directions: left and right twists. Four twisted-tapes were grouped together to become a set of quadruple twisted-tapes and were arranged to obtain counter-twisted tapes as can be seen in Fig. 5.7b. The rectangular baffle made of 0.3 mm aluminum strip was formed in V-shape to become a V-baffle with a V-tip half angle of 30° and attached on the edge of each twisted-tape by putting the V-tip of the strip on the cut edge of the tape. The V-baffles were arranged in in-line arrays and were placed only on four walls of the test duct. The effects of four baffle- to duct-height ratios, R_B=e/H=0.075, 0.1, 0.15 and 0.2 and four baffle-pitch to tape–width ratios, R_P=P/w=4, 8, 12 and 16 at a single attack angle (α) of 30° are investigated.

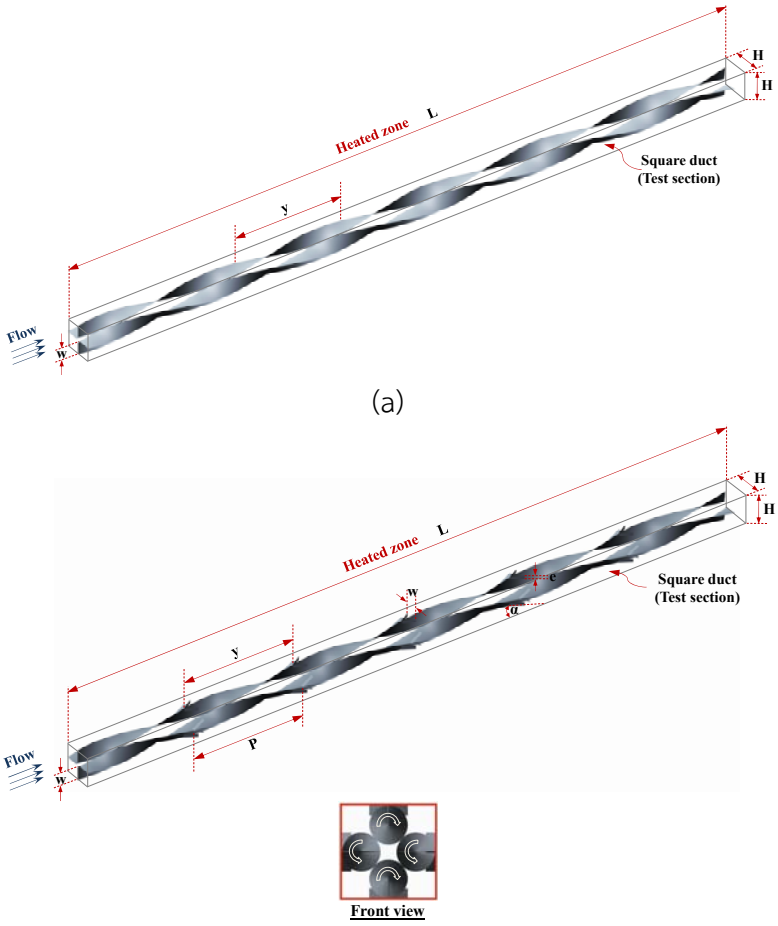

Figure 5.7 Test duct with (a) four twisted-tapes alone and (b) combined four counter-twisted tapes and V-baffles on four walls (4W).

Figure 5.8a and b presents the relationship of Nu and *f* with Re for the combined four twisted-tapes and V-baffles, respectively. The experimental results reveal that the inserted duct yields the considerable heat transfer augmentation with

the similar trends in comparison with the smooth duct and the Nu increases with the increment of Re as seen in Fig. 5.8a. In Fig. 5.8b, it is also found that the use of the combined swirl/vortex generators leads to the substantial increase in *f* above that of the smooth duct with no insert and the *f* shows the decreasing tendency with the rise of Re, especially for the higher R_B case.

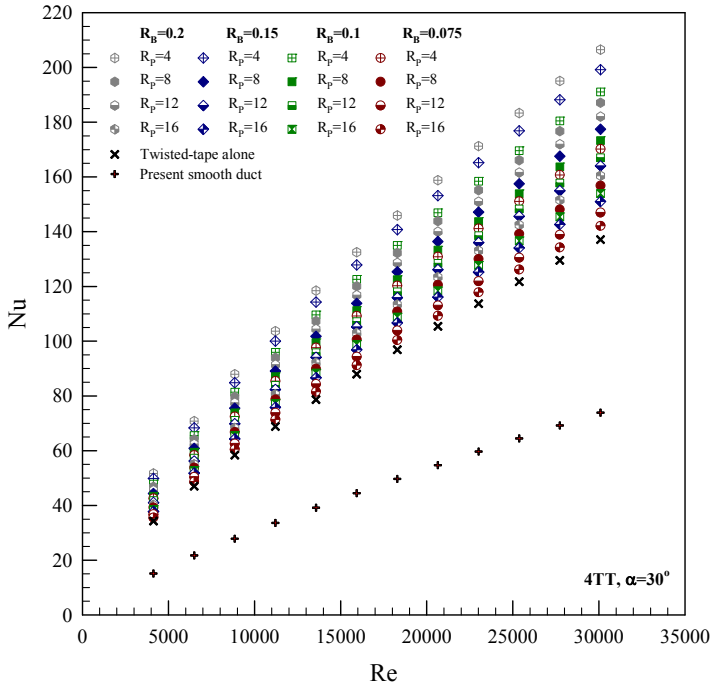

(a)

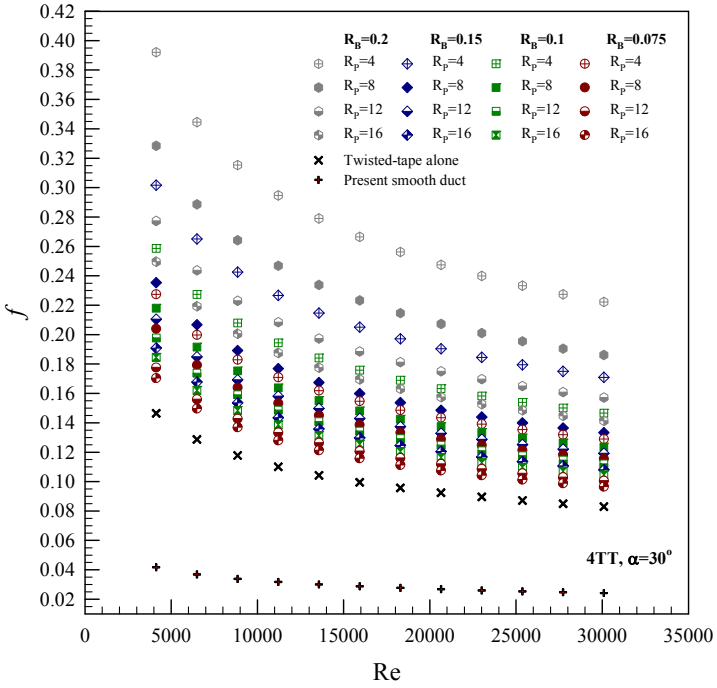

(b)

Figure 5.8 Variations of (a) Nu and (b) *f* with Re.

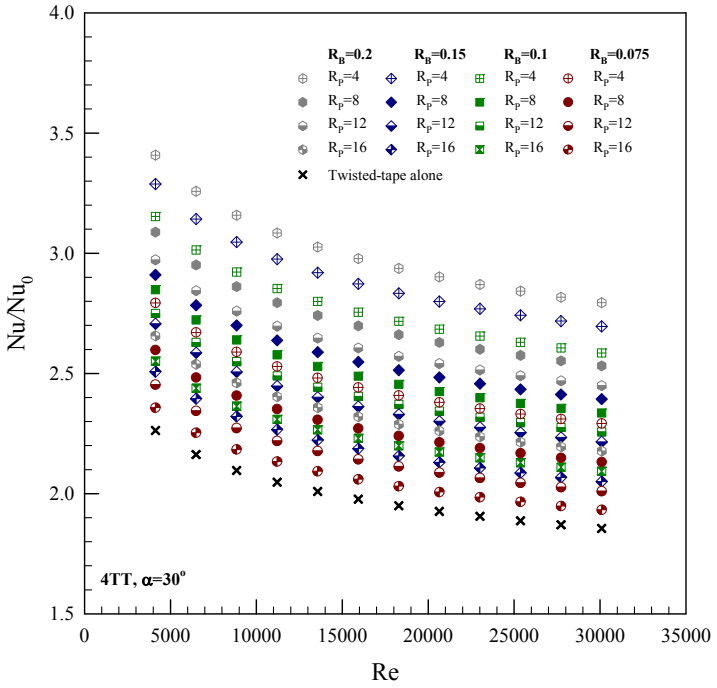

(a)

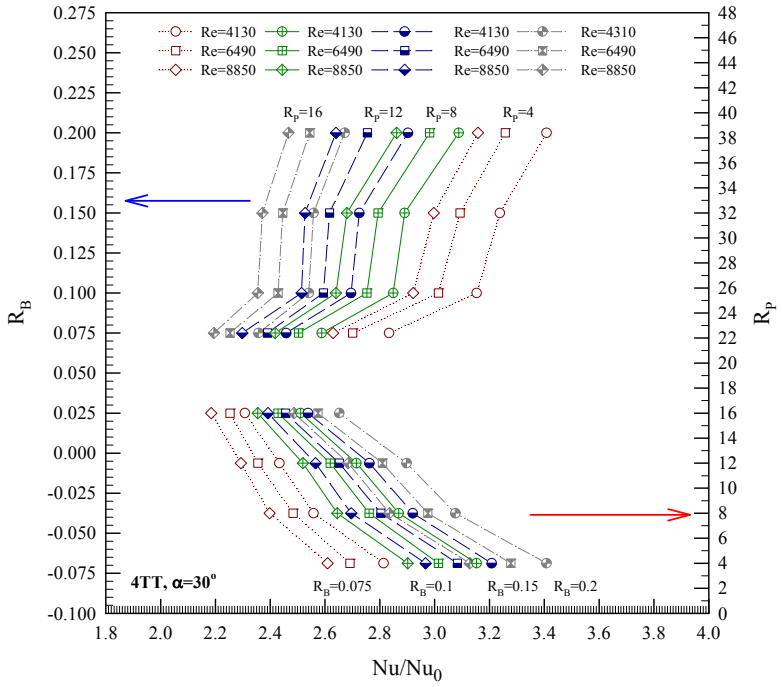

(b)

Figure 5.9 Variation of Nu/Nu_0 (a) with Re and (b) with R_B and R_P.

5.2.1 Effect of R_B and R_P on heat transfer

The variations of Nu/Nu_0 with Re and with R_B, R_P are displayed in Fig. 5.9a and b, respectively. It can be observed in the figure that the increase of R_B results in the increase in Nu/Nu_0 while the rise of R_P gives the reversing trend of Nu/Nu_0. This is because the effect of the swirl/vortex flows from the combined twisted-tape and V-

baffle can help increase the turbulence intensity/vortex strength and to transport fluid from the central core to the near-wall regions. Also, the swirl/vortex flows can interupt the thermal boundary layer thickness, leading to higher heat transfer rate in the test duct. At a given R_P, the combined four twisted-tapes and V-baffles provide the Nu/Nu_0 at about 2.2-3.4, 2.1-3.3, 2.0-3.2 and 1.9-2.8 for R_B=0.2, 0.15, 0.1 and 0.075, respectively whereas the quadruple twisted-tapes alone yield the Nu/Nu_0 at about 1.8-2.3. It is worth noting that, at R_P=4, the Nu/Nu_0 for the combined four twisted-tape and V-baffles with R_B=0.2 is highest at about 3.5-7.0%, 4.5-7.7% and 11.4-18.3% above that with R_B=0.15, 0.1 and 0.075, respectively and around 33.6% higher than that for the four twisted-tapes alone. This is caused by higher flow blockage of using R_B=0.2 and R_P=4 leading to stronger vortex strength of the flow and thus promoting high levels of mixing over the others.

5.2.2 Effect of R_B and R_P on friction loss

Figure 5.10a and b shows the variations of f/f_0 with Re and with R_B and R_P, respectively. It is seen that the f/f_0 is considerably increased with increasing R_B but with decreasing R_P. However, the f/f_0 is found to decrease slightly with the increment in Re. The R_B=0.2 and R_P=4 yeilds the highest f/f_0. This is because the use of R_B=0.2 and R_P=4, caused higher flow blockage, larger surface areas from having more the number of V-baffles and the act caused by the reversing flow leading to substantial increase in resistance of flow in duct. The f/f_0 values for the combined four twisted-tapes and V-baffles with R_B=0.2, 0.15, 0.1 and 0.075 are around 5.7-9.4, 4.5-7.2, 4.3-6.0 and 4.1-5.3, respectively while those for the four twisted-tape alone are about 3.4-3.5 times. It is noted that the f/f_0 maximum at R_B=0.2 and R_P=4 is about 21.4-27.6%, 24.6-36.3% and 28.2-43.1% higher than that at R_B=0.15, 0.1 and 0.075, respectively and around 62.6% above the four twisted-tapes alone.

5.2.3 Performance evaluation

The variation of the thermal enhancement factor (η) with Re for various R_B and R_P values is depicted in Fig. 5.11. In the figure, the η shows the downtrend with the rise in Re for all the cases studied. The η of the combined four twisted-tapes and V-baffles is higher than that of the twisted-tape alone. It is seen that the maximum η is found at R_B=0.1, R_P=4 and Re=4130 and therefore, these points are considered to be the optimal operating condition in this work. The maximum η of about 1.74 is 2.1–15.9% higher than the other cases.

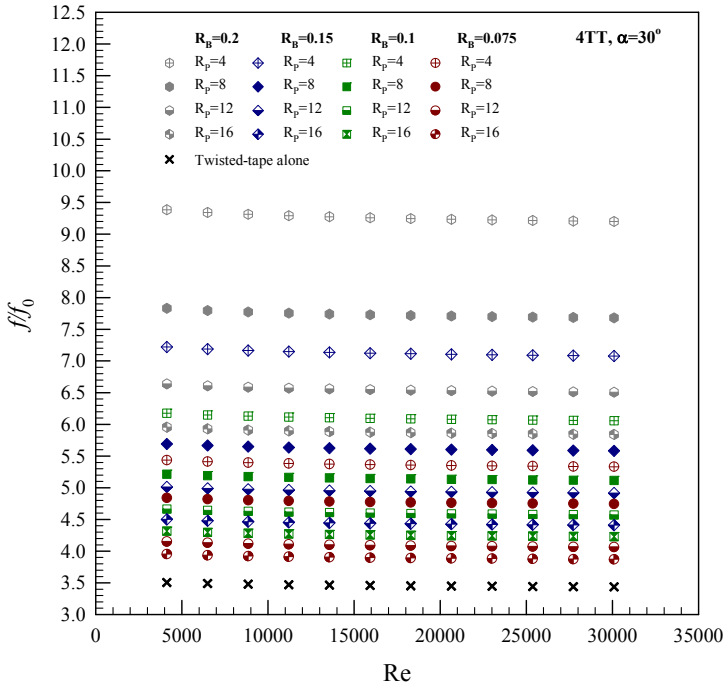

(a)

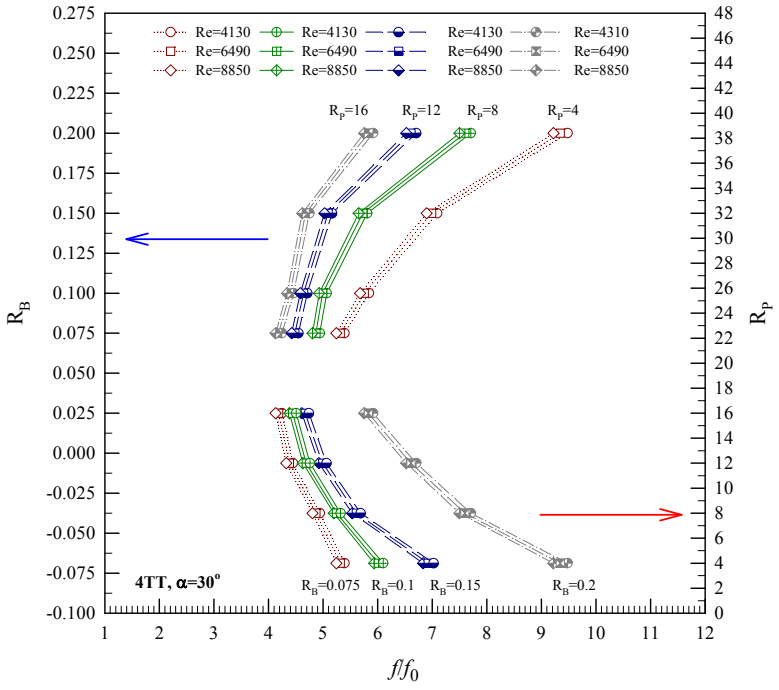

(b)

Figure 5.10 Variation of f/f_0 (a) with Re and (b) with R_B and R_P.

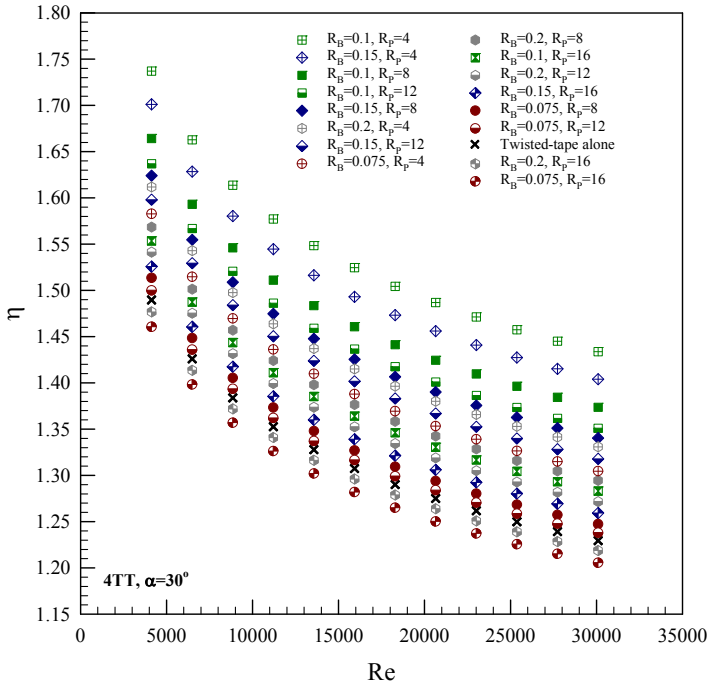

Figure 5.11 Variation of η with Re.

The Nu and *f* values for the combined four twisted-tapes and V-baffles are correlated as functions of Reynolds number (Re), Prandtl number (Pr), baffle blockage ratio (R_B), pitch ratio (R_P) and twist ratio (Y). These correlations of Nu and *f* for the combined four twisted-tapes and V-baffles valid for R_B=0.2, 0.15 0.1 and 0.075; R_P=4, 8, 12 and 16 in the Re range of 4000 to 30,000 are written by:

Nu correlation:

$$Nu = 0.2831 Re^{0.6976} Pr^{0.4} R_P^{-0.1406} R_B^{0.1492} \quad (5.7)$$

f correlation:

$$f = 10.6370 Re^{-0.2860} R_P^{-0.2648} R_B^{0.4153} \quad (5.8)$$

The plots of the Nu and *f* of the combined four twisted-tapes and V-baffles predicted by Eqs. (7) and (8) with the measured data are depicted in Fig. 5.12a and b, respectively. In the figure, the majority of the measured data falls within ±7% and ±10% for the predicted Nu and *f*, respectively.

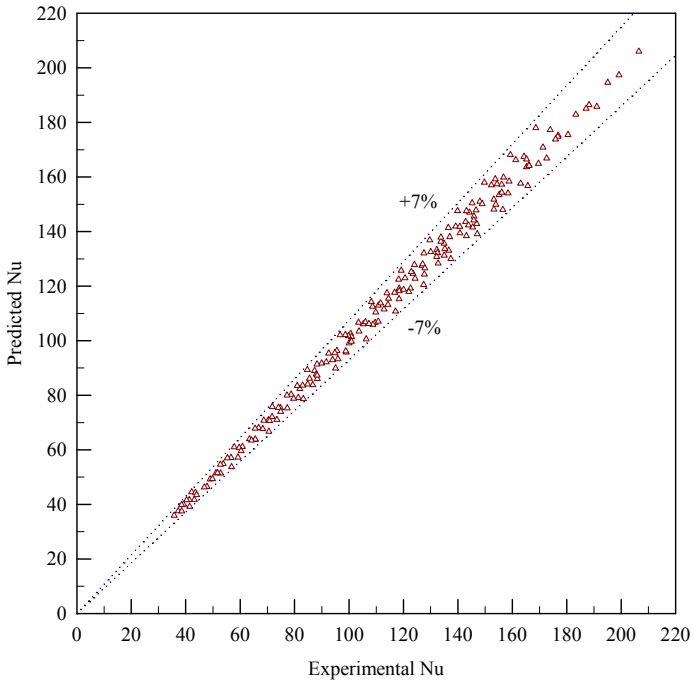

(a)

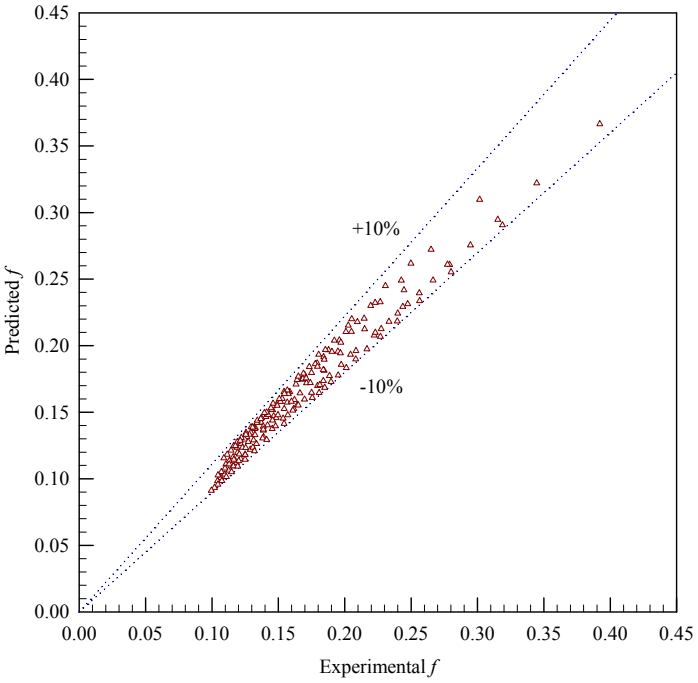

(b)

Figure 5.12 Predicted data of (a) Nu and (b) *f* versus experimental data.

5.3 Comparison between combined single and four twisted-tapes with V-baffles

This section deals with the comparison of the experimental results between the conbined single and four twisted-tapes with V-baffles at the best operating condition after the improvement.

Figure 5.13 displays the plots of Nu and Nu/Nu_0 against Re for both types of swirl/vortex generators as mentioned ealier in Sections 5.1 and 5.2. It is visible in the figure that the combined four twisted-tapes with V-baffles provide the heat transfer higher than the combined single ones at around 10.5%. It is because the geometrical arrangement for the device of combined four twisted-tapes and V-baffles is intended to promote vortex strength and the mixing between the central-core and the near-wall regimes and create rotating/ secondary flow higher than the single twisted-tape with V-baffle, leading to the increase of local heat transfer coefficients.

The variation of f and f/f_0 with Re is shown in Fig. 5.14. In the figure it can be observed that the use of the four twisted-tapes with V-baffles yields about 13.6% higher friction factor than that of the single one due to higher flow resistance.

The relationship between thermal enhancement factor (η) and Re is depicted in Fig. 5.15. It is seen that the η for the four twisted-tapes with V-baffles is about 7% higher than that for the single one.

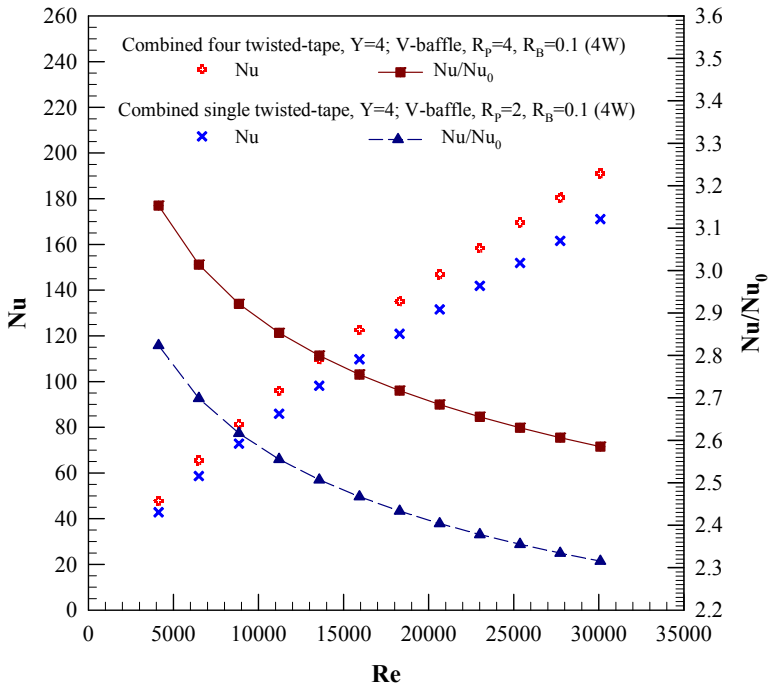

Figure 5.13 Variation of Nu and Nu/Nu_0 with Re.

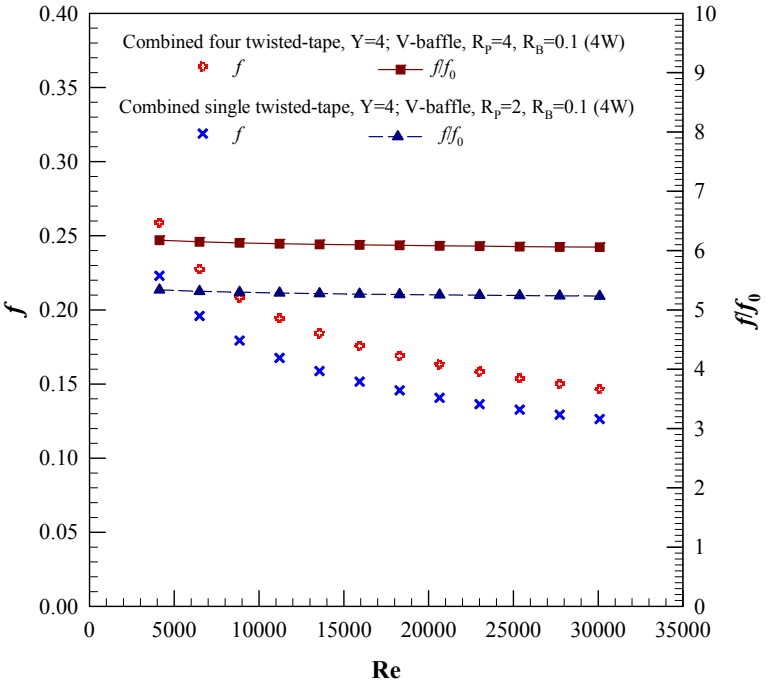

Figure 5.14 Variation of f and f/f_0 with Re.

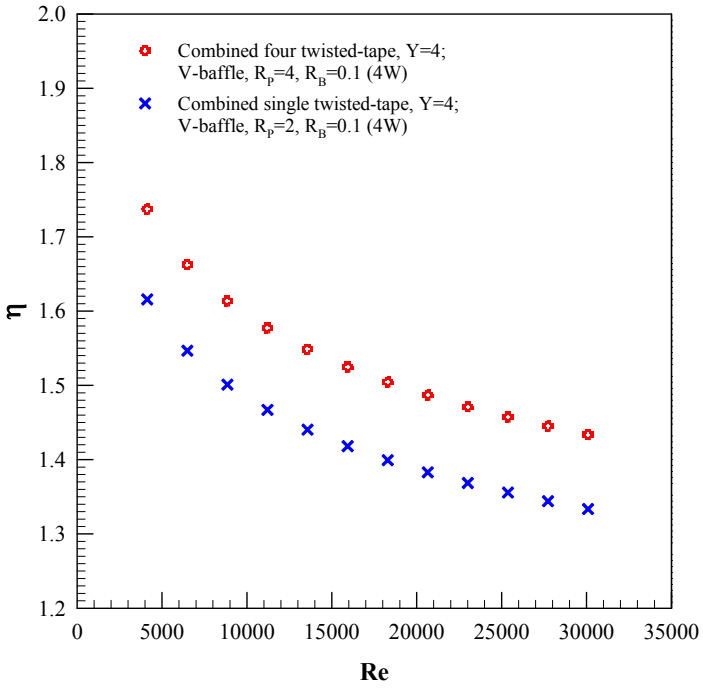

Figure 5.15 Variation of η with Re.

CHAPTER 6
DISCRETE AND TRAPEZOIDAL V-BAFFLES

This chapter presents an experimental investigation on heat transfer and thermal performance behaviors in a square-duct inserted diagonally with V–baffled tapes. This new enhancement device is proposed and developed to provide higher thermal performance than the device of combined twisted-tapes and baffles as mentioned earlier in chapter 5. The concept and principle is similar to previous work. With a view to pressure reduction in the test duct, two types of V-baffles were introduced: discrete V-baffles and trapezoidal V-baffles. Both V-baffle types were placed on a double-sided straight tape before diagonally inserting it into a square-duct. This arrangement of the V-baffles is expected to yield greater heat transfer rate but lower pressure drop than that in the previous work. Thus, the main aim in this chapter is to investigate the heat transfer and flow friction characteristics for turbulent duct flows in a square-duct fitted with modified V-baffled tapes.

6.1 Discrete V–baffles

Figure 6.1 presents the schematic of the test section fitted with discrete V–baffles placed on a double-sided tape. The diagonal straight tape was made of aluminum sheet with its dimension of 63×1200×0.5 mm^3. The V-baffles made of 0.3 mm aluminum strip were attached on both sides of a straight tape. Four baffle sizes were 3.375, 4.5, 6.75 and 9 mm high (e) with 0.3 mm thickness (t), equivalent to baffle-to duct-height ratios, R_B=e/H=0.075, 0.1, 0.15 and 0.2, respectively. The baffle parameters were four baffle-pitch to duct-height ratios, R_P=P/H=0.5, 1, 1.5 and 2, and three attack angles, α=30°, 45° and 60°, with two V-baffle arrangements: V-tip pointing upstream and downstream (called “V-upstream” and “V-downstream”).

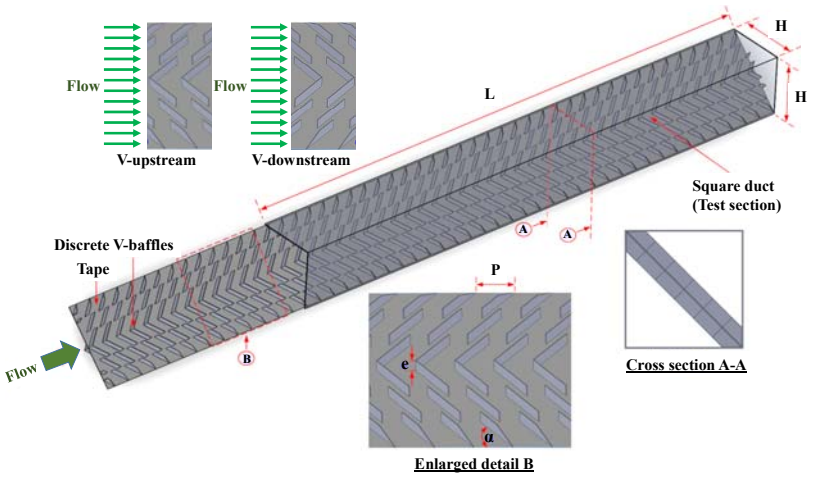

Figure 6.1 Test section with discrete V-baffles placed on a straight tape.

6.1.1 Discrete 60° V-upstream baffles

The present experimental result on the heat transfer rate in a square-duct with discrete V-baffe inserts presented in the form of Nusselt number ratio, Nu/Nu_0 against Re at various R_B and R_P values for the α=60°, V-upstream baffles is displayed in Fig. 6.2. It is visible in the figure that at a given Re, the Nu/Nu_0 increases with the increment of R_B but with decreasing R_P. This is because the higher R_B and lower R_P values provide stronger turbulence intensity and vortex strength that helps to transport the central core flow to the near-wall region. It is noted that for similar operating conditions, the highest Nu/Nu_0 is found at R_B=0.2 and R_P=0.5; about 13-29% above the other R_B; and about 8-22% over the other R_P.

The effect of R_B and R_P on isothermal pressure drop in terms of friction factor ratio, f/f_0 for α=60°, V-upstream is depicted in Fig. 6.3. It is observed that, apart from showing the decreasing trend with the fall of Re, the f/f_0 tends to increase with increasing R_B but shows the reversing trend with increasing R_P. This is because the discrete V-baffed tape gives rise to higher flow blockage and larger surface area. The f/f_0 for R_B=0.2 and R_P=0.5 is maximum and about 41-73% above that for R_B=0.15, 0.1 and 0.075; and about 29-57% higher than that for R_P=1.0, 1.5 and 2.0. It is also observed that the Nu/Nu_0 has a slight decrease for smaller R_B while the f/f_0 is increased continuously for the rise of R_B. This indicates that the results of heat transfer and friction factor are more sensitive to R_B rather than R_P. At a given R_P, the Nu/Nu_0 and f/f_0 values are, respectively, about 3.3-4.5, 3.0-4.0, 2.8-3.7 and 2.5-3.2; and 18.8-53.1, 13.1-31.5, 6.6-19.4 and 6.0-14.5 for R_B=0.2, 0.15, 0.1 and 0.075.

The thermal enhancement factor (η) for the α=60°, V-upstream plotted against Re is shown in Fig. 6.4. In the figure, the η is decreased as the Re increases for all cases. For a fixed R_P, the η values for R_B=0.2, 0.15, 0.1 and 0.075 are about 1.13-1.38, 1.18-1.39, 1.28-1.62 and 1.24-1.48, respectively.

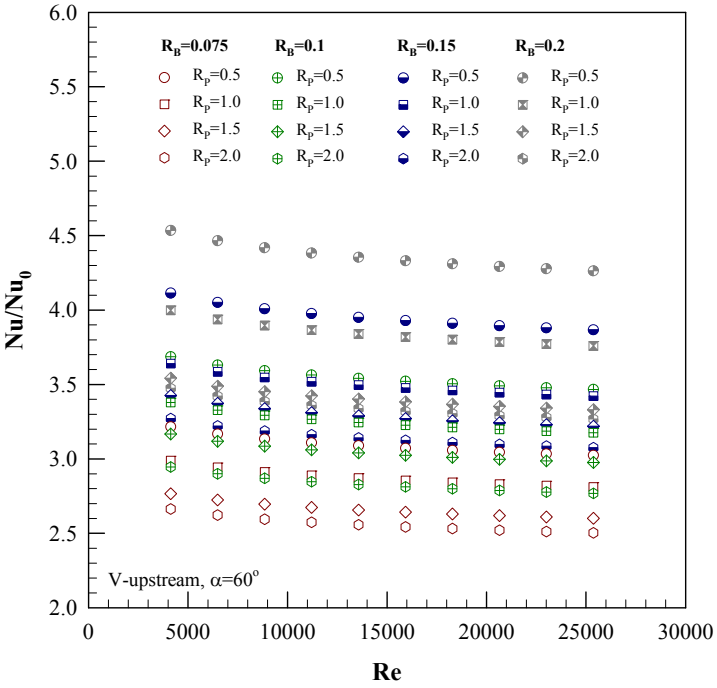

Figure 6.2 Variation of Nu/Nu_0 with Re for 60° V-upstream baffles.

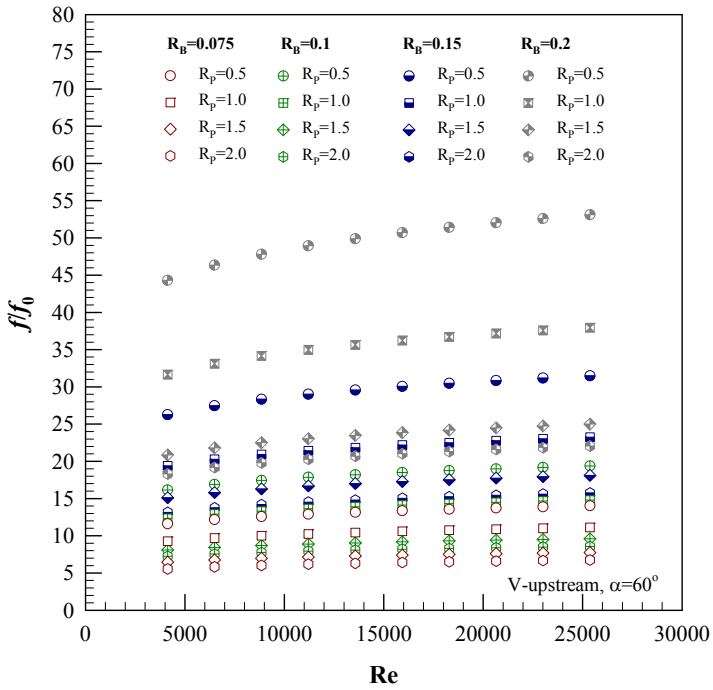

Figure 6.3 Variation of f/f_0 with Re for 60° V-upstream baffles.

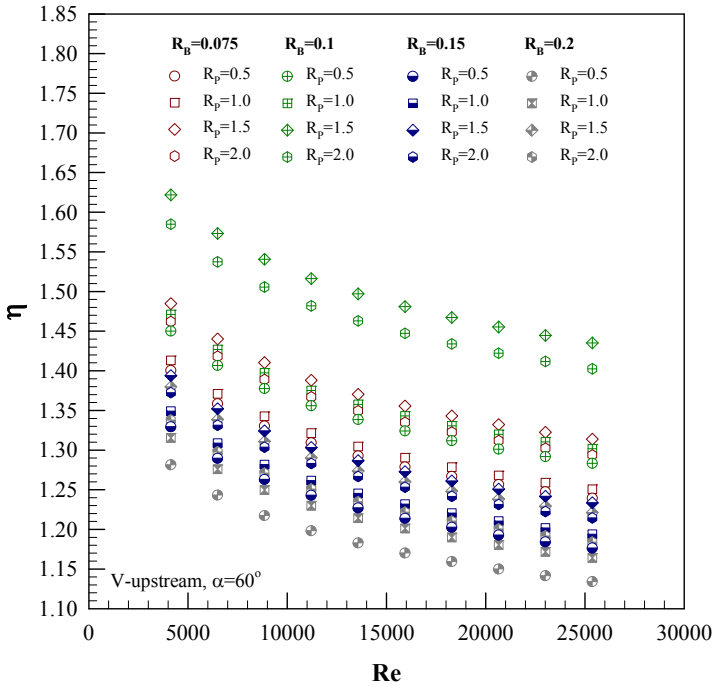

Figure 6.4 Variation of η with Re for 60° V-upstream baffles.

6.1.2 Discrete 60° V-downstream baffles

Figures 6.5, 6.6 and 6.7 shows the relationships between Nu/Nu_0, f/f_0 and η with Re for α=60°, V-downstream, respectively. In Figs. 6.5 and 6.6, it can be observed that at a given R_P, the Nu/Nu_0 and f/f_0 values for R_B=0.2, 0.15, 0.1 and 0.075 are in the range of 3.1-4.3, 2.8-3.7, 2.6-3.5 and 2.4-3.0; and 16.0-48.3, 11.5-30.3, 6.0-18.6 and 5.6-13.7, respectively. The η values are about 1.11-1.37, 1.12-1.39, 1.23-1.58 and 1.18-1.46 for R_B= 0.2, 0.15, 0.1 and 0.075, respectively, as seen in Fig. 6.7. It is noted that the results of the V-downstream baffles are in similar trend patterns with those of the V-upstream ones.

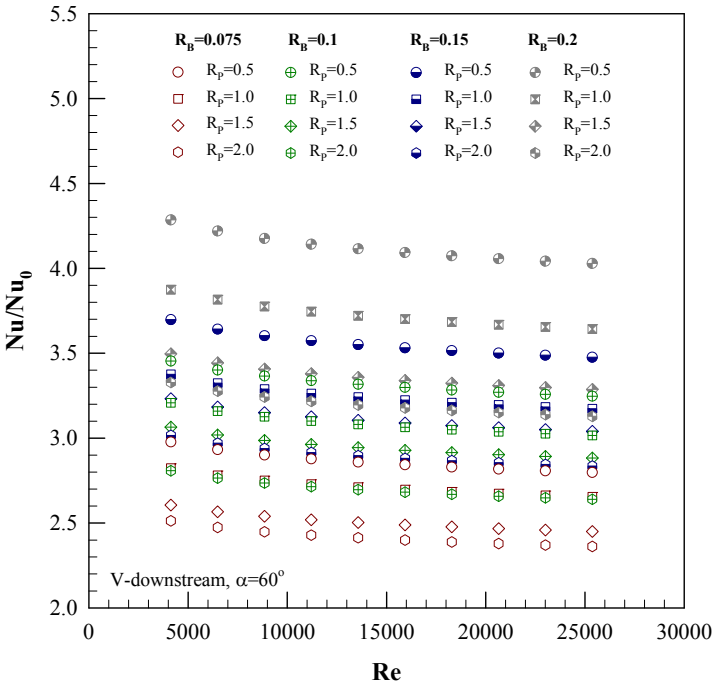

Figure 6.5 Variation of Nu/Nu_0 with Re for discrete 60° V-downstream baffles.

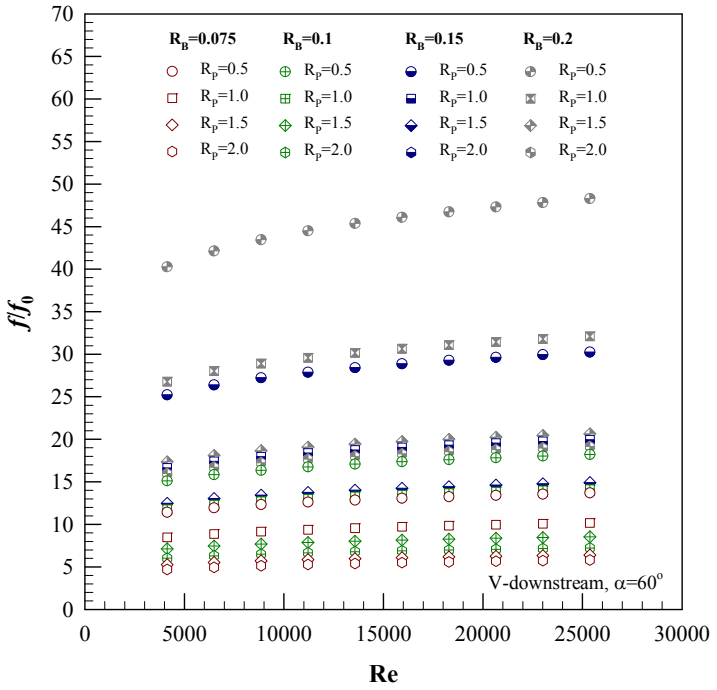

Figure 6.6 Variation of f/f_0 with Re for discrete 60° V-downstream baffles.

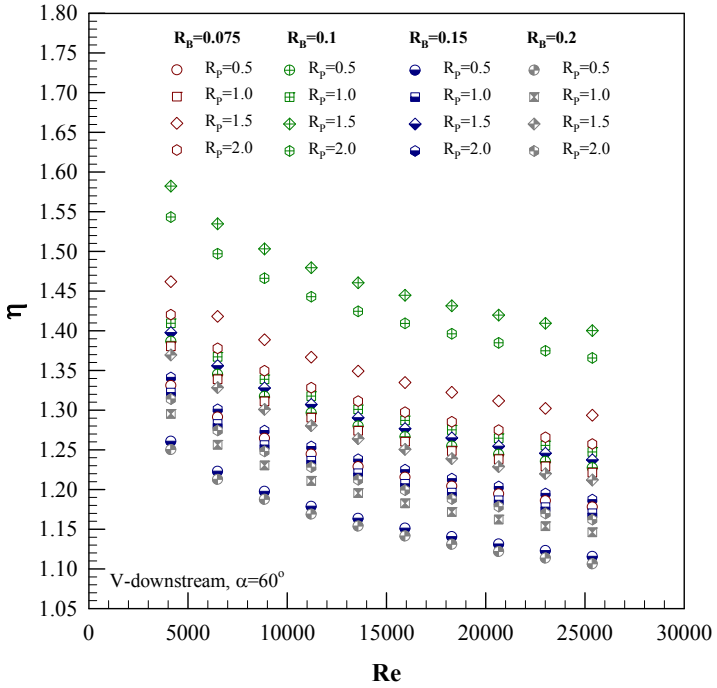

Figure 6.7 Variation of η with Re for discrete 60° V-downstream baffles.

6.1.3 Comparison between V-upstream and V-downstream baffles

The comparative study of the effect of V-upstream and V-downstream baffles on Nu/Nu_0 and f/f_0; and η is depicted in Fig. 6.8a and b, respectively. Figure 6.8a displays the relation of Nu/Nu_0 and f/f_0 with Re at a fixed R_B=0.1 and R_P=1.5 for α=60°. In the figure, it is visible that the V-upstream baffles provide the Nu/Nu_0 and f/f_0 around 4.5%, and 6.1% higher than the V-downstream ones. Also, the η of the V-upstream baffles is about 2.4% above that of the V-downstream ones. Therefore, considering all aspects and for the sake of brevity, only the V-upstream baffles will be presented in the next section.

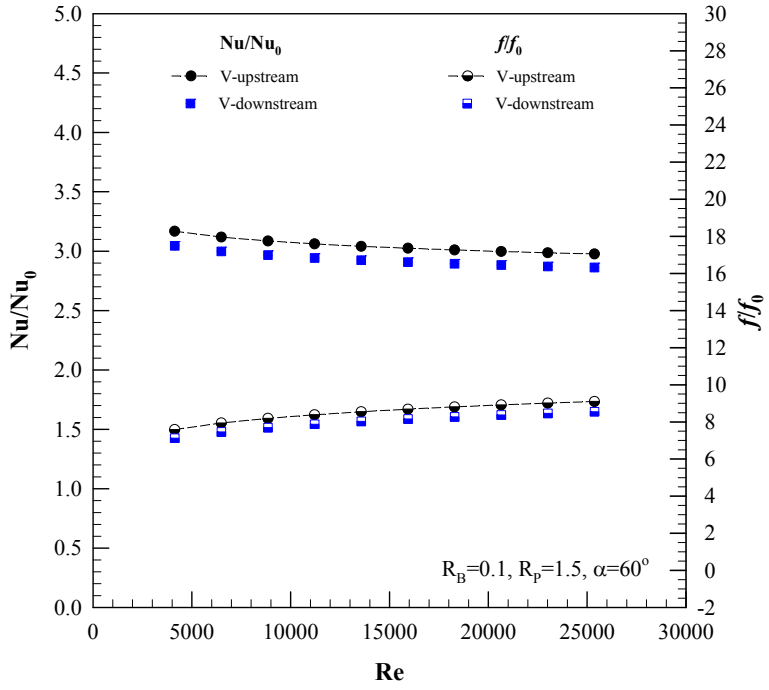

(a)

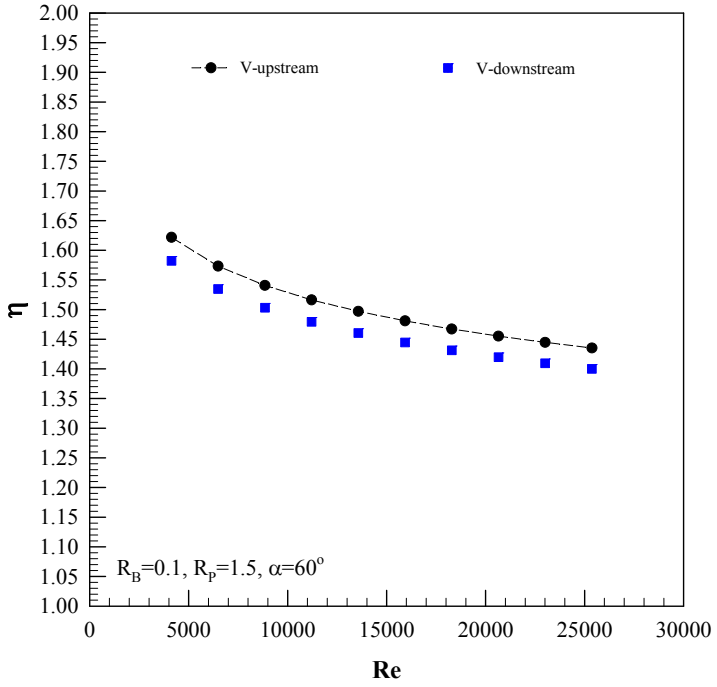

(b)

Figure 6.8 Variation of (a) Nu/Nu_0 and f/f_0 and (b) η with Re for 60° V-baffles.

6.1.4 Discrete 45° V-upstream baffles

Figures 6.9, 6.10 and 6.11 show the variations of Nu/Nu_0, f/f_0 and η with Re for discrete 45° V-upstream baffles, respectively. At a given R_P, the Nu/Nu_0 and f/f_0 values for R_B= 0.2, 0.15, 0.1 and 0.075 are, respectively, about 3.0-3.9, 2.9-3.5, 2.8-3.4 and 2.4-2.8; and 8.8-26.3, 7.1-17.9, 5.1-13.1 and 3.8-8.8. It can be observed

that the increase rate of f/f_0 is higher than that of Nu/Nu_0 for a prescribed R_B and R_P. Therefore, the use of larger R_B and smaller R_P should be avoided if higher thermal performance of a heat exchanger is required. In Fig. 6.11, the η values for R_B=0.2, 0.15, 0.1 and 0.075 are about 1.30-1.50, 1.33-1.55, 1.42-1.69 and 1.35-1.60, respectively. The maximum η around 1.69 is found at R_B=0.1, R_P=1.5 and Re=4130.

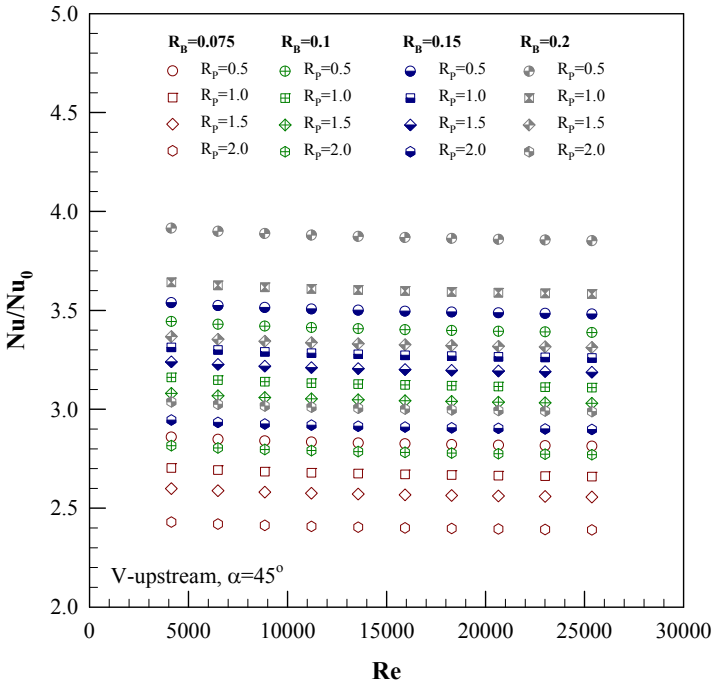

Figure 6.9 Variation of Nu/Nu_0 with Re for discrete 45° V-upstream baffles.

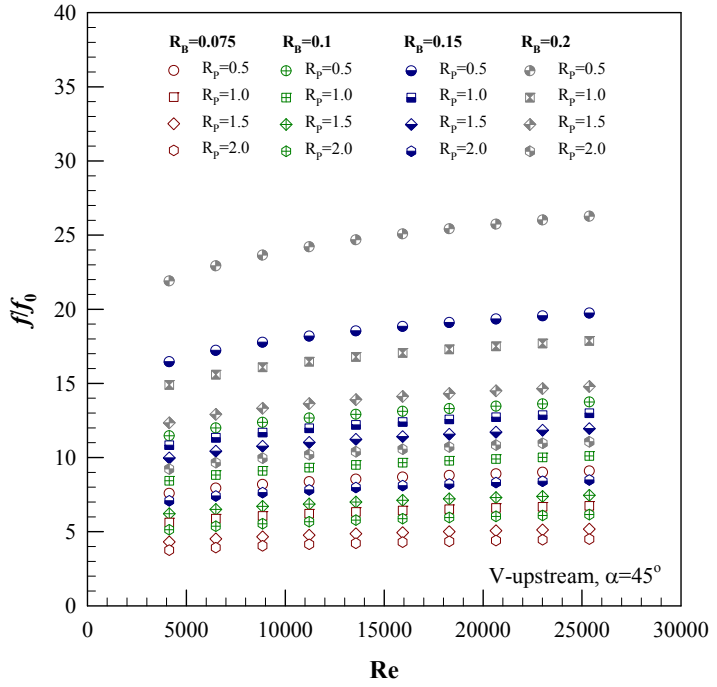

Figure 6.10 Variation of f/f_0 with Re for discrete 45° V-upstream baffles.

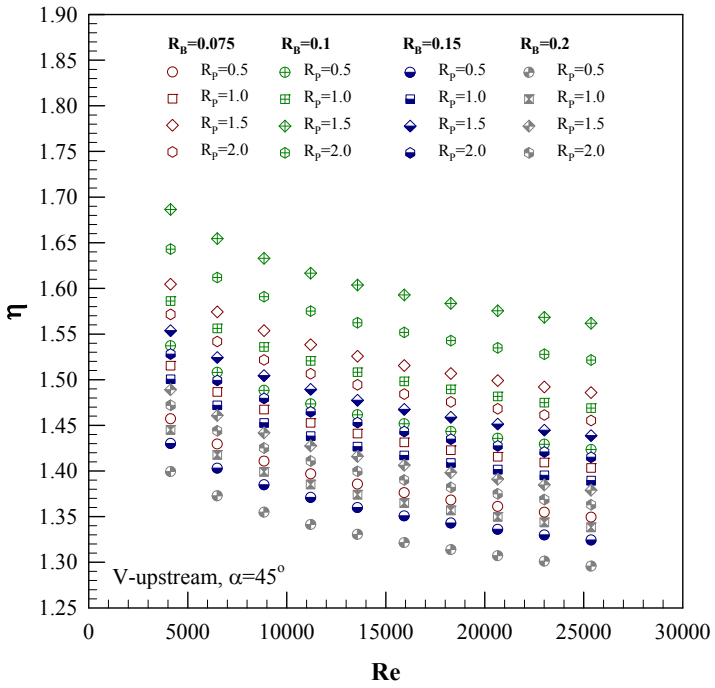

Figure 6.11 Variation of η with Re for discrete 45° V-upstream baffles.

6.1.5 Discrete 30° V-upstream baffles

The relationships of Nu/Nu_0, f/f_0 and η with Re for using discrete 30° V-upstream baffles are depicted in Figures 6.12, 6.13 and 6.14, respectively. A close examination of Figs. 6.12 and 6.13 reveals that at a given R_P, the Nu/Nu_0 and f/f_0 values for R_B= 0.2, 0.15, 0.1 and 0.075 are, respectively, about 2.9-3.9, 2.9-3.6, 2.7-3.4 and 2.4-2.8; and 8.0-24.4, 6.4-15.3, 4.4-11.8 and 3.4-7.9. Also, at a fixed R_B and R_P the increase rate of f/f_0 is considerably higher than that of Nu/Nu_0, especially for larger R_B. To investigate its thermal performance, the η is around 1.31-1.53, 1.35-1.62, 1.46-1.76 and 1.37-1.66 for R_B= 0.2, 0.15, 0.1 and 0.075 under the R_P range studied, respectively and its maximum of about 1.76 is at R_B=0.1, R_P=1.5 and Re=4130, similar locations as the cases of the discrete 60° and 45° V-upstream baffles.

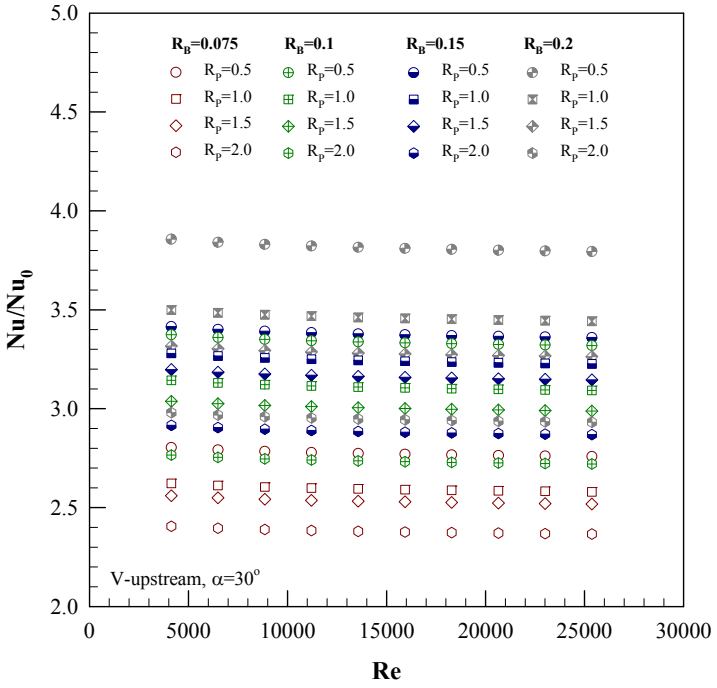

Figure 6.12 Variation of Nu/Nu_0 with Re for discrete 30° V-upstream baffles.

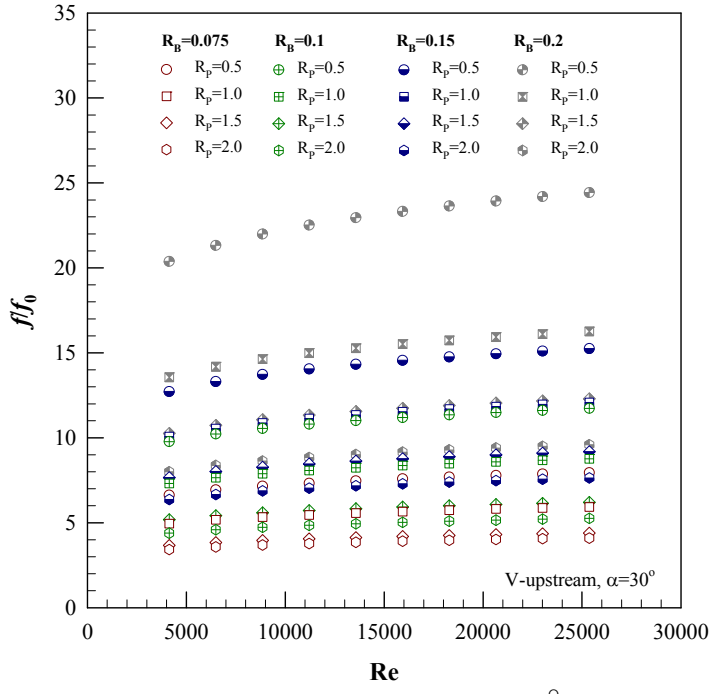

Figure 6.13 Variation of f/f_0 with Re for discrete 30° V-upstream baffles.

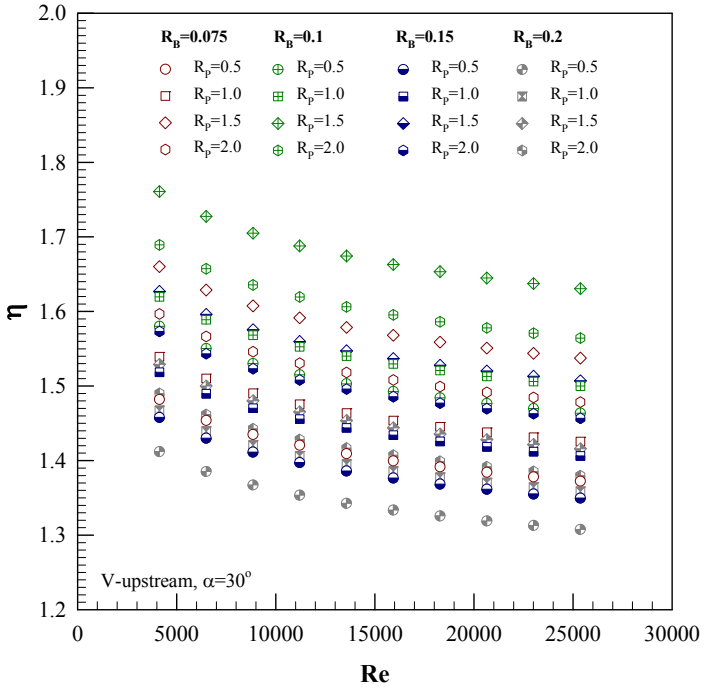

Figure 6.14 Variation of η with Re for discrete 30° V-upstream baffles.

6.1.6 Performance comparison among discrete V–baffles

From the previous sections, the maximum η is found at R_B=0.1 and R_P=1.5 for all the attack angles. Thus, the optimum parameter of the present work is at R_B=0.1 because at this point, the highest η is achieved no matter what R_P is. Figures 6.15 and 6.16 exhibit the comparison of Nu/Nu_0, f/f_0 and η at a fixed R_B and R_P but diferent α values.

The effect of α on the heat transfer rate and pressure drop is displayed in Fig. 6.15. In the figure it is seen that the V-baffles at R_B=0.1 and R_P=1.5 provide the considerable increase in Nu/Nu_0 with the rise of α. The Nu/Nu_0 tends to slightly decrease while the f/f_0 shows the reversing trend with the increment of Re. The Nu/Nu_0 and f/f_0 values are maximum for α=60° due to highly interrupting the flow and promoting higher levels of vortex strength, and are around 2-9% and 20-41% higher than those for α=45° and 30°, respectively. Figure 6.16 shows the variation of η with Re for various α values. In the figure, it is observed that the η is highest for α=30°, and about 4% and 10% above that for α=45° and 60° respectively. This indicates that the optimal η is found at α=30° and thus, the modified baffles will be presented only for α=30° in the next section.

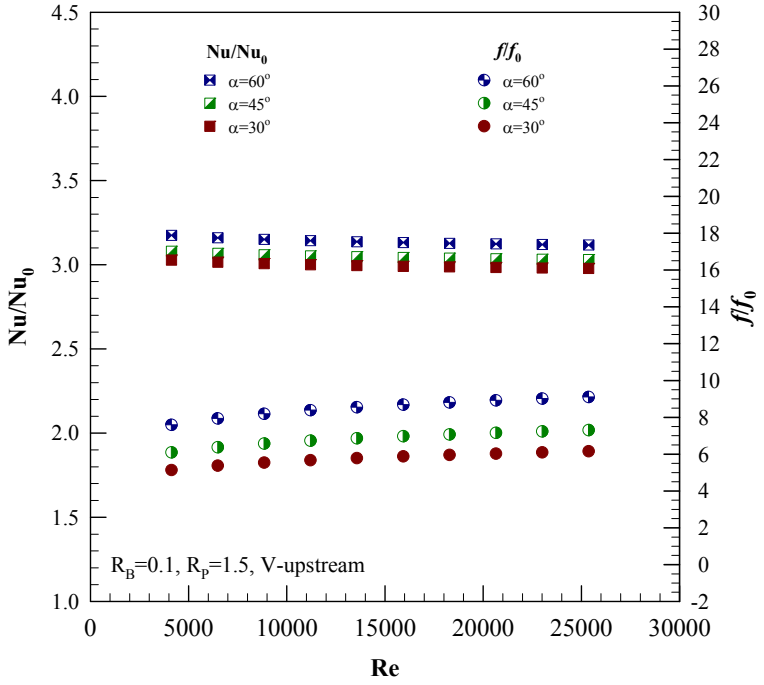

Figure 6.15 Variation of Nu/Nu_0 and f/f_0 with Re for various α values.

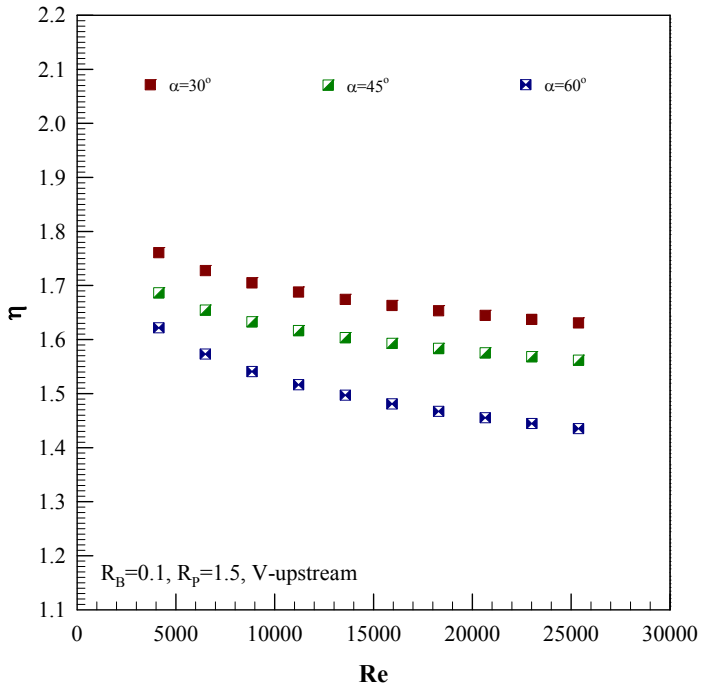

Figure 6.16 Variation of η with Re for various α values.

6.1.7 Prediction correlations of Nu and *f* for discrete V–baffes

The Nu and *f* values for discrete V–baffle inserts are correlated as functions of Reynolds number (Re), Prandtl number (Pr), baffle blockage ratio (R_B), and pitch ratio (R_P). These correlations of Nu and *f* for the discrete V–baffles valid for R_B=0.2, 0.15 0.1 and 0.075; R_P=0.5, 1.0, 1.5 and 2.0; α=60°, 45° and 30°; V-upstream and V-downstream in the Re range of 4000 to 25,000 are written as:

Discrete 60° V–upstream baffles,

Nusselt number correlation:

$$Nu = 0.1945 Re^{0.7667} Pr^{0.4} R_P^{-0.1496} R_B^{0.3079} \quad (6.1)$$

Friction factor correlation:

$$f = 40.8973 Re^{-0.1836} R_P^{-0.5903} R_B^{1.2607} \quad (6.2)$$

Discrete 60° V–downstream baffles;

Nusselt number correlation:

$$Nu = 0.1773 Re^{0.7667} Pr^{0.4} R_P^{-0.1498} R_B^{0.2938} \quad (6.3)$$

Friction factor correlation:

$$f = 30.3712 Re^{-0.1836} R_P^{-0.6437} R_B^{1.1693} \quad (6.4)$$

Discrete 45° V–upstream baffles;

Nusselt number correlation:

$$Nu = 0.1271 Re^{0.7917} Pr^{0.4} R_P^{-0.1302} R_B^{0.2508} \quad (6.5)$$

Friction factor correlation:

$$f = 13.0030 Re^{-0.1836} R_P^{-0.5521} R_B^{0.9632} \quad (6.6)$$

Discrete 30° V–upstream baffles;

Nusselt number correlation:

$$Nu = 0.1250 Re^{0.7917} Pr^{0.4} R_P^{-0.1259} R_B^{0.2511} \quad (6.7)$$

Friction factor correlation:

$$f = 12.3458 Re^{-0.1836} R_P^{-0.5645} R_B^{0.9939} \quad (6.8)$$

The plot of Nu and *f* for the discrete V–baffles predicted by Eqs. (6.1) - (6.12) against measured data is depicted in Fig. 6.17a and b, respectively. In the figure, the majority of the measured data falls within ±10% and ±9% for the predicted Nu and *f*, respectively.

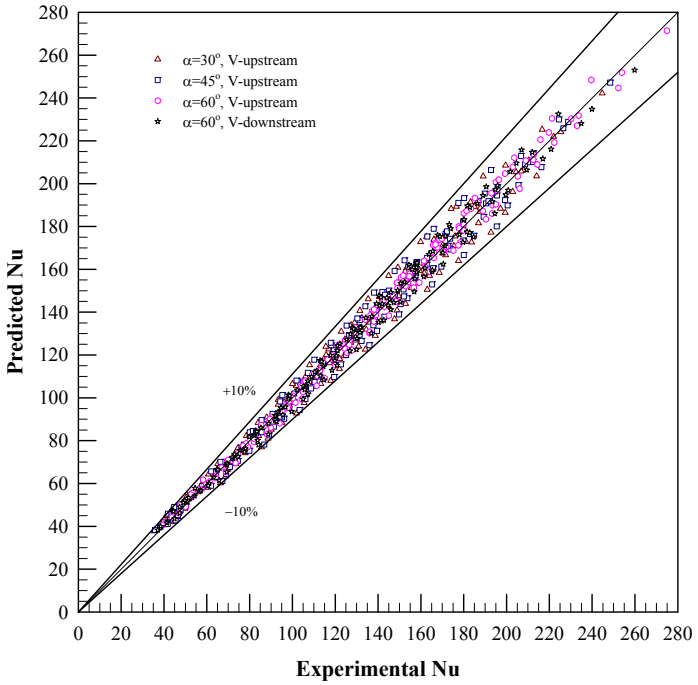

(a)

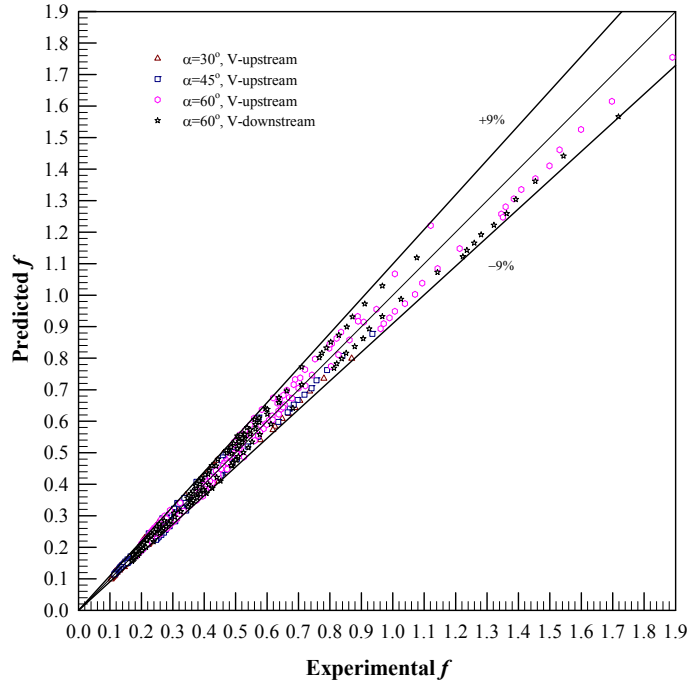

(b)

Figure 6.17 Predicted data of (a) Nu and (b) *f* versus experimental data.

6.2 Trapezoidal V-Baffles

This section presents the new improvement of V-baffle vortex generator. Figure 6.18 portrays the test duct with trapezoidal V-baffles placed on double sides of a straight tape that inserted diagonally into the duct. The V-baffle parameters of R_B and R_P values are the same as used in the previous section of discrete V-baffles while only one attack angle, α=30°; V-cut angle, β=10°; and V-upstream direction are offered. This arrangement of trapezoidal V-baffles is expected to yield greater heat transfer rate than that of the discrete V–baffles. The purpose of cutting the V-tip at V-cut angle, β=10° is to help reduce pressure drop across the V-baffles.

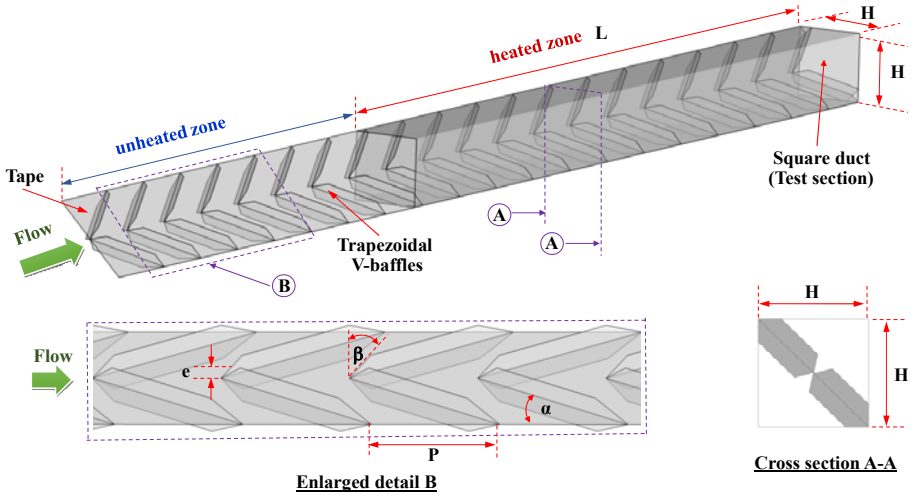

Figure 6.18 Test section with trapezoidal V-baffles.

Figures 6.19 and 6.20 show the relationship of Nu/Nu_0 and f/f_0 against Re for the 30° trapezoidal V-baffles at various R_B and R_P. In the figures, it is visible that at a given R_P, the Nu/Nu_0 and f/f_0 for R_B=0.2, 0.15, 0.1 and 0.075 are approximately 4.1-5.0, 3.7-4.4, 3.3-3.8 and 2.5-2.9; and 22.0-50.2, 11.8-28.1, 6.7-15.5 and 3.9-8.6, respectively. Again, it can be observed that the increase rate of f/f_0 is considerably higher than that of Nu/Nu_0. However, for small R_B, the increase rates of Nu/Nu_0 and f/f_0 are not much different.

The thermal enhancement factor (η) for the trapezoidal V-baffles plotted against Re is displayed in Fig. 6.21. In the figure, the η is maximum around 1.81 is found at R_B=0.1, R_P=1.5 and Re=4130; and is about 1.32-1.54, 1.41-1.73, 1.51-1.81 and 1.40-1.70 for R_B=0.2, 0.15, 0.1 and 0.075, respectively is depending on the Re value.

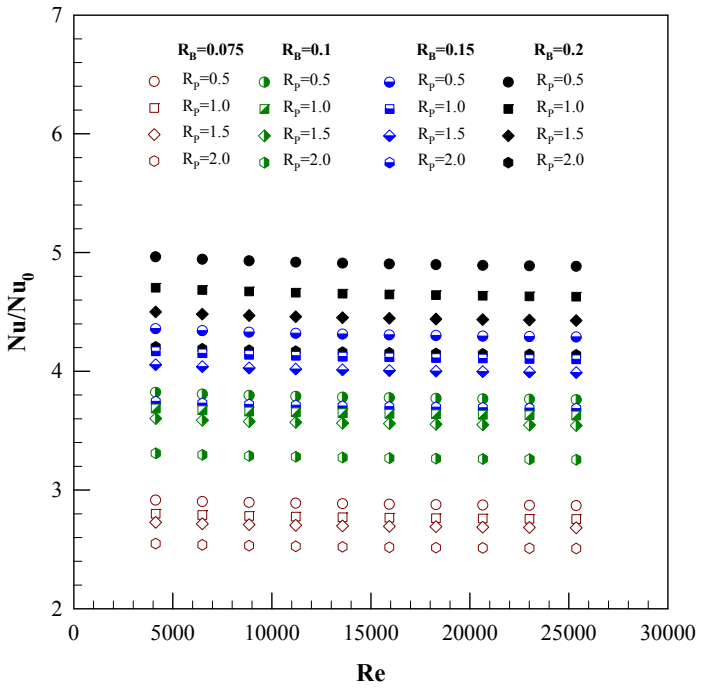

Figure 6.19 Variation of Nu/Nu_0 with Re for trapezoidal V-baffles.

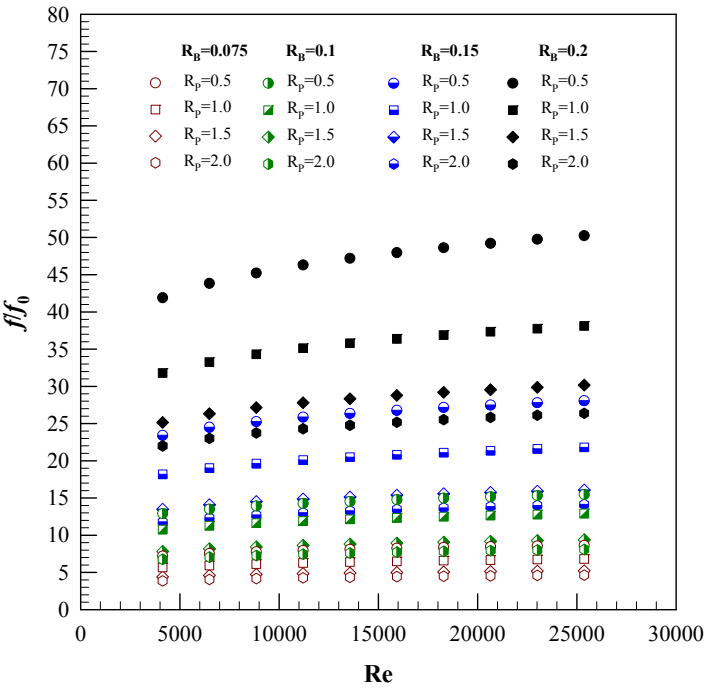

Figure 6.20 Variation of f/f_0 with Re for trapezoidal V-baffles.

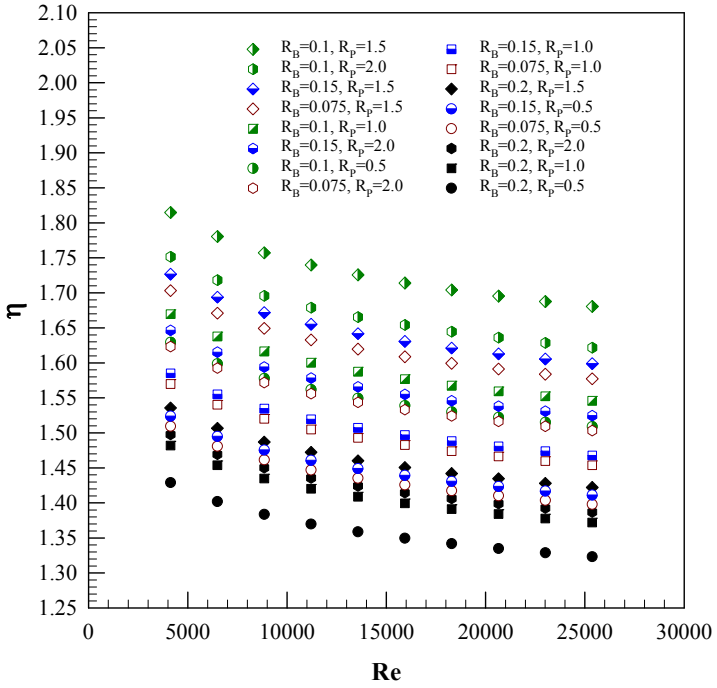

Figure 6.21 Variation of η with Re for trapezoidal V-baffles.

6.2.1 Prediction correlations of Nu and *f* for trapezoidal V–baffles

The Nu and *f* values for the trapezoidal V–baffles placed on double sides of a tape are correlated as functions of Reynolds number (Re), Prandtl number (Pr), baffle blockage ratio (R_B), and pitch ratio (R_P). These correlations of Nu and *f* for the trapezoidal V–baffles valid for R_B=0.2, 0.15 0.1 and 0.075; R_P=0.5, 1.0, 1.5 and 2.0; α=30° in the Re range of 4000 to 25,000 are written by:

Nusselt number correlation:

$$Nu = 0.2493 Re^{0.7917} Pr^{0.4} R_P^{-0.0982} R_B^{0.4910} \quad (6.9)$$

Friction factor correlation:

$$f = 93.0677 Re^{-0.1836} R_P^{-0.4844} R_B^{1.7276} \quad (6.10)$$

The plots of Nu and *f* of the trapezoidal V–baffles mounted on a tape predicted by Eqs. (6.13) - (6.14) against the measured data are depicted in Fig. 6.22a and b, respectively. In the figure, the majority of the measured data fall within ±10% for both the predicted Nu and *f*.

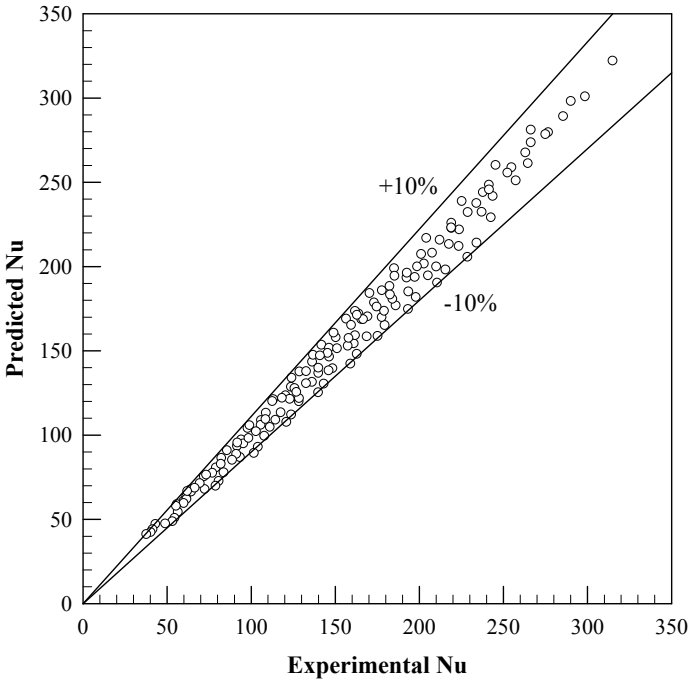

(a)

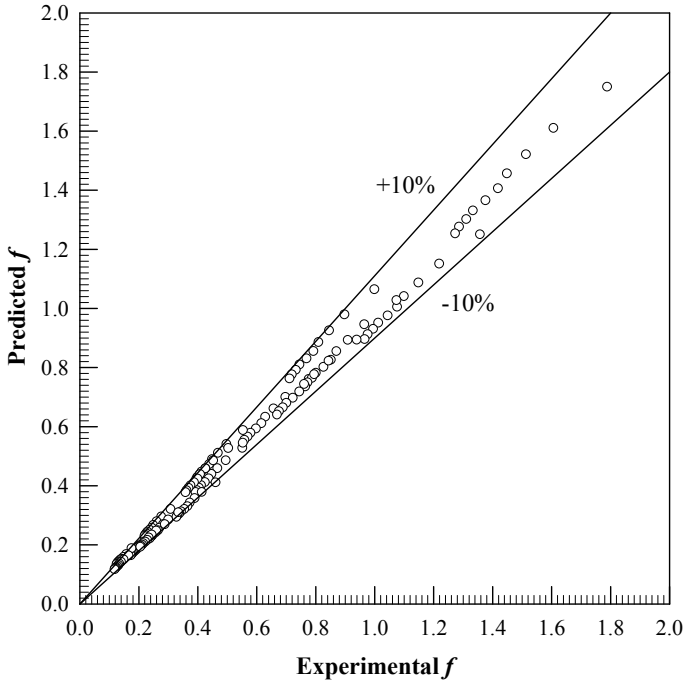

(b)

Figure 6.22 Predicted data of (a) Nu and (b) *f* versus experimental data.

6.3 Comparison between trapezoidal and discrete V-Baffles

This section presents the performance comparison between trapezoidal V-baffles and discrete V-baffles at a fixed R_P=1.5; R_B=0.2, 0.15, 0.1 and 0.075; α=30° and V-upstream direction.

Figures 6.23, 6.24 and 6.25 display the comparison of Nu/Nu_0, f/f_0, and η with Re for the trapezoidal and discrete V-baffles, respectively. In Figs. 6.23 and 6.24, the Nu/Nu_0 and f/f_0 for the trapezoidal V-baffles are about 6-26% and 11-59% higher than those of the discrete ones for the corresponding conditions, respectively. As can be seen in Fig. 6.25, the η is maximum around 1.81 for the trapezoidal V-baffles at R_P=1.5, R_B=0.1 and is about 3-16% above the discrete V-baffles for similar operating condition.

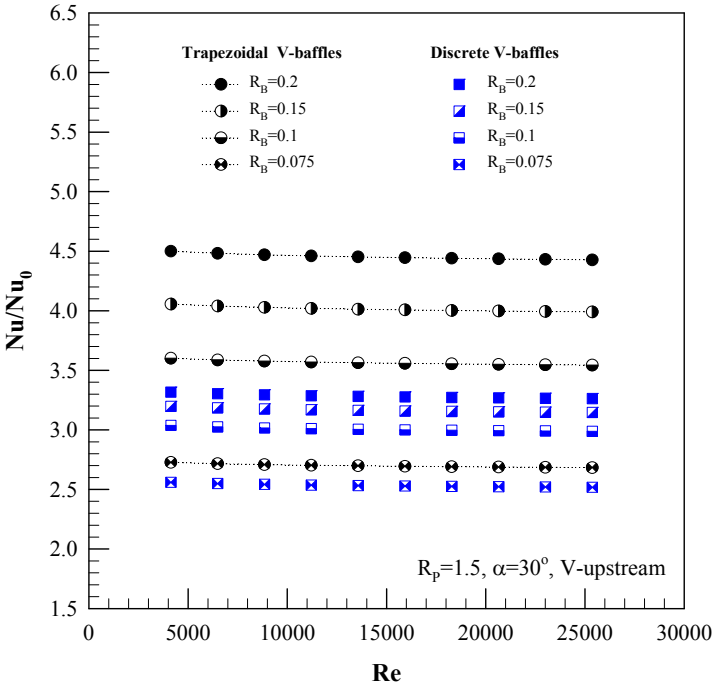

Figure 6.23 Comparison of Nu/Nu_0 between trapezoidal and discrete V-baffles.

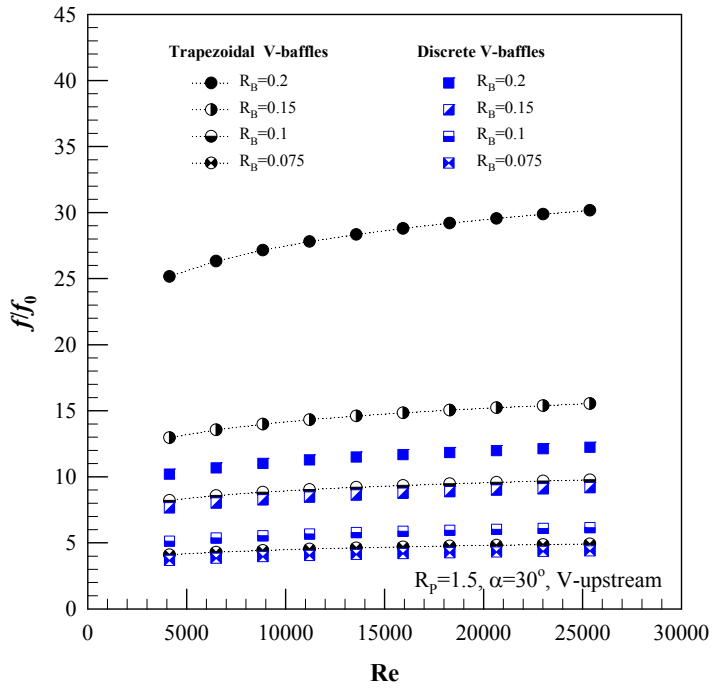

Figure 6.24 Comparison of f/f_0 between trapezoidal and discrete V-baffles.

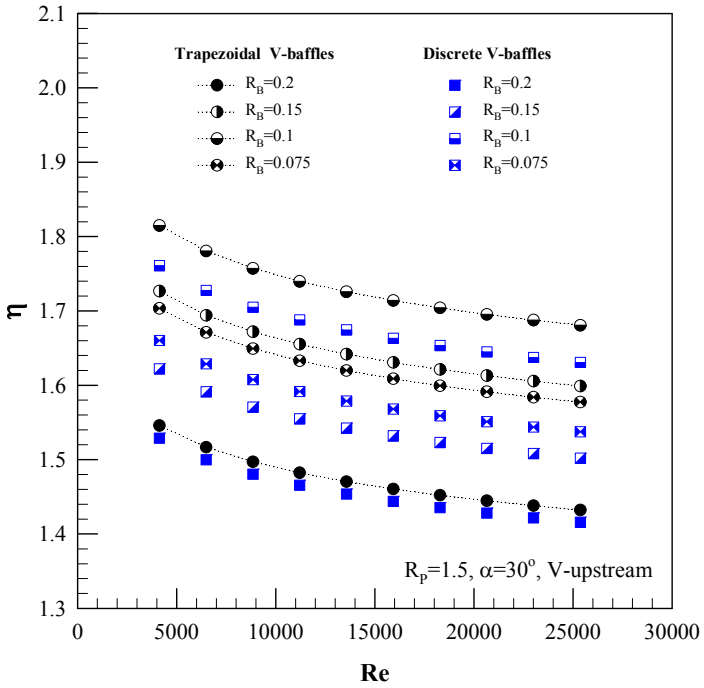

Figure 6.25 Comparison of η between trapezoidal and discrete V-baffles.

6.4 Performance prediction between trapezoidal and discrete V-Baffles

In this section, the performance prediction of discrete V-baffles and trapezoidal V-baffles is presented by using the response surface method (RSM) to optimize them. The RSM is the mathematic and statistic method for designing the model and analysis of problem to achieve the optimal response paramrter.

Figures 6.26, 6.27; and 6.28, 6.29 displays the prediction of η with respect to R_B and R_P in 2D, 3D for the discrete V-baffles and 2D, 3D for trapezoidal ones, respectively. In the figures, all curves in graphs are obtained from the regression equations. In Figs. 6.26 and 6.27, the maximum η of around 1.66 is at R_B=0.1 and R_P=1.7 for the discrete V-baffles while that of about 1.74 is at R_B=0.12 and R_P=1.6 for the trapezoidal ones, as seen in Figs. 6.28 and 6.29.

The η values for discrete V–baffle and trapezoidal V-baffles inserts are correlated as functions of baffle blockage ratio (R_B), and pitch ratio (R_P). These correlations of η for α= 30°; V-upstream and Re=4130 are written as:

The η correlation for discrete V–baffle:

$$\eta = 1.1467 + 3.7372R_B + 0.3927R_P - 0.2777R_BR_P - 16.1732R_B^2 - 0.1089R_P^2 \quad (6.11)$$

The η correlation for trapezoidal V-baffles:

$$\eta = 0.9456 + 7.5623R_B + 0.4312R_P - 0.3355R_BR_P - 30.2657R_B^2 - 0.1198R_P^2 \quad (6.12)$$

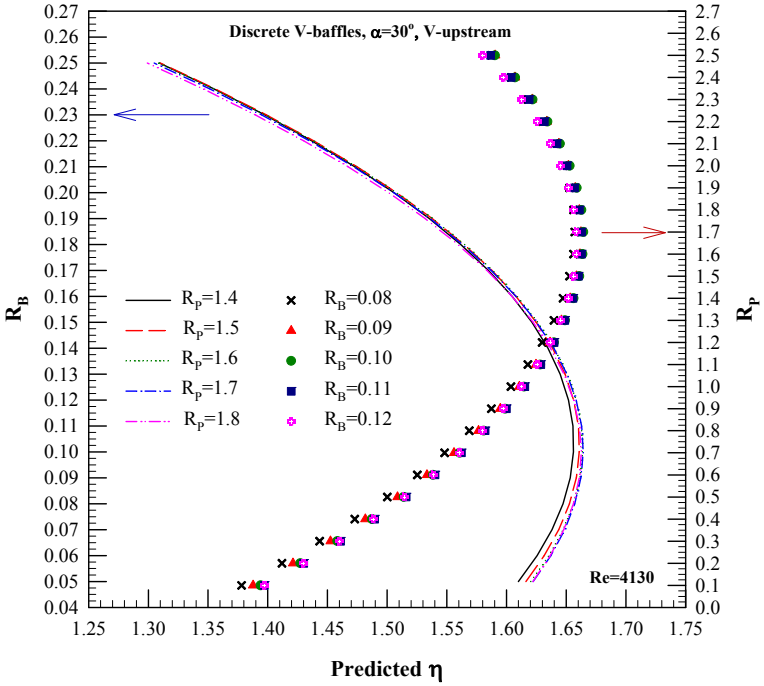

Figure 6.26 Variation of predicted η with R_B and R_P for 30° discrete V-baffles.

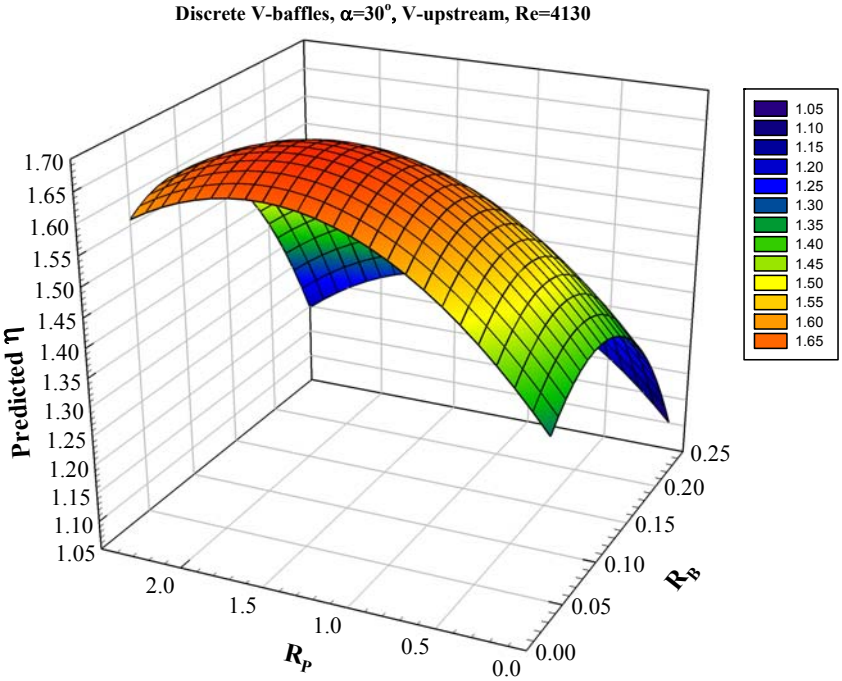

Figure 6.27 Three dimensional η by the RSM for 30° discrete V-baffles.

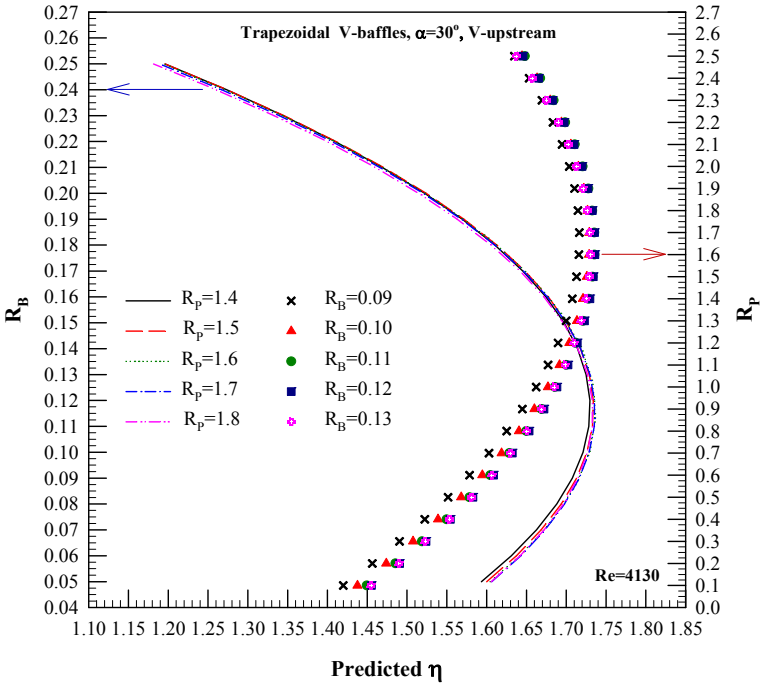

Figure 6.28 Variation of predicted η with R_B and R_P for 30° trapezoidal V-baffles.

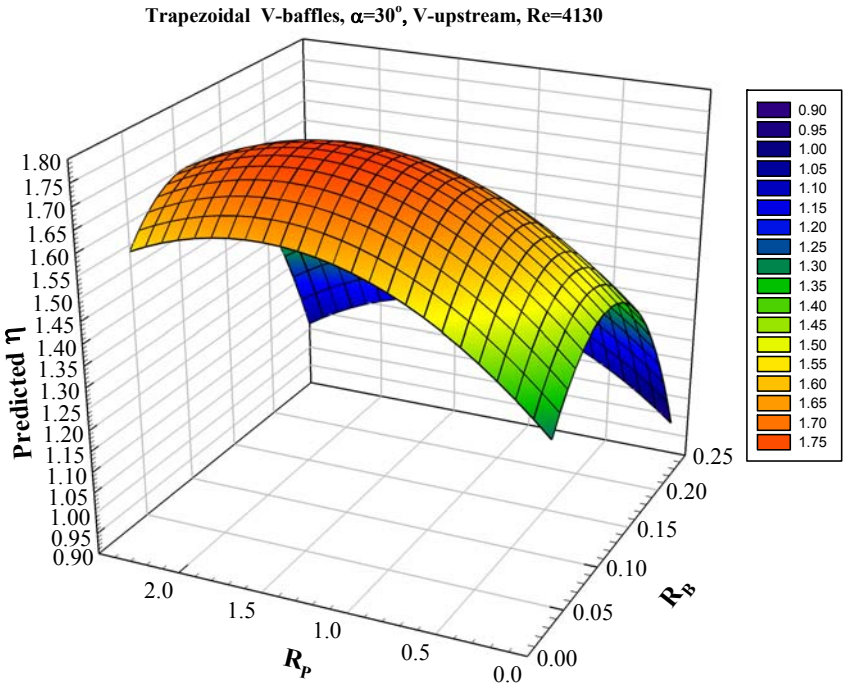

Figure 6.29 Three dimensional η by the RSM for 30° trapezoidal V-baffles.

CHAPTER 7
BAFFLES ON TWO OPPOSITE WALLS

7.1 Introduction

This chapter presents the insertion of baffle vortex generators placed on two opposite walls of a square duct while in the previous chapter the baffles were placed in central core flow. From the achievement in chapter 6, the improvement and development of a new form of vortex generator arrangements is proposed. Therefore, this chapter is dedicated to the increase in thermal performance in a square-duct inserted with baffles placed on the duct walls. The configurations of the baffles are classified into 2 types: angled and V-shaped baffles. Both the baffle types are placed on two opposite walls of the duct by using a straight tape as a support to keep those baffles closest to the wall surfaces.

7.2 Angled baffles

The schematic of the test section with angled baffles placed on two opposite walls of a square duct is depicted in Fig. 7.1. The straight tape made of an aluminum sheet with its dimension of 44×1200×0.5 mm^3 was employed as a support to keep the baffles closest to the wall surfaces. The baffles made of 0.3 mm aluminum strip were attached on both edges of the straight tape as shown in Fig. 7.1. The two baffle sizes were 4.5 and 9.0 mm high (e) with 0.3 mm thickness (t), equivalent to baffle- to duct-height ratios, R_B=e/H=0.1 and 0.2 respectively. There were three baffle-pitch to duct-height ratios (R_P=P/H=0.5, 1.0, and 2.0), all at a single attack angle, α=30°.

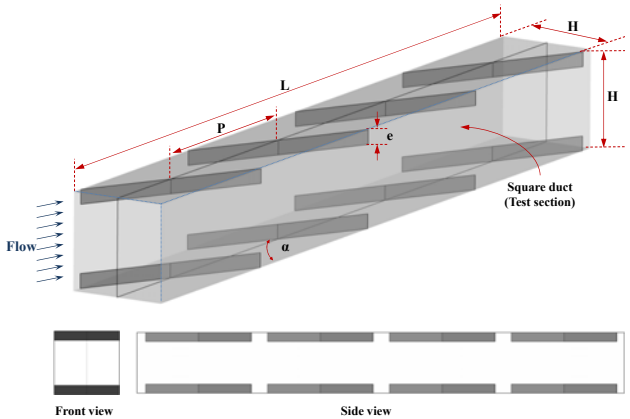

Figure 7.1 Test section with angled baffles on two opposite walls.

7.2.1 Effect of angled baffles on Nu/Nu_0 and f/f_0

The relationship between Nu/Nu_0 and Re for using the angled baffles with α=30°; R_B=0.2 and 0.1; and R_P=0.5, 1 and 2 is displayed in Fig. 7.2. In the figure, it is observed that the Nu/Nu_0 shows the slight downtrend pattern with the rise of Re and R_P but with the decrease of R_B. The R_B=0.2 provides the Nu/Nu_0 higher than the R_B=0.1 for all R_P values and the maximum Nu/Nu_0 found at R_B=0.2 and R_P=0.5 is about 6-39% higher than the others. This is because the use of the baffles leads to axial vortex flows through the test duct helping to increase stronger fluid mixing between the core flow and the wall regions. It is visible that the Nu/Nu_0 values for R_B=0.2 and 0.1 are about 4.8-4.9, 4.5-4.6 and 4.1-4.2; and 4.0-4.1, 3.6-3.7 and 2.9-3.0 times at R_P=0.5, 1.0 and 2.0, respectively.

Figure 7.3 shows the variation of f/f_0 with Re for using the 30° angled baffles with various R_B and R_P values. In the figure, it is seen that the highest f/f_0 values found at R_B=0.2 and R_P=0.5 are about 14-78% higher that the others. It is noted that the f/f_0 tends to increase with the rise of Re and R_B values while shows a reversing trend with increasing R_P. This can be attributed to higher flow blockage and larger surface areas form the baffles. The f/f_0 values of the R_B=0.2 are higher than those of the R_B=0.1 and at R_B=0.2 and 0.1 are, respectively, around 25.9-31.1, 22.3-26.8 and 18.0-21.6; and 11.0-13.2, 8.6-10.2 and 5.7-6.8 for R_P=0.5, 1.0 and 2.0.

7.2.2 Thermal performance

The variation of η for using the 30° angled baffles is shown in Fig. 7.4. In the figure, η is decreased as Re increases for all cases. The maximum η seen at R_B=0.1, R_P=0.5 and Re=4130 is about 1.86 and around 4-13% higher than the others. It is observed that the highest η is at lower Re, R_B and R_P values. It can be attributed to the much lower friction loss for using the small height value of the baffles. Although the larger R_B provides high Nu/Nu_0, it yields higher f/f_0. This means that the increase rate of f/f_0 is steeper than that of Nu/Nu_0 leading to lower thermal performance for using larger R_B. The η values for R_B=0.2 and 0.1 are, respectively, approximately 1.53-1.66, 1.52-1.64 and 1.49-1.61; and 1.72-1.86, 1.67-1.79 and 1.68-1.56 at R_P=0.5, 1.0 and 2.0.

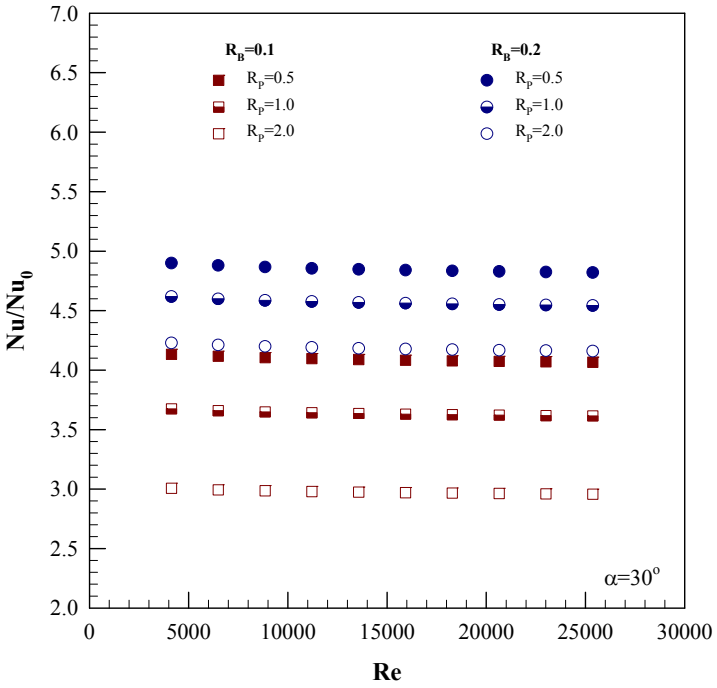

Figure 7.2 Variation of Nu/Nu_0 with Re for angled baffles with various R_B and R_P.

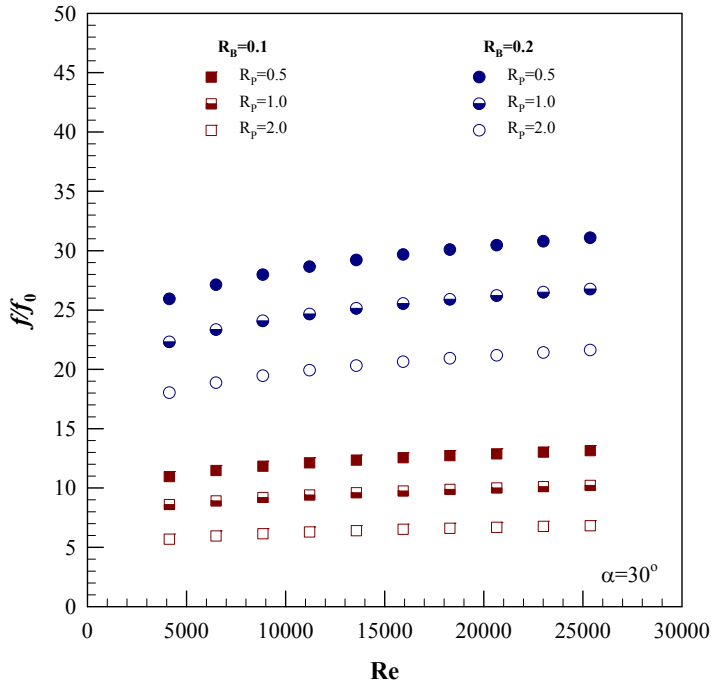

Figure 7.3 Variation of f/f_0 with Re for angled baffles with various R_B and R_P.

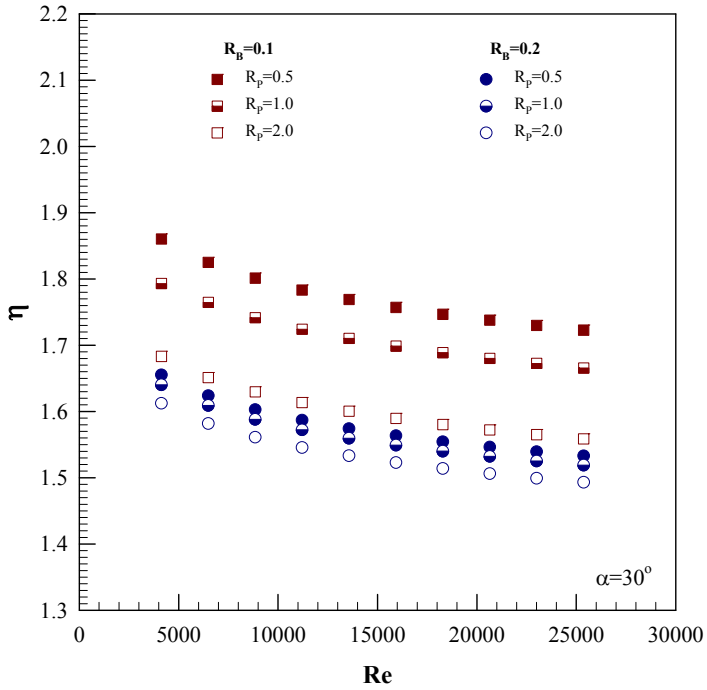

Figure 7.4 Variation of η with Re for angled baffles with various R_B and R_P.

7.3 V-baffles

In section 7.2, the results of the 30° angled baffles placed on two opposite duct walls revealed that the baffles at R_B=0.1 and R_P=0.5 yield the highest thermal performance. Thus, to continue improvement of its thermal performance, the baffle geometry was changed from the angled baffles to the V-shaped ones with a view to streamlining the baffle shape. This new baffle vortex generator geometry is expected to increase its thermal performance due to the reduction of pressure loss from using the streamlined baffles.

Figure 7.5 shows the test duct with V-shaped baffles placed on two opposite walls using a straight tape as the support. The straight tape was made of aluminum with its dimension of 44×1200×0.5 mm^3 while the V-baffles made of 0.3 mm aluminum strip were attached on both edges of the tape. The four baffle sizes were 3.375, 4.5, 6.75 and 9.0 mm high (e) with 0.3 mm thickness (t), equivalent to baffle-to duct-height ratios, R_B=e/H=0.075, 0.1, 0.15 and 0.2 respectively. There were four baffle-pitch to duct-height ratios (R_P=P/H=0.5, 1.0, 1.5 and 2.0) and three baffle attack angles (α) of 20°, 30°, and 45°. The V-baffles arranged by letting V-tip point upstream were placed on the tape edges as can be seen in Fig. 7.5.

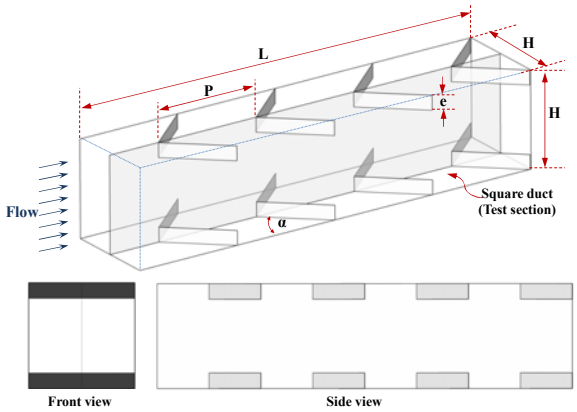

Figure 7.5 Test section with V-baffles placed repeatedly on two opposite walls.

7.3.1 Effect of V-baffles on Nu/Nu_0, f/f_0 and η

Figures 7.6, 7.7 and 7.8 display, respectively, the variations of Nu/Nu_0, f/f_0 and η with Re for various R_P at fixed R_B=0.1. In the figure, it is noted that the inserted duct with R_P=0.5 provides the maximum Nu/Nu_0, f/f_0 and η values. It is observed in Figs. 7.7 and 7.8 that the Nu/Nu_0 and f/f_0 values for R_P=0.5, 1.0, 1.5 and 2.0 are around 4.2-4.3, 3.6-3.7, 3.3-3.4 and 3.0-3.1; and 11.5-13.8, 8.7-10.5, 6.8-8.1 and 5.8-6.9, respectively. This indicates that the decrease rate of f/f_0 is higher than that of Nu/Nu_0 for the increment in R_P, for example, the reductions of Nu/Nu_0 and f/f_0 of about 25% and 50% for the change of R_P=0.5 to 2.0. It is interesting to note that the η values are approximately 1.75-1.89, 1.67-1.80, 1.63-1.76 and 1.57-1.70 of R_P=0.5, 1.0, 1.5 and 2.0, respectively. The maximum η of 1.89 is seen at Re=4130 for using R_P=0.5 and R_B=0.1.

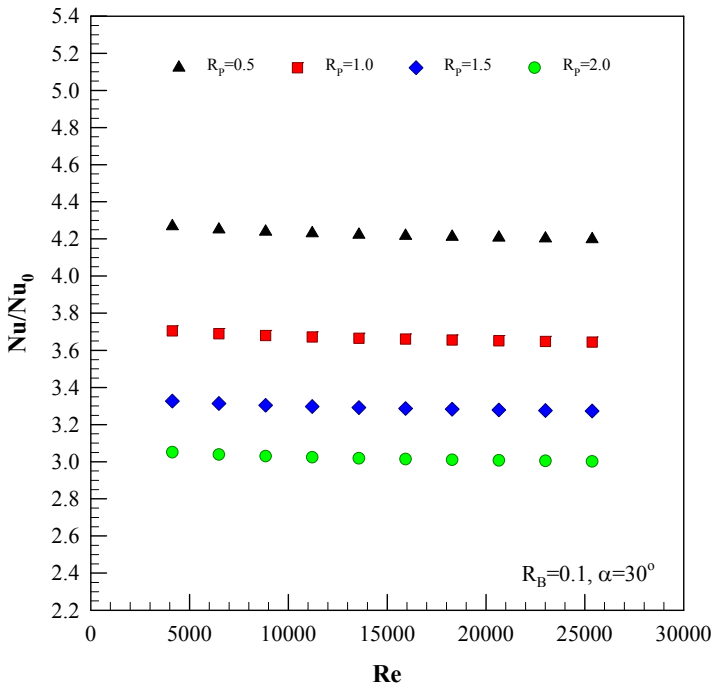

Figure 7.6 Variation of Nu/Nu_0 with Re for various R_P.

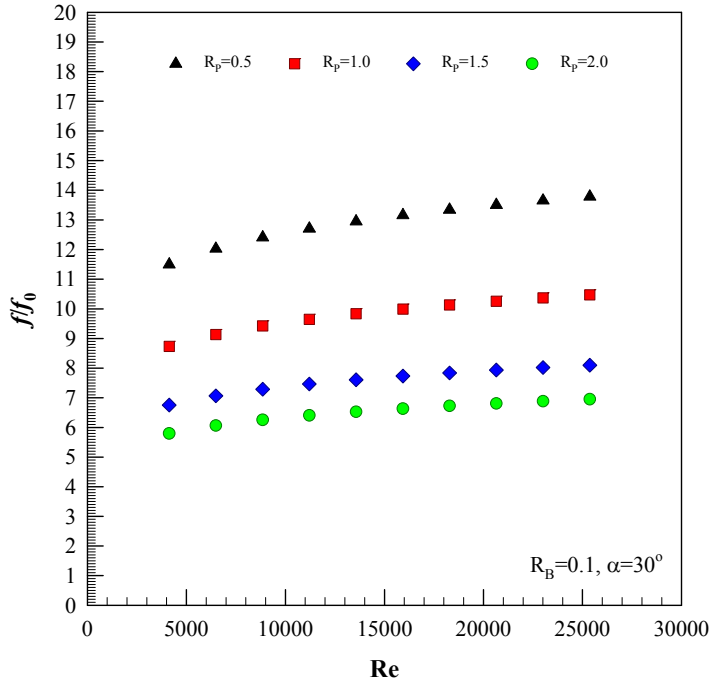

Figure 7.7 Variation of f/f_0 with Re for various R_P.

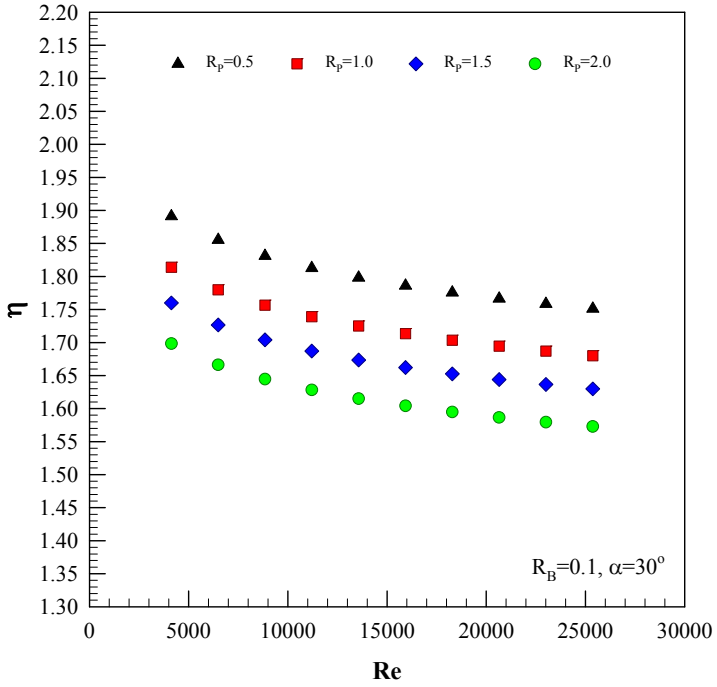

Figure 7.8 Variation of η with Re for various R_P.

7.3.2 Performance comparison between angled and V-shaped baffles

The comparisons of Nu/Nu_0, f/f_0 and η with Re for various R_P and a fixed R_B between the angled and V-shaped baffles are shown in Figures 7.9, 10 and 11, respectively. In the figures, it is visible that the V-baffles provides the Nu/Nu_0, f/f_0 and η values slightly higher than the angled ones for all cases. It is

apparent that the Nu/Nu_0, f/f_0 and η values for the V-baffles are about 1-3%, 1-5% and 1-2% above those for the angled ones.

The performance comparison between the two baffle types reveals that the optimal thermal performance is for the V-baffle type at R_P=0.5. Therefore, the optimum R_B is needed and will be done in the next sub-section.

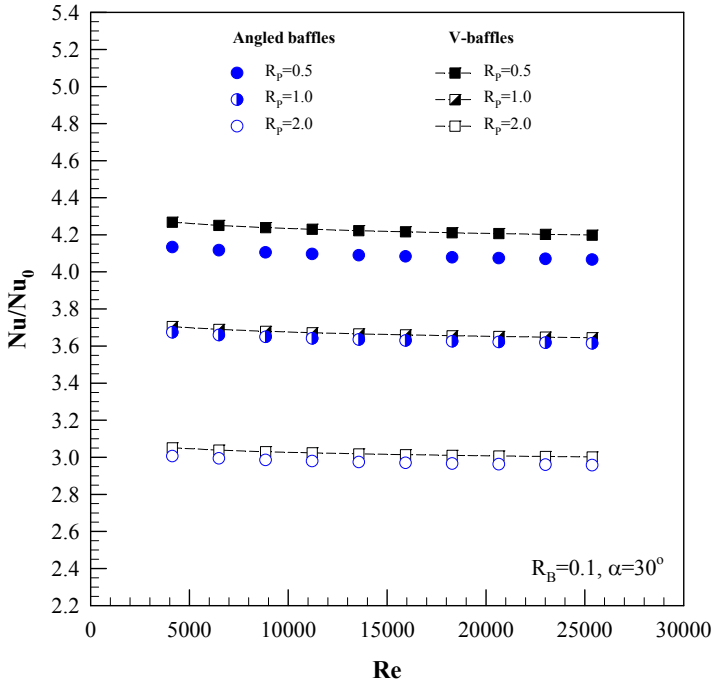

Figure 7.9 Variation of Nu/Nu_0 with Re for different baffle types.

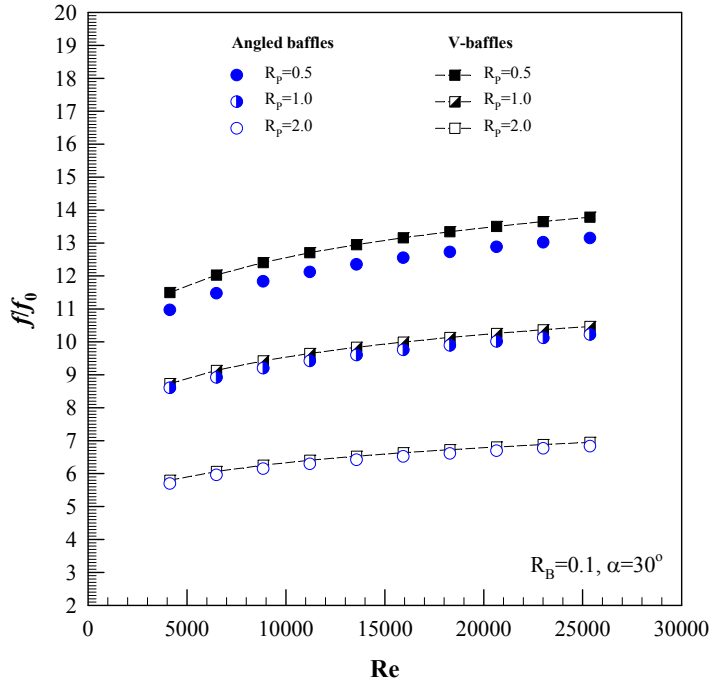

Figure 7.10 Variation of f/f_0 with Re for different baffle types.

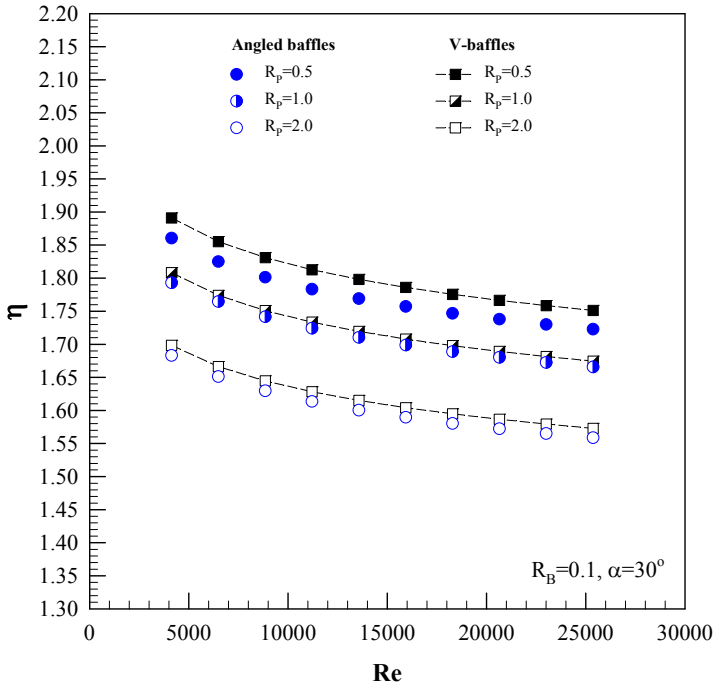

Figure 7.11 Variation of η with Re for different baffle types.

7.3.3 V-baffles with R_B optimization

Figures 7.12, 7.13 and 7.14 present the variations of Nu/Nu_0, f/f_0 and η with Re for various R_B at a fixed R_P, respectively. In the figures, it is observed that the inserted duct with R_B = 0.2 provides the maximum Nu/Nu_0 and f/f_0 values while the one with R_B = 0.075 yields the highest η. It is visible in Figs. 7.12 and 7.13 that the Nu/Nu_0 and f/f_0 values are about 5.0-5.1, 4.6-4.7, 4.2-4.3 and 3.7-3.8; and 29.7-35.6, 20.3-24.3, 11.5-13.8 and 7.8-9.4 for R_B=0.2, 0.15, 0.1 and 0.075, respectively. The η values are, respectively, 1.52-1.64, 1.60-1.73, 1.75-1.89 and 1.77-1.92 at R_B = 0.2, 0.15, 0.1 and 0.075 as seen in Fig. 7.14. Thus, the maximum η found at R_B = 0.075, R_P = 0.5 and Re=4130 is around 1.92.

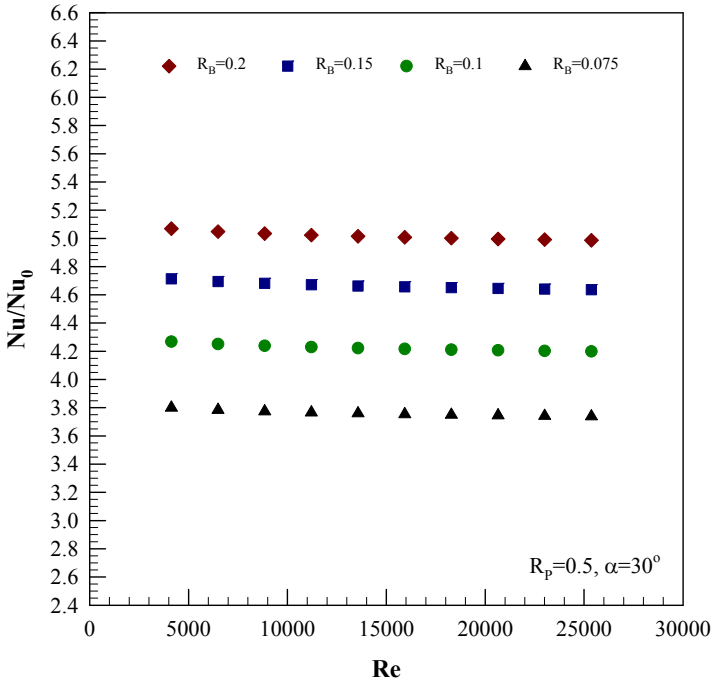

Figure 7.12 Variation of Nu/Nu_0 with Re for various R_B.

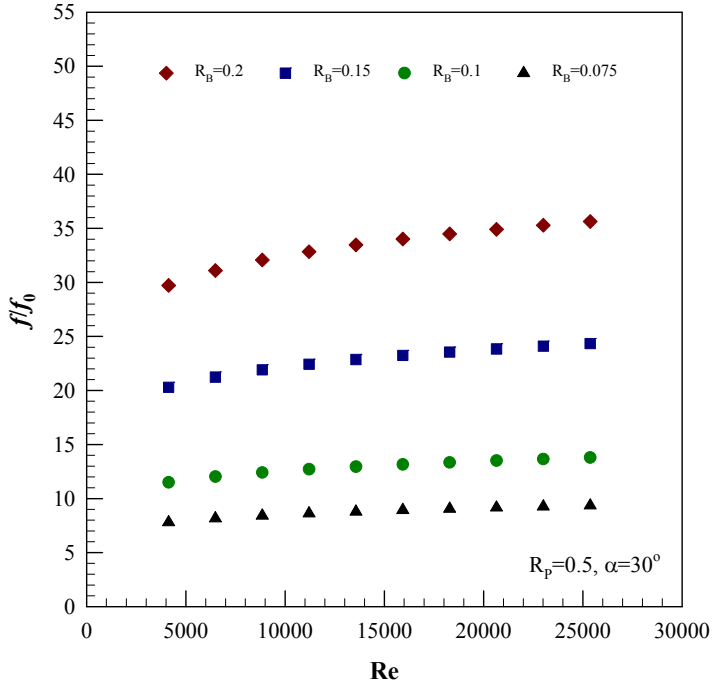

Figure 7.13 Variation of f/f_0 with Re for various R_B.

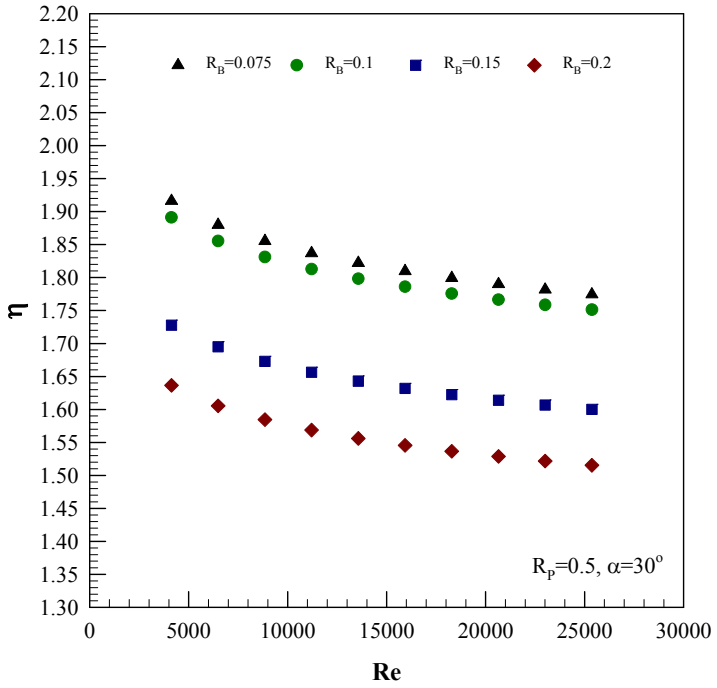

Figure 7.14 Variation of η with Re for various R_B.

7.3.4 Effect of attack angle

In previous sections, the optimum thermal performance of the 30° V-baffles is found at R_P=0.5 and R_B=0.075. Thus, the optimum attack angle at a fixed R_P and R_B is next performed to obtain the optimum thermal performance.

Figures 7.15, 7.16 and 7.17 presents, respectively the variation of the Nu/Nu_0, f/f_0 and η with Re for α=45°, 30° and 20° at the fixed R_P=0.5 and R_B=0.075. In the figures, it can be observed that the α=45° gives the highest Nu/Nu_0 and f/f_0 values while the α=20° yields the maximum η value. It is visible in Figs. 7.15 and 7.16 that the Nu/Nu_0 and f/f_0 values are about 3.9-4.0, 3.7-3.8 and 3.6-3.7; and 10.4-12.4, 7.8-9.4 and 6.5-7.8 for α=45°, 30° and 20°, respectively. In scrutiny of Fig. 7.17, the η values are, respectively, approximately 1.68-1.82, 1.77-1.92 and 1.84-1.99 and 1.77-1.92 for α=45°, 30° and 20° depending on Re values. The η of the inserted duct with α=20° is, respectively, around 4 and 9% higher than that of the one with α=30° and 45°. At α=20°, the highest η is about 2.0 at R_P=0.5, R_B=0.075 and Re=4130 in which these conditions yield the best thermal performance.

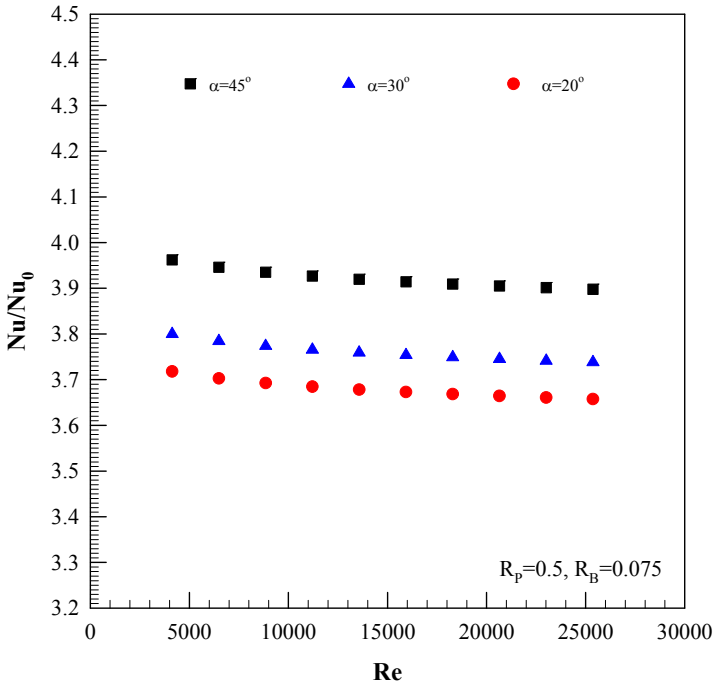

Figure 7.15 Variation of Nu/Nu_0 with Re for various α values.

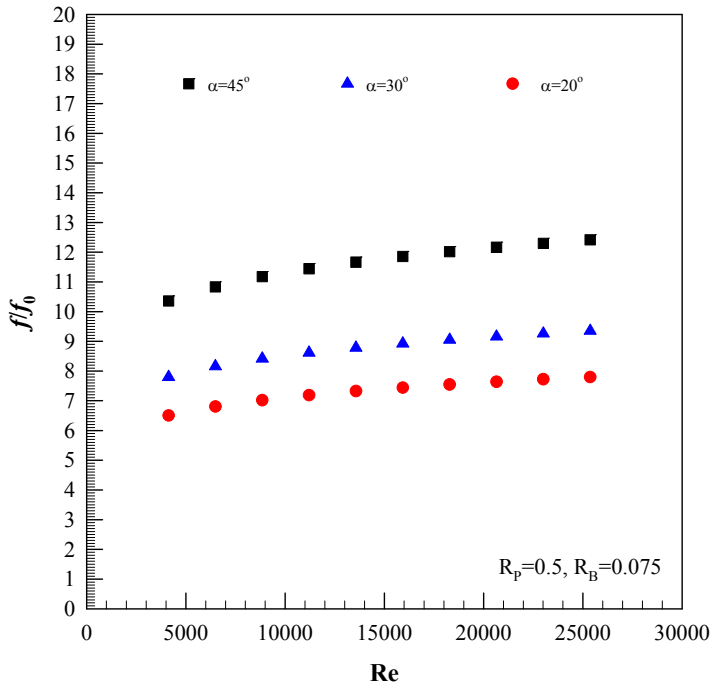

Figure 7.16 Variation of f/f_0 with Re for various α values.

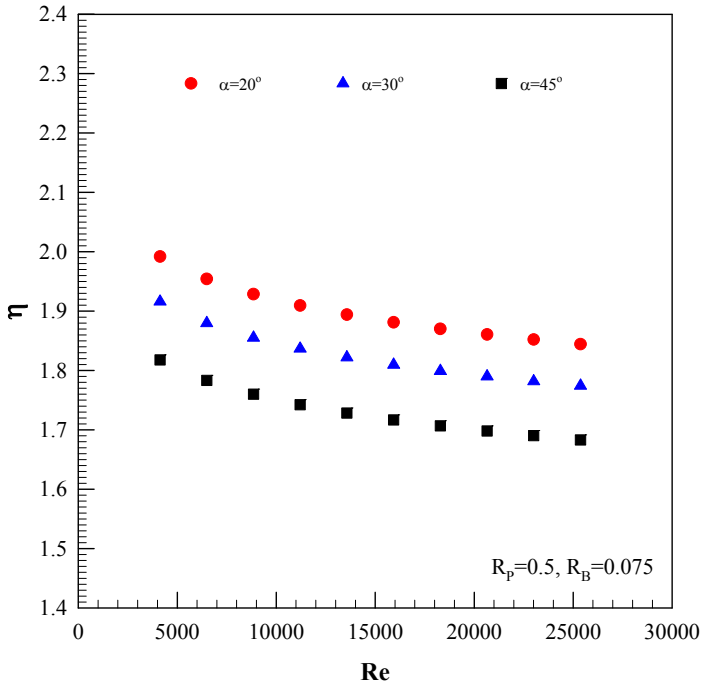

Figure 7.17 Effect of α values on η.

CHAPTER 8
CONCLUSIONS

The present research efforts have been made to investigate experimentally the effect of different types of turbulators or swirl/vortex flow generators fitted in a square duct heat exchanger on the heat transfer rate, pressure drop and thermal performance characteristics. The choice of vortex flow generators was decided after the extensive literature survey. Several turbulators have been suggested in this effort for possibility to achieve the target of higher thermal performance.

Main findings of the present work have been described in some details in chapters 5 (combined twisted-tape and V-baffles), 6 (V-baffled tapes) and 7 (baffled tape on two opposite walls). This chapter summarizes the major conclusions including suggestions for further studies.

8.1 Combined twisted-tape and V-baffles

8.1.1 Single twisted-tape with V-baffles

The twisted tapes were formed with two different twist ratios, Y=y/w=4 and 5. The V-baffles were arranged with three blockage ratios, R_B=0.1, 0.15 and 0.2, four pitch ratios R_P=2, 2.5, 4 and 5 at a single attack angle, α=30°.

The combined devices provide the Nu/Nu_0 of about 1.91-3.22 while the twisted tapes alone yield that of 1.49-1.90. The highest Nu/Nu_0 is found at Y=4, R_P=2 and R_B=0.2; and around 3.9-44% higher than the other cases. The f/f_0 is some 3.94-9.44 for the combined devices whereas is about 2.44-2.62 for twisted-tape alone. The highest f/f_0 is seen at Y=4, R_P=2 and R_B=0.2 and about 6.9-73.6% above other cases. The highest η of 1.62 is seen at Y=4; R_B=0.1 and R_P=2 and around 2–17% higher than other cases.

8.1.2 Quadruple twisted-tapes with V-baffles

Four twisted tapes were formed with a single twist-ratio, Y=y/w=4. For V-baffles, there were three blockage ratios, R_B=0.075, 0.1, 0.15 and 0.2; four pitch ratios, R_P=4, 8, 12 and 16 at a single attack angle, α=30°.

The Nu/Nu_0 is around 1.9-3.4 for a combination of four twisted-tapes and V-baffles while is about 1.8-2.3 for the four twisted-tapes alone. The highest Nu/Nu_0 is at R_P=4 and R_B=0.2 and around 3.5-33.6% above the other cases. The f/f_0 is 4.3-9.4 for the compound devices whereas about 3.4-3.5 for the four twisted-tapes alone. The maximum η of about 1.74 is achieved for the combined devices at R_B=0.1 and R_P=4 and around 2.1–15.9 % higher than the other cases.

8.2 V-baffles in central core flow

8.2.1 Discrete V–baffles

The discrete V–baffles placed on double sides of a tape were performed with four blockage ratios, R_B=0.075, 0.1, 0.15 and 0.2; four pitch ratios, R_P=0.5, 1, 1.5 and 2; three attack angles, α=30°, 45°, and 60°; with two arrangements of V-tip pointing upstream and downstream.

The Nu/Nu_0 increases with the increment of R_B but with decreasing R_P. The V-upstream baffles with R_B=0.2 and R_P=0.5 provide the highest Nu/Nu_0. At given R_P and α=60°, the Nu/Nu_0 values of R_B=0.2 is 13-29% above the R_B=0.15, 0.1 and 0.075 while at a prescribed R_B, those of R_P=0.5 is about 8-22% over the R_P=1.0, 1.5 and 2.0. The f/f_0 tends to increase with increasing R_B but with decreasing R_P. The f/f_0 for R_B=0.2 and R_P=0.5 is about 41-73% above that for R_B=0.15, 0.1 and 0.075; and 29-57% higher than that for R_P=1.0, 1.5 and 2.0.

The V-upstream baffles at fixed R_B=0.1 and R_P=1.5 for α=60° provides the Nu/Nu_0, f/f_0 and η at about 4.5%, 6.1% and 2.4%, respectively higher than the V-downstream ones at similar α. The 60° V-baffles provide the maximum heat transfer and around 2-7% and 4-9% higher than the 45° and 30° ones whereas the f/f_0 for the 60° V-baffles is highest and about 20-35% and 28-41% higher than that for the 45° and 30° ones, respectively. The Nu/Nu_0 and f/f_0 for the discrete V-baffles are, respectively, in the range of 2.3-4.5 and 3.4-53.1 while the thermal enhancement factor is around 1.11-1.76.

8.2.2 Trapezoidal V–baffles

The parameters of the trapezoidal V–baffles included four blockage ratios, R_B=0.075, 0.1, 0.15 and 0.2; four pitch ratios, R_P=0.5, 1, 1.5 and 2; and a single attack angle, α=30° with V-upstream direction.

The Nu/Nu_0 and f/f_0 values for the trapezoidal V–baffles are, respectively, about 2.5-5.0 and 3.9-50.2 times whereas the η is maximum at R_B=0.1, R_P=1.5 and is in the range of 1.32-1.81, depending on R_B and R_P values.

8.3 Baffles on two opposite walls

8.3.1 Angled baffles

The angled baffles were placed on both edges of a tape with two blockage ratios, R_B=0.1 and 0.2; three pitch ratios, R_P=0.5, 1.0, and 2.0; at a single attack angle α=30°.

The Nu/Nu_0 and f/f_0 values having a maximum at R_B=0.2 and R_P=0.5, are in the range of 2.9-4.9 and 5.7-31.1 and are about 6-39% and 14-78% above the other cases, respectively. The η value is between 1.49-1.86 and its maximum is seen at R_B=0.1, R_P=0.5 and is 4-13% higher than the other cases.

8.3.2 V-baffles

The V-baffles were mounted on the edges of a straight tape with four blockage ratios, R_B=0.075, 0.1, 0.15 and 0.2, four pitch ratios, R_P=0.5, 1.0, 1.5 and 2.0 and four baffle attack angle α=20°, 30°and 45° with V-upstream direction.

The maximum of Nu/Nu_0 and f/f_0 for the inserted duct is at the lowest R_P while at the highest R_B for a prescribed α value. The maximum of η is found to be about 2.0 at R_P=0.5, R_B=0.075 and α=20°.

8.4 Suggestions for future work

From the present research, an experimental investigation on heat transfer rate, pressure drop and thermal performance behaviors in a square-duct heat exchanger fitted with various turbulators or swirl/vortex generators. The knowledge obtained from this work can be applied to future work as follows:

8.4.1 Further study on the effect of V-baffles on two opposite walls by extending the values of R_B, R_P and α to find the optimum their values.

8.4.2 Modification of the turbulators in chapter 5, for example, such as opening of V-tip by cutting edge-tip (similar to trapezoidal baffles), double V-baffles or integrating it into a wavy-surfaced tape instead of plain tapes etc.

8.4.3 Changing the working fluid from air to another fluid such as nanofluid.

REFERENCES

[1] Eiamsa-ard S., Somkleang P., Nuntadusit C. and Thianpong C. “Heat Transfer Enhancement in Tube by Inserting Uniform/Non-uniform Twisted-Tapes with Alternate Axes: Effect of Rotated-Axis Length” **Appl. Therm. Eng.**, Vol. 54, 2013. pp. 289–309.

[2] Bas H. and Ozceyhan V. “Heat Transfer Enhancement in a Tube with Twisted Tape Inserts Placed Separately From the Tube Wall” **Exp. Therm. Fluid Sci.**, Vol. 41, 2012. pp. 51–58.

[3] Eiamsa-ard S. and Seemawute P. “Decaying Swirl Flow in Round Tubes with Short-Length Twisted Tapes” **Int. Commun. Heat Mass Transfer.**, Vol. 39, 2012. pp. 649–656.

[4] Eiamsa-ard S., Yongsiri K., Nanan K. and Thianpong C. “Heat Transfer Augmentation by Helically Twisted Tapes as Swirl and Turbulence Promoters” **Chem. Eng. Process.**, Vol. 60, 2012. pp. 42-48.

[5] Ferroni P., Block R.E., Todreas N.E. and Bergles A.E. “Experimental Evaluation of Pressure Drop in Round Tubes Provided with Physically Separated, Multiple, Short-Length Twisted Tapes” **Exp. Therm. Fluid Sci.**, Vol. 35, 2011. pp. 1357–1369.

[6] Wongcharee K. and Eiamsa-ard S. “Heat Transfer Enhancement by Twisted Tapes with Alternate-Axes and Triangular, Rectangular and Trapezoidal Wings” **Chem. Eng. Process.**, Vol. 50, 2011. pp. 211-219.

[7] Wongcharee K. and Eiamsa-ard S. “Friction and Heat Transfer Characteristics of Laminar Swirl Flow Through the Round Tubes Inserted with Alternate Clockwise and Counter-Clockwise Twisted-Tapes” **Int. Commun. Heat Mass Transfer.**, Vol. 38, 2011. pp. 348–352.

[8] Hejazi V., Akhavan-Behabadi M.A. and Afshari A. “Experimental Investigation of Twisted Tape Inserts Performance on Condensation Heat Transfer Enhancement and Pressure Drop” **Int. Commun. Heat Mass Transfer.**, Vol. 37, 2010. pp. 1376–1387.

[9] Eiamsa-ard S., Thianpong C. and Eiamsa-ard P. “Turbulent Heat Transfer Enhancement by Counter/Co-Swirling Flow in a Tube Fitted with Twin Twisted Tapes” **Exp. Therm. Fluid Sci.**, Vol. 34, 2010. pp. 53–62.

[10] Eiamsa-ard S., Wongcharee K., Eiamsa-ard P. and Thianpong C. “Heat Transfer Enhancement in a Tube Using Delta-Winglet Twisted Tape Inserts” **Appl. Therm. Eng.**, Vol. 30, 2010. pp. 310–318.

[11] Eiamsa-ard S. and Promvonge P. “Performance Assessment in a Heat Exchanger Tube with Alternate Clockwise and Counter-Clockwise Twisted-Tape Inserts” **Int. J. Heat Mass Transfer.**, Vol. 53, 2010. pp. 1354–1372.

[12] Eiamsa-ard S., Thianpong C., Eiamsa-ard P. Promvonge P. “Thermal Characteristics in a Heat Exchanger Tube Fitted with Dual Twisted Tape Elements in Tandem” **Int. Commun. Heat Mass Transfer.**, Vol. 37, 2010. pp. 39–46.

[13] . Eiamsa-ard S., Thianpong C., Eiamsa-ard P. Promvonge P. “Convective Heat Transfer in a Circular Tube with Short-Length Twisted Tape Insert” **Int. Commun. Heat Mass Transfer.**, Vol. 36, 2009. pp. 365–371.

[14] Nanan K., Thianpong C., Promvonge P. and Eiamsa-ard S. “Investigation of Heat Transfer Enhancement by Perforated Helical Twisted-Tapes” **Int. Commun. Heat Mass Transfer.**, Vol. 52, 2014. pp. 106–112.

[15] Nanan K., Yongsiri K., Wongcharee K., Thianpong C. and Eiamsa-ard S.. “Heat Transfer Enhancement by Helically Twisted Tapes Inducing Co- and Counter-Swirl Flows” **Int. Commun. Heat Mass Transfer.**, Vol. 46, 2013. pp. 67–73.

[16] Bhuiya M.M.K., Sayem A.S.M., Islam M., Chowdhury M.S.U. and Shahabuddin M. “Performance Assessment in a Heat Exchanger Tube Fitted with Double Counter Twisted Tape Inserts” **Int. Commun. Heat Mass Transfer.**, Vol. 50, 2014. pp. 25–33.

[17] Bhuiya M.M.K., Chowdhury M.S.U., Saha M. and Islam M.T. “Heat Transfer and Friction Factor Characteristics in Turbulent Flow Through a Tube Fitted with Perforated Twisted Tape Inserts” **Int. Commun. Heat Mass Transfer.**, Vol. 46, 2013. pp. 49–57.

[18] Bhuiya M.M.K., Chowdhury M.S.U., Shahabuddin M, Saha M. and Memon L.A. “Thermal Characteristics in a Heat Exchanger Tube Fitted with Triple Twisted Tape Inserts” **Int. Commun. Heat Mass Transfer.**, Vol. 48, 2013. pp. 124–132.

[19] Chang S.W. and Guo M.H. “Thermal Performances of Enhanced Smooth and Spiky Twisted Tapes for Laminar and Turbulent Tubular Flows” **Int. J. Heat Mass Transfer.**, Vol. 55, 2012. pp. 7651–7667.

[20] Murugesan P., Mayilsamy K. and Suresh S. “Turbulent Heat Transfer and Pressure Drop in Tube Fitted with Square-Cut Twisted Tape” **Chem. Eng. Process.**, Vol. 18, 2010. pp. 609-617.

[21] Murugesan P., Mayilsamy K. and Suresh S. “Heat Transfer and Friction Factor Studies in a Circular Tube Fitted with Twisted Tape Consisting of Wire-Nails” **Chem. Eng. Process.**, Vol. 18, 2010. pp. 1038-1042.

[22] Seemawute P. and Eiamsa-ard S. “Thermohydraulics of Turbulent Flow Through a Round Tube by a Peripherally-Cut Twisted Tape with an Alternate Axis” **Int. Commun. Heat Mass Transfer.**, Vol. 37, 2010. pp. 652–659.

[23] Eiamsa-ard S. and Promvonge P. “Thermal Characteristics in Round Tube Fitted with Serrated Twisted Tape” **Appl. Therm. Eng.**, Vol. 30, 2010. pp. 1673–1682.

[24] Eiamsa-ard S., Seemawute P. and Wongcharee K. “Influences of Peripherally-Cut Twisted Tape Insert on Heat Transfer and Thermal Performance Characteristics in Laminar and Turbulent Tube Flows” **Exp. Therm. Fluid Sci.**, Vol. 34, 2010. pp. 711–719.

[25] Chang S.W., Jan Y.J. and Liou J.S. “Turbulent Heat Transfer and Pressure Drop in Tube Fitted with Serrated Twisted Tape” **Int. J. Therm. Sci.**, Vol. 46, 2007. 506–518.

[26] Chang S.W., Yang T.L. and Liou J.S. “Heat Transfer and Pressure Drop in Tube with Broken Twisted Tape Insert” **Exp. Therm. Fluid Sci.**, Vol. 32, 2007. pp. 489–501

[27] Eiamsa-ard S. and Wongcharee K. “Heat Transfer Characteristics in Micro-Fin Tube Equipped with Double Twisted Tapes: Effect of Twisted Tape and Micro-Fin Tube Arrangements” **Journal of Hydrodynamics.**, Vol. 25, 2013. pp. 205–214.

[28] Eiamsa-ard S., Kongkaitpaiboon V. and Nanan K. “Thermohydraulics of Turbulent Flow Through Heat Exchanger Tubes Fitted with Circular-rings and Twisted Tapes” **Chin. J. Chem. Eng.**, Vol. 21, 2013. pp. 585–593.

[29] Nagarajan P.K., Mukkamala Y. and Sivashanmugam P. “Studies on Heat Transfer and Friction Factor Characteristics of Turbulent Flow Through a Micro-Finned Tube Fitted with Left-Right Inserts” **Appl. Therm. Eng.**, Vol. 30, 2010. pp. 1666–1672.

[30] Eiamsa-ard S., Nivesrangsan P., Chokphoemphun S. and Promvonge P. “Influence of Combined Non-Uniform Wire Coil and Twisted Tape Inserts on Thermal Performance Characteristics” **Int. Commun. Heat Mass Transfer.**, Vol. 37, 2010. pp. 850–856.

[31] Promvonge P. “Thermal Augmentation in Circular Tube with Twisted Tape and Wire Coil Turbulators” **Energy Convers. Manage.**, Vol. 49, 2008. pp. 2949–2955.

[32] Promvonge P. and Eiamsa-ard S. “Heat Transfer Behaviors in a Tube with Combined Conical-Ring and Twisted-Tape Insert” **Int. Commun. Heat Mass Transfer.**, Vol. 34, 2007. pp. 849–859.

[33] Promvonge P., Pethkool S., Pimsarn M. and Thianpong C. “Heat Transfer Augmentation in a Helical-Ribbed Tube with Double Twisted Tape Inserts” **Int. Commun. Heat Mass Transfer.**, Vol. 39, 2012. pp. 953–959.

[34] Thianpong C., Eiamsa-ard P., Wongcharee K. and Eiamsa-ard S. "Compound Heat Transfer Enhancement of a Dimpled Tube with a Twisted Tape Swirl Generator" **Int. Commun. Heat Mass Transfer.**, Vol. 36, 2009. pp. 698–704.

[35] Bharadwaj P., Khondge A.D. and Date A.W. "Heat Transfer and Pressure Drop in a Spirally Grooved Tube with Twisted Tape Insert" **Int. J. Heat Mass Transfer.**, Vol. 52, 2009. pp. 1938–1944

[36] Mengna H., Xianhe D., Kuo H. and Zhiwu L. "Compound Heat Transfer Enhancement of a Converging-Diverging Tube with Evenly Spaced Twisted-Tapes" **Chin. J. Chem. Eng.**, Vol. 15, 2007. pp. 814–820.

[37] Naik M.T., Fahad S.S., Sundar L.S. and Singh M.K. "Comparative Study on Thermal Performance of Twisted Tape and Wire Coil Inserts in Turbulent Flow Using CuO/Water Nanofluid" **Exp. Therm. Fluid Sci.**, Vol. 57, 2014. pp. 65–76.

[38] Azmi W.H., Sharma K.V., Sarma P.K., Mamat R. and Anuar S. "Comparison of Convective Heat Transfer Coefficient and Friction Factor of TiO_2 Nanofluid Flow in a Tube with Twisted Tape Inserts" **Int. J. Therm. Sci.**, Vol. 81, 2014. pp. 84–93.

[39] Esmaeilzadeh E., Almohammadi H., Nokhosteen A., Motezaker A. and Omrani A.N. "Study on Heat Transfer and Friction Factor Characteristics of γ-Al_2O_3/Water Through Circular Tube with Twisted Tape Inserts with Different Thicknesses" **Int. J. Therm. Sci.**, Vol. 82, 2014. pp. 72–83.

[40] Wongcharee K. and Eiamsa-ard S. "Heat Transfer Enhancement by Using CuO/Water Nanofluid in Corrugated Tube Equipped with Twisted Tape" **Int. Commun. Heat Mass Transfer.**, Vol. 39, 2012. pp. 251–257.

[41] Eiamsa-ard S. and Wongcharee K. "Single-Phase Heat Transfer of CuO/Water Nanofluids in Micro-Fin Tube Equipped with Dual Twisted-Tapes" **Int. Commun. Heat Mass Transfer.**, Vol. 39, 2012. pp. 1453–1459.

[42] Promvonge P., Koolnapadol N., Pimsarn M. and Thianpong C. "Thermal Performance Enhancement in a Heat Exchanger Tube Fitted with Inclined Vortex Rings" **Appl. Therm. Eng.**, Vol. 62, 2014. pp. 285–292.

[43] Thianpong C., Yongsiri K., Nanan K. and Eiamsa-ard S. "Thermal Performance Evaluation of Heat Exchangers Fitted with Twisted-Ring Turbulators" **Int. Commun. Heat Mass Transfer.**, Vol. 39, 2012. pp. 861–868.

[44] Eiamsa-ard S. and Promvonge P. "Influence of Double-sided Delta-Wing Tape Insert with Alternate-Axes on Flow and Heat Transfer Characteristics in a Heat Exchanger Tube" **Chin. J. Chem. Eng.**, Vol. 19, 2011. pp. 410–423.

[45] Eiamsa-ard S. and Promvonge P. "Thermal Characterization of Turbulent Tube Flows Over Diamond-Shaped Elements in Tandem" **Int. J. Therm. Sci.**, Vol. 49, 2010. pp. 1051–1062.

[46] Lee M.S., Jeong S.S., Ahn S.W. and Han J.C. "Effects of Angled Ribs on Turbulent Heat Transfer and Friction Factors in a Rectangular Divergent Channel" **Int. J. Therm. Sci.**, Vol. 84, 2014. pp. 1–8.

[47] Liu J., Gao J., Gao T. and Shi X. "Heat Transfer Characteristics in Steam-Cooled Rectangular Channels with Two Opposite Rib-Roughened Walls" **Appl. Therm. Eng.**, Vol. 50, 2013. pp. 104–111.

[48] Tang X.Y. and Zhu D.S. "Flow Structure and Heat Transfer in a Narrow Rectangular Channel with Different Discrete Rib Arrays" **Chem. Eng. Process.**, Vol. 69, 2013. pp. 1-14.

[49] Shui L., Gao J., Shi X. and Liu J. "Effect of Duct Aspect Ratio on Heat Transfer and Friction in Steam-Cooled Ducts with 60° Angled Rib Turbulators" **Exp. Therm. Fluid Sci.**, Vol. 49, 2013. pp. 123–134.

[50] Xie G., Zheng S., Zhang W. Sundén B. "A Numerical Study of Flow Structure and Heat Transfer in a Square Channel with Ribs Combined Downstream Half-Size or Same-Size Ribs" **Appl. Therm. Eng.**, Vol. 61, 2013. pp. 289–300.

[51] Karwa R. and Chitoshiya G. "Performance Study of Solar Air Heater Having V-Down Discrete Ribs on Absorber Plate" **Energy**, Vol. 55, 2013. pp. 939-955.

[52] Sriromreun P., Thianpong C. and Promvonge P. "Experimental and Numerical Study on Heat Transfer Enhancement in a Channel with Z-Shaped Baffles" **Int. Commun. Heat Mass Transfer.**, Vol. 39, 2012. pp. 945–952.

[53] Promvonge P., Skullong S., Kwankaomeng S. and Thianpong C. "Heat Transfer in Square Duct Fitted Diagonally with Angle-Finned Tape—Part 1: Experimental Study" **Int. Commun. Heat Mass Transfer.**, Vol. 39, 2012. pp. 617–624.

[54] Promvonge P., Skullong S., Kwankaomeng S. and Thianpong C. "Heat Transfer in Square Duct Fitted Diagonally with Angle-Finned Tape—Part 2: Numerical Study" **Int. Commun. Heat Mass Transfer.**, Vol. 39, 2012. pp. 625–633.

[55] Promvonge P., Jedsadaratanachai W., Kwankaomeng S. and Thianpong C. "3D Simulation of Laminar Flow and Heat Transfer in V-Baffled Square Channel" **Int. Commun. Heat Mass Transfer.**, Vol. 39, 2012. pp. 85–93.

[56] Promvonge P., Changcharoen W., Kwankaomeng S. and Thianpong C. "Numerical Heat Transfer Study of Turbulent Square-Duct Flow Through Inline V-Shaped Discrete Ribs" **Int. Commun. Heat Mass Transfer.**, Vol. 38, 2011. pp. 1392–1399.

[57] Jedsadaratanachai W., Suwannapan S. and Promvonge P. "Numerical Study of Laminar Heat Transfer in Baffled Square Channel with Various Pitches" **Energy Procedia.**, Vol. 9, 2011. pp 630–642.

[58] Peng W., Jiang P.X., Wang Y.P. and Wei B.Y. "Experimental and Numerical Investigation of Convection Heat Transfer in Channels with Different Types of Ribs" **Appl. Therm. Eng.**, Vol. 31, 2011. pp. 2702–2708.

[59] Singh S., Chander S. and Saini J.S. “Heat Transfer and Friction Factor Correlations of Solar Air Heater Ducts Artificially Roughened with Discrete V-Down Ribs” **Energy.**, Vol. 36, 2011. pp 5053-5064.

[60] Lanjewar A., Bhagoria J.L. and Sarviya R.M. “Heat Transfer and Friction in Solar Air Heater Duct with W-Shaped Rib Roughness on Absorber Plate” **Energy.**, Vol. 36, 2011. pp 4531-4541.

[61] Tanda G. “Effect of Rib Spacing on Heat Transfer and Friction in a Rectangular Channel with 45° Angled Rib Turbulators on One/Two Walls” **Int. J. Heat Mass Transfer.**, Vol. 54, 2011. pp. 1081–1090.

[62] Promvonge P. “Heat Transfer and Pressure Drop in a Channel with Multiple 60° V-Baffles” **Int. Commun. Heat Mass Transfer.**, Vol. 37, 2010. pp. 835–840.

[63] Hans V.S., Saini R.P. and Saini J.S. “Heat Transfer and Friction Factor Correlations For a Solar Air Heater Duct Roughened Artificially with Multiple V-Ribs” **Solar Energy.**, Vol. 84, 2010. pp. 898–911.

[64] Song W.M., Meng J.A. and Li Z.X. “Numerical Study of Air-Side Performance of a Finned Flat Tube Heat Exchanger with Crossed Discrete Double Inclined Ribs” **Appl. Therm. Eng.**, Vol. 30, 2010. pp. 1797–1804.

[65] Promvonge P. and Kwankaomeng S. “Periodic Laminar Flow and Heat Transfer in a Channel with 45° Staggered V-Baffles” **Int. Commun. Heat Mass Transfer.**, Vol. 37, 2010. pp. 841–849.

[66] Kwankaomeng S. and Promvonge P. “Numerical Prediction on Laminar Heat Transfer in Square Duct with 30° Angled Baffle on One Wall” **Int. Commun. Heat Mass Transfer.**, Vol. 37, 2010. pp. 857–866.

[67] Promvonge P., Sripattanapipat S. and Kwankaomeng S. “Laminar Periodic Flow and Heat Transfer in Square Channel with 45° Inline Baffles on Two Opposite Walls” **Int. J. Therm. Sci.**, Vol. 49, 2010. pp. 963–975.

[68] Promvonge P., Sripattanapipat S., Tamna S., Kwankaomeng S. and Thianpong C. “Numerical Investigation of Laminar Heat Transfer in a Square Channel with 45° Inclined Baffles” **Int. Commun. Heat Mass Transfer.**, Vol. 37, 2010. pp. 170–177.

[69] Promvonge P., Jedsadaratanachai W. and Kwankaomeng S. “Numerical Study of Laminar Flow and Heat Transfer in Square Channel with 30° Inline Angled Baffle Turbulators” **Appl. Therm. Eng.**, Vol. 30, 2010. pp. 1292–1303.

[70] Thianpong C., Chompookham T., Skullong S. and Promvonge P. “Thermal Characterization of Turbulent Flow in a Channel with Isosceles Triangular Ribs” **Int. Commun. Heat Mass Transfer.**, Vol. 36, 2009. pp. 712–717.

[71] Aharwal K.R., Gandhi B.K. and Saini J.S. “Heat Transfer and Friction Characteristics of Solar Air Heater Ducts Having Integral Inclined Discrete Ribs on Absorber Plate” **Int. J. Heat Mass Transfer.**, Vol. 52, 2009. pp. 5970–5977.

[72] Karwa R. and Maheshwari B.K. “Heat Transfer and Friction in an Asymmetrically Heated Rectangular Duct with Half and Fully Perforated Baffles at Different Pitches” **Int. Commun. Heat Mass Transfer.**, Vol. 36, 2009. pp. 264–268.

[73] Islam M.D., Oyakawa K., Yaga M. and Kubo I. “The Effects of Duct Height on Heat Transfer Enhancement of a Co-Rotating Type Rectangular Finned Surface in Duct” **Exp. Therm. Fluid Sci.**, Vol. 33, 2009. pp. 348–356.

[74] SriHarsha V., Prabhu S.V. and Vedula R.P. “Influence of Rib Height on the Local Heat Transfer Distribution and Pressure Drop in a Square Channel with 90° Continuous and 60° V-Broken Ribs” **Appl. Therm. Eng.**, Vol. 29, 2009. pp. 2444–2459.

[75] Sripattanapipat S. and Promvonge P. “Numerical Analysis of Laminar Heat Transfer in a Channel with Diamond-Shaped Baffles” **Int. Commun. Heat Mass Transfer.**, Vol. 36, 2009. pp. 32–38.

[76] Kamali R. and Binesh A.R. “The Importance of Rib Shape Effects on the Local Heat Transfer and Flow Friction Characteristics of Square Ducts with Ribbed Internal Surfaces” **Int. Commun. Heat Mass Transfer.**, Vol. 35, 2008. pp. 1032–1040.

[77] Gupta A., SriHarsha V., Prabhu S.V. and Vedula R.P. “Local Heat Transfer Distribution in a Square Channel with 90° Continuous, 90° Saw Tooth Profiled and 60° Broken Ribs” **Exp. Therm. Fluid Sci.**, Vol. 32, 2008. pp. 997–1010.

[78] Aharwal R.K., Gandhi B.K. and Saini J.S. “Experimental Investigation on Heat-Transfer Enhancement Due to a Gap in an Inclined Continuous Rib Arrangement in a Rectangular Duct of Solar Air Heater” **Renewable Energy.**, Vol. 33, 2008. pp. 585–596.

[79] Promvonge P. and Thianpong C. “Thermal Performance Assessment of Turbulent Channel Flows Over Different Shaped Ribs” **Int. Commun. Heat Mass Transfer.**, Vol. 35, 2008. pp. 1327–1334.

[80] Khan R.K., Ali M. A.T. and Akhanda M.A.R. “Heat Transfer Augmentation in Developing Flow Through a Ribbed Square Duct” **J. of Therm. Sci.**, Vol.15, 2006. pp. 251-256.

[81] Dutta P. and Hossain A. “Internal Cooling Augmentation in Rectangular Channel Using Two Inclined Baffles” **Int. J. Heat and Fluid Flow.**, Vol. 26 2005. pp. 223–232.

[82] Chandra P.R., Alexander C.R. and Han J.C. “Heat Transfer and Friction Behaviors in Rectangular Channels with Varying Number of Ribbed Walls” **Int. J. Heat Mass Transfer.**, Vol. 46, 2003. pp. 481–495.

[83] Momin A.M.E., Saini J.S. and Solanki S.C. “Heat Transfer and Friction in Solar Air Heater Duct With V-Shaped Rib Roughness on Absorber Plate” **Int. J. Heat Mass Transfer.**, Vol. 45, 2002. pp. 3383–3396.

[84] Murata A. and Mochizuki S. “Comparison Between Laminar and Turbulent Heat Transfer in a Stationary Square Duct with Transverse or Angled Rib Turbulators” **Int. J. Heat Mass Transfer.**, Vol. 44, 2001. pp. 1127–1141.

[85] Tsia J.P. and Hwang J.J. “Measurements of Heat Transfer and Fluid Flow in a Rectangular Duct with Alternate Attached-Detached Rib-arrays” **Int. J. Heat Mass Transfer.**, Vol. 42, 1999. pp. 2071–2083.

[86] Skullong S. and Promvonge P. “Experimental Investigation on Turbulent Convection in Solar Air Heater Channel Fitted with Delta Winglet Vortex Generator” **Chin. J. Chem. Eng.**, Vol. 22, 2014. pp. 1–10.

[87] Zhou G. and Ye Q. “Experimental Investigations of Thermal and Flow Characteristics of Curved Trapezoidal Winglet Type Vortex Generators” **Appl. Therm. Eng.**, Vol. 37, 2012. pp. 241–248.

[88] Min C., Qi C., Kong X. and Dong J. “Experimental Study of Rectangular Channel with Modified Rectangular Longitudinal Vortex Generators” **Int. J. Heat Mass Transfer.**, Vol. 53, 2010. pp. 3023–3029.

[89] Promvonge P., Khanoknaiyakarn C., Kwankaomeng S. and Thianpong C. “Thermal Behavior in Solar Air Heater Channel Fitted with Combined Rib and Delta-Winglet” **Int. Commun. Heat Mass Transfer.**, Vol. 38, 2011. pp. 749–756.

[90] Promvonge P., Chompookham T., Kwankaomeng S. and Thianpong C. “Enhanced Heat transfer in a Triangular Ribbed Channel with Longitudinal Vortex Generators” **Energy Convers. Manage.**, Vol. 51, 2010. pp. 1242–1249.

[91] Chompookham T., Thianpong C., Kwankaomeng S. and Promvonge P. “Heat Transfer Augmentation in a Wedge-Ribbed Channel Using Winglet Vortex Generators” **Int. Commun. Heat Mass Transfer.**, Vol. 37, 2010. pp. 163–169.

[92] Alam T., Saini R.P. and Saini J.S. “Heat and Flow Characteristics of Air Heater Ducts Provided with Turbulators-A Review” **Renew Energy.**, Vol. 31, 2014. pp. 289–304.

[93] Skullong S., Kwankaomeng S., Thianpong C. and Promvonge P. “Thermal Performance of Turbulent Flow in a Solar Air Heater Channel with Rib-Groove Turbulators” **Int. Commun. Heat Mass Transfer.**, Vol. 50, 2014. pp. 34–43.

[94] Mohammed H.A., Al-Shamani A.N. and Sheriff J.M. “Thermal and Hydraulic Characteristics of Turbulent Nanofluids Flow in a Rib–Groove Channel” **Int. Commun. Heat Mass Transfer.**, Vol. 39, 2012. pp. 1584–1594.

[95] Eiamsa-ard S. and Promvonge P. “Thermal Characteristics of Turbulent Rib-Grooved Channel Flows” **Int. Commun. Heat Mass Transfer.**, Vol. 36, 2009. pp. 705–711.

[96] Promvonge P. and Eiamsa-ard S. “Numerical Study on Heat Transfer of Turbulent Channel Flow Over Periodic Grooves” **Int. Commun. Heat Mass Transfer.**, Vol. 35, 2008. pp. 844–852.

[97] Parsazadeh M., Mohammed H.A. and Fathinia F. “Influence of Nanofluid on Turbulent Forced Convective Flow in a Channel with Detached Rib-Arrays” **Int. Commun. Heat Mass Transfer.**, Vol. 46, 2013. pp. 97–105.

[98] Nassan T.H., Heris S.Z. and Noie S.H. “A Comparison of Experimental Heat Transfer Characteristics for Al_2O_3/Water and CuO/Water Nanofluids in Square Cross-Section Duct” **Int. Commun. Heat Mass Transfer.**, Vol. 37, 2010. pp. 924–928.

[99] Bopche S.B. and Tandale M.S. “Experimental Investigations on Heat Transfer and Frictional Characteristics of a Turbulator Roughened Solar Air Heater Duct” **Int. J. Heat Mass Transfer.**, Vol. 52, 2009. pp. 2834–2848.

[100] Eiamsa-ard S., Koolnapadol N. and Promvonge P. “Heat Transfer Behavior in a Square Duct with Tandem Wire Coil Element Insert” **Chin. J. Chem. Eng.**, Vol. 20, 2012. pp. 863–869.

[101] Saha S.K. “Thermal and Friction Characteristics of Turbulent Flow Through Rectangular and Square Ducts with Transverse Ribs and Wire-Coil Inserts” **Exp. Therm. Fluid Sci.**, Vol. 34, 2010. pp. 575–589.

[102] Ray S. and Date A.W. “Friction and Heat Transfer Characteristics of Flow Through Square Duct with Twisted Tape Insert” **Int. J. Heat Mass Transfer.**, Vol. 46, 2003. pp. 889–902.

[103] Fox R.W. and McDonald A.M. **Introduction to Fluid Mechanics**. 5th ED. New York: John Wiley, 1998.

[104] Cengel, Y.A., Cimbala J.M. and Turner R.H. **Fundamentals of Thermal-Fluid Sciences**. 4th ED. Singapore: McGraw-Hill, 2012.

[105] Webb, R. L. **Principles of Enhanced Heat Transfer**., New York: John-Wiley & Sons, 1992.

[106] Montgomery D.C., Peck E.A. and Vining G.G. **Introduction to Linear Regression Analysis**. 5th ED. Hoboken, NJ: John Wiley, 2012.

[107] Sen A. and Srivastava M. **Regression Analysis: Theory, Methods, and Applications**. New York: Springer-Verlag, 1990.

[108] Montgomery D.C. **Design and Analysis of Experiments**. 8th ED. Hoboken, NJ: John Wiley, 2013.

[109] Incropera F., Dewitt P.D. **Introduction to Heat Transfer**. 5th ED. John Wiley & Sons Inc, 2006.

[110] ANSI/ASME, **Measurement Uncertainty**, PTC 19, 1–1985. Part I, 1986.

APPENDIX

Appendix A
Publications

International Journal

---

1. Pongjet Promvonge, **Supattarachai Suwannapan**, Monsak Pimsarn, Chinaruk Thianpong, “Experimental Study on Heat Transfer in Square Duct with Combined Twisted-Tape and Winglet Vortex Generators”, accepted by International Communications in Heat and Mass Transfer, 2014.
2. **Supattarachai Suwannapan**, Panuwat Hoonpong, Pongjet Promvonge, Sirisawat Juengjaroennirachon, Monsak Pimsarn, “Experimental Study on Flow Friction and Heat Transfer in a Square-Duct Heat Exchanger with Winglet Turbulators”, Advanced Materials Research, Vols. 931-932, 2014, pp. 1183-1187.
3. **Supattarachai Suwannapan**, Ratsak Poomsalood, Pongjet Promvonge, Withada Jedsadaratanachai, Thitipat Limkul, “Heat Transfer Improvement in a Square Duct with Diagonal Inclined Ribs”, Advanced Materials Research, Vols. 931-932, 2014, pp. 1144-1148.

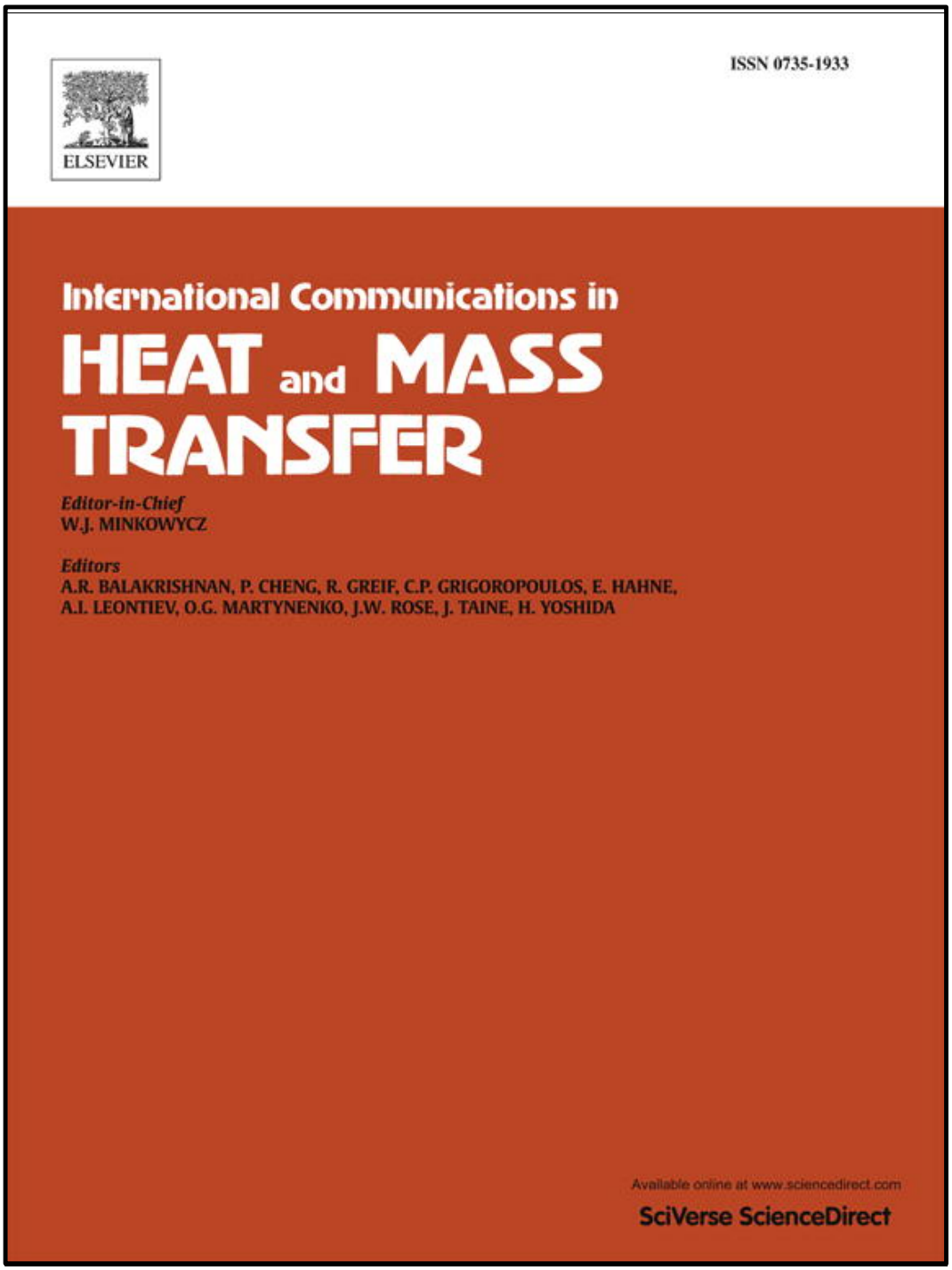
ISSN 0735-1933
ELSEVIER
International Communications in
HEAT and MASS
TRANSFER
Editor-in-Chief
W.J. MINKOWYCZ
Editors
A.R. BALAKRISHNAN, P. CHENG, R. GREIF, C.P. GRIGOROPOULOS, E. HAHNE,
A.I. LEONTIEV, O.G. MARTYNENKO, J.W. ROSE, J. TAINE, H. YOSHIDA
Available online at www.sciencedirect.com
SciVerse ScienceDirect

ARTICLE IN PRESS
ICHMT-03078; No of Pages 8
International Communications in Heat and Mass Transfer xxx (2014) xxx–xxx
Contents lists available at ScienceDirect
International Communications in Heat and Mass Transfer
journal homepage: www.elsevier.com/locate/ichmt

Experimental study on heat transfer in square duct with combined twisted-tape and winglet vortex generators ☆

Pongjet Promvonge *, Supattarachai Suwannapan [1], Monsak Pimsarn [1], Chinaruk Thianpong [1]

Department of Mechanical Engineering, Faculty of Engineering, King Mongkut's Institute of Technology Ladkrabang, Bangkok 10520, Thailand

ARTICLE INFO

Available online xxxx

Keywords:
Heat exchanger
Square duct
Twisted tape
Winglet
Vortex generators

ABSTRACT

The article presents an experimental investigation on thermal performance enhancement in a constant heat-fluxed square duct fitted with combined twisted-tape and winglet vortex generators. The experiments are carried out for the airflow rate through the tested square duct fitted with both the vortex generators for Reynolds number from 4000 to 30,000. The effect of the combined twisted tape and rectangular winglet inserts on heat transfer and pressure drop presented in terms of respective Nusselt number and friction factor is experimentally investigated. The characteristics of the combined twisted-tape and winglet include two twist ratios ($Y = 4$ and 5), three winglet- to duct-height ratios, ($R_B = 0.1$, 0.15 and 0.2), four winglet-pitch to tape-width ratios, ($R_P = 2$, 2.5, 4 and 5) and a single attack angle of winglet, $\alpha = 30°$. The experimental results reveal that the Nusselt number and friction factor for the combined twisted-tape and V-winglet increase with increasing R_B but decreasing R_P. The inserted duct at $R_B = 0.2$, $R_P = 2$ and $Y = 4$ provides the highest heat transfer rate and friction factor but the one at $R_B = 0.1$, $R_P = 2$ and $Y = 4$ yields the highest thermal performance. The application of combined vortex-flow devices gives thermal performance around 17% higher than the twisted tape alone.

1. Introduction

Many engineering techniques have been devised for enhancing the rate of convective heat transfer from the wall surface. One of the popular passive techniques for increasing thermal performance in cooling/heating duct systems is the application of vortex generators such as fins, baffles, ribs, twisted tapes, wire coils, winglets, etc. to thin or interrupt the boundary layer development in such ducts. Apart from enhancing the heat transfer rate, the insertion of the vortex generators also yields the substantial increase in pressure drop. Therefore, to achieve optimal thermal performance the pertinent parameters of the vortex generators are to be considered such as the blockage height, pitch spacing and angle of attack.

Several investigations have been made to examine the effect of the parameters of vortex generators on heat transfer and friction factor behaviors in tubes/ducts. Promvonge et al. [1,2] investigated experimentally and numerically the turbulent convection heat transfer in a square duct inserted diagonally with 30° angle-finned tapes. They indicated that the finned tapes with smaller fin pitch yielded the highest heat transfer and friction factor and the thermal performance for the finned-tape insert was much higher than that of the wire-coil/twisted-tape acting alone. Eiamsa-ard et al. [3] studied the influence of using the tandem wire-coil element inserts on thermal behaviors in a square duct and reported that the heat transfer and friction factor characteristics for the full-length wire-coil were higher than those for the tandem wire-coil elements. Promvonge et al. [4] examined numerically the heat transfer enhancement of turbulent flow through a square duct fitted with inline 60° discrete V-ribs on two opposite duct walls. Chompookham et al. [5] reported the application of combined ribs and winglet vortex generators (WVGs) to increase the heat transfer rate in a channel. They found that the heat transfer and flow friction behaviors for using the ribs in common with the WVGs were much higher than those for the ribs or the WVGs alone. Sri Harsha et al. [6] and Gupta et al. [7] investigated the local Nusselt number distribution and friction loss in a square duct fitted with various ribs and reported that the heat transfer augmentation by the 60° V-discrete ribs was higher than that by the 90° continuous and profiled ribs. Tanda [8] studied the heat transfer and flow friction characteristics in a rectangular duct by using the transverse, discrete ribs; angled, angled discrete ribs; V-shaped, V-shaped discrete ribs and parallel discrete ribs. Chandra et al. [9] conducted an experiment on the heat transfer rate and friction loss in a square channel fitted with continuous ribs placed on four channel walls and found the heat transfer augmentation rose with the increase in the number of ribbed walls. Murata and Mochizuki [10] examined the laminar and turbulent heat transfer distribution in a square duct with transverse or angled rib turbulators. Han et al. [11,12] carried out experiments on the heat transfer augmentation in a square channel with parallel, crossed, and V-shaped angled ribs on two opposite walls. Lau et al. [13] proposed the use of V-shaped rib arrays to increase the

☆ Communicated by W.J. Minkowycz

* Corresponding author. Tel.: +66 2 3298350, 51; fax: +66 2 3298352.
E-mail address: kppongje@kmitl.ac.th (S. Suwannapan).
[1] Tel.: +66 2 3298350, 51; fax: +66 2 3298352.

http://dx.doi.org/10.1016/j.icheatmasstransfer.2014.10.005
0735-1933/

Please cite this article as: P. Promvonge, et al., Experimental study on heat transfer in square duct with combined twisted-tape and winglet vortex generators, Int. Commun. Heat Mass Transf. (2014), http://dx.doi.org/10.1016/j.icheatmasstransfer.2014.10.005

Nomenclature

A	convection heat transfer area of duct, m^2
A_c	cross-sectional area, m^2
C_p	specific heat capacity of air, J/kgK
D_h	hydraulic diameter of duct (=H), m
e	winglet height, m
f	friction factor
H	duct height, m
h	average heat transfer coefficient, W/m^2K
k	thermal conductivity of air, W/mK
L	length of test duct, m
$\dot{m}$	mass flow rate of air, kg/s
Nu	Nusselt number
P	winglet pitch spacing, m
P_w	wetted perimeter of cross-section, m
ΔP	pressure drop, Pa
Pr	Prandtl number
R_B	winglet blockage ratio, e/H
Re	Reynolds number
R_P	winglet pitch ratio, P/w
Q	heat transfer, W
T	temperature, K
TT	twisted tape
t	thickness of winglet, m
U	mean velocity, m/s
w	tape width, m
Y	twist ratio, y/w
y	pitch length of twisted tape (180° rotation), m

Greek letters

α	attack angle of winglet, °
η	thermal enhancement factor, $(Nu/Nu_0)/(f/f_0)^{1/3}$
ν	kinematics viscosity, m^2/s
ρ	density of air, kg/m^3

Subscripts

b	bulk
0	smooth duct
conv	convection
i	inlet
o	outlet
bp	blowing power
s	duct surface

heat transfer rate of fully turbulent developed flow through a square channel.

For twisted-tapes (TT), several modified twisted tapes were presented with different types by targeting the increase in the heat transfer rate rather than the decrease of pressure loss due to low flow resistance of itself, for example, the perforated/serrated/jagged/broken twisted tapes and so on. Nanan et al. [14] and Eiamsa-ard et al. [15] reported the application of helical twisted-tapes can help increase the thermal performance in a circular tube at around 10–15% higher than that of twisted-tapes alone. Thianpong et al. [16] studied experimentally the use of twisted-rings to promote the heat transfer rate in a round tube and found that the heat transfer and friction factor tend to increase with increasing width ratio but with decreasing pitch ratio. Eiamsa-ard and Seemawute [17] examined experimentally and numerically the local heat transfer and friction behaviors in a circular tube inserted with short-length twisted tapes. Wongcharee and Eiamsa-ard [18] investigated thermal characteristics in a round tube with the insertion of twisted tapes with alternate-axes and triangular, rectangular and trapezoidal wings. Eiamsa-ard [19] carried out a measurement to examine the influence of multiple TT vortex generators on the heat transfer and fluid friction characteristics in turbulent channel flow. Eiamsa-ard et al. [20–22] studied the thermal performance enhancement in a round tube with short-length twisted tape, delta-winglet-cut twisted tape and peripherally-cut twisted tape inserts and indicated that the winglet-cut twisted tape provided higher thermal performance and the peripherally-cut twisted tape produced more turbulence around the tube wall than the typical one. Rahimi et al. [23] experimentally and numerically investigated on heat transfer and friction factor characteristics in a tube with modified twisted tapes and concluded that the jagged twisted tape insert provides the highest thermal performance. Chang et al. [24,25] examined the turbulent heat transfer and pressure drop in a tube with serrated and broken twisted tapes. Eiamsa-ard and Promvonge [26] found that the heat transfer rate in a tube can be increased by serrated twisted tape inserts.

For twisted tapes in conjunction with other vortex generators, Promvonge et al. [27] investigated the turbulent convective heat transfer characteristics in a helical-ribbed tube fitted with twin twisted tapes and found that the co-swirling inserted tube performs much better than the ribbed/smooth tube alone. Eiamsa-ard et al. [28] examined thermal performance behaviors in a tube fitted with the combined devices between the twisted tape and constant/periodically varying wire coil pitch ratio. Promvonge and Eiamsa-ard [29] investigated experimentally the heat transfer and friction factor characteristics in a circular tube fitted with conical-ring and twisted-tape swirl generator. Bharadwaj et al. [30] studied experimentally the friction factor and heat transfer characteristics of water flow in a 75-start spirally grooved tube with twisted-tape inserts. Ray and Date [31] presented numerical prediction of characteristics of laminar and turbulent flow and heat transfer in a square duct with twisted tape inserts.

Most of the literature review above reveal that typical or modified twisted-tape vortex generators are often used in circular tubes to intensify fluid mixing between the central-core and the wall regions while fin/baffle/rib/winglet vortex generators are always employed in ducts/channels or flat surfaces to increase the degree of turbulence intensity. The combined twisted-tape and V-winglet has never been reported in the literature. In general, the twisted-tape vortex generator has low flow resistance and ease in manufacturing but lower vortex strength leading to lower thermal performance while the winglet vortex generator is superior to thermal performance due to the lowest penalty of pressure drop. Therefore, with consideration of the merits of both the vortex generators, a newly designed enhancement device by integrating the V-winglet into the twisted-tape is proposed and expected to provide higher swirl/vortex strength or turbulence intensity at the near-wall region from the V-winglet and stronger fluid mixing by transporting the fluid in the central-core to the near-wall regimes from using the twisted-tape and thus, improve heat transfer rate in the duct surface.

2. Experimental setup

2.1. Apparatus and vortex generator characteristics

A schematic diagram of the experimental apparatus is presented in Fig. 1 whereas the vortex generator types and the detail of combined twisted tape and rectangular V-winglet in a square duct are shown in Figs. 2 and 3, respectively. In Fig. 1, a circular pipe was connected between a high-pressure blower and a settling tank while an orifice flow meter was placed in this pipeline. The square duct connected to the other side of the settling tank had overall length of 3000 mm and was divided into two sections: calm section and test section. The test section duct made of 3 mm thick aluminum sheets having a cross section of $45 \times 45\ mm^2$ was 1000 mm long (L). In Fig. 2a, the twisted tape was made of aluminum sheet with its dimension of $42 \times 1200 \times 0.8\ mm^3$.

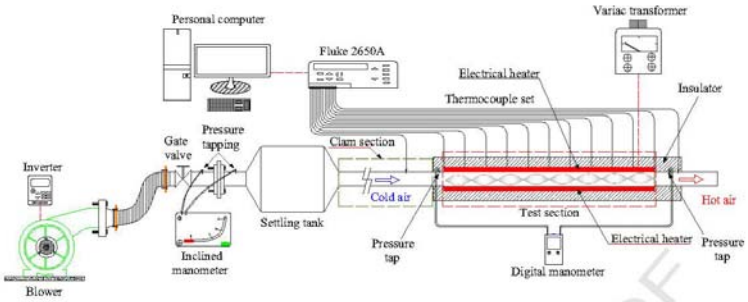

Fig. 1. Schematic diagram of experimental apparatus.

Two different twist-ratios of twisted tapes, $Y = y/w = 4$ and 5 were offered where twist ratio is defined as a ratio of twist length (y) in 180° rotation to tape width (w). The rectangular winglet made of 0.3 mm aluminum strip was formed in V-shape to become a V-winglet with a V-tip half angle of 30°. The V-winglet elements were attached on the two opposite edges of the twisted-tape by putting the V-tip of the element on the cut edges of the tape as shown in Fig. 2b and c. This arrangement would let the V-winglets place on the two opposite duct walls (2 W) for P = y or on the four walls (4 W) for P = y/2 as can be seen in Fig. 3. The three winglet sizes were 4.5, 6.75 and 9.0 mm high (e), equivalent to three winglet- to duct-height ratios, $R_e = e/H = 0.1$, 0.15 and 0.2, respectively and were placed on the tape edges to obtain four winglet-pitch to tape-width ratios ($R_P = P/w = 2$, 4 and 2.5, 5 for $Y = 4$ and 5, respectively) at $\alpha = 30°$.

2.2. Procedure and function

The test duct used in the present experiment was composed of the four heating walls. The AC power supply was the source of power for the plate-type heater employed for heating all the walls of test duct to maintain a uniform surface heat-flux. Air as the test fluid was directed into the systems by a 1.45 kW high-pressure blower. To achieve the desired airflow rates, the operating speed of the blower was controlled using an inverter. An orifice flowmeter was utilized to measure the airflow rate in the system. The temperature distributions along the test duct were measured by twenty-eight thermocouples fitted into the outer duct walls. The thermocouples were attached in holes drilled from the outer surface and centered of the duct walls with the respective junctions located within 1.5 mm of the inner wall surface with axial separation of about 100 mm apart. The inlet and outlet bulk temperatures were measured using two thermocouples located at the entry and the exit of the test duct. All thermocouples were type K, 1.5 mm diameter wire and their temperature signals were read by a data logger (Fluke 2650A) and recorded by a personal computer. A digital differential pressure was employed to measure the pressure drop across the test duct used for calculation of friction factor.

The uncertainty calculation was based on Ref. [32]. The maximum uncertainties of non-dimensional parameters were ±5% for Reynolds number, ±7% for Nusselt number and ±9% for friction factor.

3. Data processing

The present experiment was conducted to investigate the heat transfer enhancement in a square duct inserted with the combined twisted-tape and V-winglet. The results obtained are displayed in dimensionless terms of Nusselt number and friction factor. The average heat transfer coefficients are calculated by using the experimental data via the following equations:

$$Q_{air} = Q_{conv} = \dot{m} C_p (T_o - T_i) \quad (1)$$

$$h = \frac{Q_{conv}}{A(\bar{T}_s - T_b)} \quad (2)$$

in which,

$$T_b = (T_o + T_i)/2 \quad (3)$$

and

$$\bar{T}_s = \sum T_s/28 \quad (4)$$

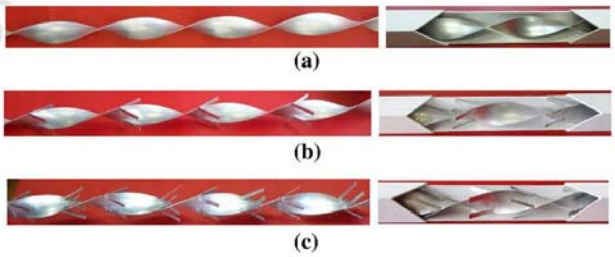

Fig. 2. Vortex generators: (a) type 1, twisted tape; (b) type 2, combined twisted-tape and V-winglets on two walls (2 W) and (c) type 3, combined twisted-tape and V-winglets on four walls (4 W).

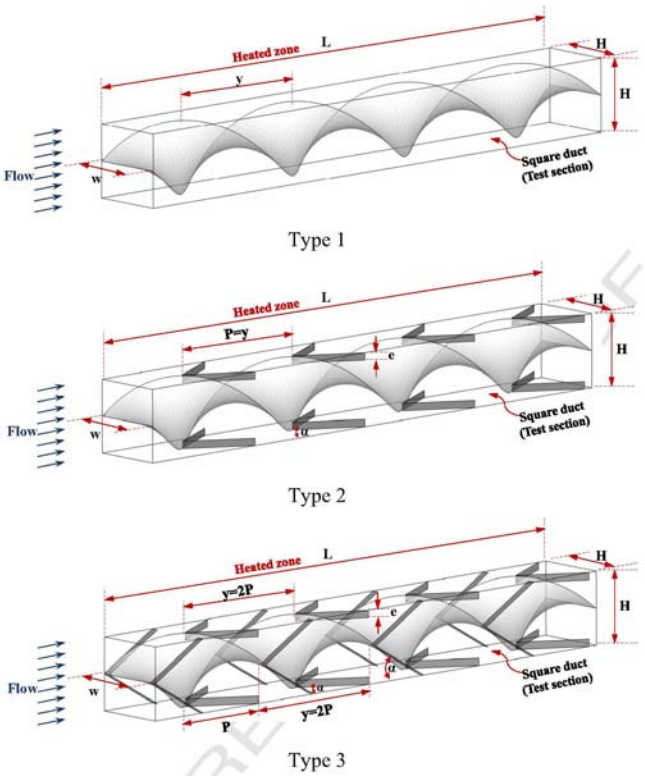

Fig. 3. Test section with various vortex generators.

where A is the heat transfer surface area of duct, T_s is the local surface temperature along the duct length, and $\bar{T}_s$ is the average surface temperature. Thus, the average Nusselt number is written as

$$\mathrm{Nu} = \frac{hD_h}{k} \tag{5}$$

The Reynolds number based on the duct hydraulic diameter (D_h) is given by

$$\mathrm{Re} = UD_h/\nu \tag{6}$$

The duct hydraulic diameter is defined by

$$D_h = \frac{4A_c}{P_w} = H \tag{7}$$

in which A_c is the cross sectional area and P_w is the wetted perimeter of the cross section.

The friction factor is evaluated by

$$f = \frac{2}{(L/D_h)}\frac{\Delta P}{\rho U^2} \tag{8}$$

where ΔP is the pressure drop across the test duct and U is the mean air velocity in the duct. All properties of air are evaluated at the overall bulk air temperature from Eq. (3).

The thermal enhancement factor (η) defined as the ratio of the heat transfer coefficient of an inserted duct, h to that of smooth duct, h_0, at a constant blowing power [33] is given by

$$\eta = \frac{h}{h_0}\Big|_{bp} = \frac{\mathrm{Nu}}{\mathrm{Nu}_0}\Big|_{bp} = \left(\frac{\mathrm{Nu}}{\mathrm{Nu}_0}\right)\left(\frac{f}{f_0}\right)^{-1/3} \tag{9}$$

4. Results and discussion

4.1. Validation of smooth square duct

The experimental results of Nusselt number and friction factor obtained from the present smooth duct are compared with those from correlations of Dittus–Boelter, Gnielinski, Blasius and Petukhov found in Ref. [34] for turbulent flow in ducts.

Dittus–Boelter's correlation,

$$\mathrm{Nu} = 0.023\mathrm{Re}^{0.8}\mathrm{Pr}^{0.4} \quad \text{for heating} \tag{10}$$

Gnielinski's correlation,

$$\mathrm{Nu} = \frac{(f/8)(\mathrm{Re}-1000)\,\mathrm{Pr}}{1+12.7(f/8)^{1/2}(\mathrm{Pr}^{2/3}-1)} \quad 3000 < \mathrm{Re} < 5\times10^{6} \tag{11}$$

Blasius's correlation,

$$f = 0.316\mathrm{Re}^{-0.25} \quad 3000 \le \mathrm{Re} \le 20{,}000 \tag{12}$$

Petukhov's correlation,

$$f = (0.79\ \ln \mathrm{Re} - 1.64)^{-2} \quad 3000 \le \mathrm{Re} \le 5\times10^{6} \tag{13}$$

The comparison of Nusselt number and friction factor obtained from the present smooth duct with those from correlations of Eqs. (10)–(13) is depicted in Fig. 4. It is seen in the figure that the present results are in good agreement within ±5% with the correlation data.

4.2. Heat transfer rate and pressure drop behaviors

The present results on the heat transfer and pressure drop in a uniform heat-fluxed square duct with combined twisted-tape and V-winglet inserts are, respectively, presented in terms of Nusselt number (Nu) and friction factor (f) against Reynolds number as depicted in Fig. 5a and b. In Fig. 5a, the inserted duct yields the considerable heat transfer enhancement with similar trend pattern in comparison with the smooth duct and thus, the Nu increases with the rise of Reynolds number. It is visible in Fig. 5b that the use of the combined vortex generators leads to a substantial increase in f above the smooth duct and the f shows the decreasing tendency with the increment of Reynolds number.

4.3. Effect of R_B and R_P on heat transfer

The Nusselt number ratio, $\mathrm{Nu}/\mathrm{Nu}_0$ plotted against Reynolds number and R_B values is displayed in Fig. 6a and b, respectively where the Nusselt number ratio, $\mathrm{Nu}/\mathrm{Nu}_0$, is defined as a ratio of the enhanced Nusselt number to Nusselt number of smooth duct. It is seen in the figure that the increment of R_B results in the increase in $\mathrm{Nu}/\mathrm{Nu}_0$ while that of R_P provides the reversing trend. This is because the effect of the vortex flows from the combined devices can help to increase the turbulence intensity and to transport the fluid from the central core to the near-wall regions. Also, the vortex flows can wash up the flow trapped in the duct corner regions normally act as ineffective heat transfer areas, leading to higher heat transfer rate in the duct.

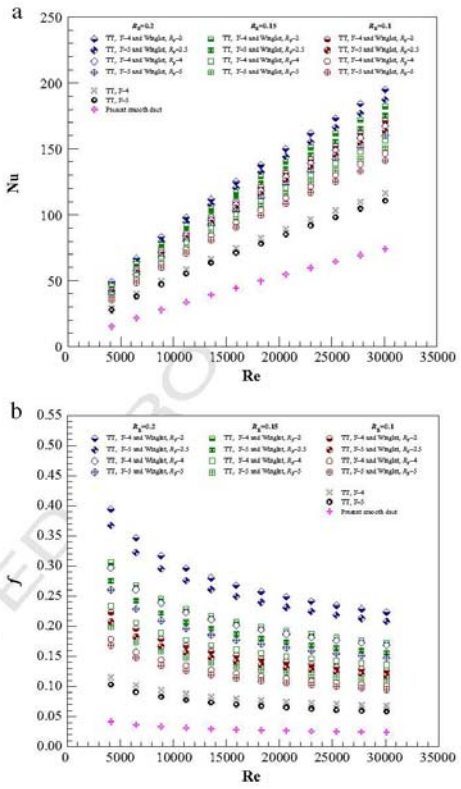

Fig. 5. Comparison of (a) Nu and (b) f with Re for various Y, R_B and R_P.

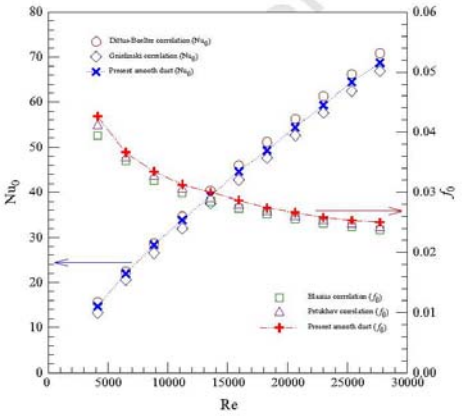

Fig. 4. Validation of Nu_0 and f_0 for smooth duct.

At a given R_P, the combined twisted-tape and V-winglet device provides the $\mathrm{Nu}/\mathrm{Nu}_0$ in the range of 2.16–3.22, 2.01–3.03 and 1.91–2.82 for $R_B = 0.2$, 0.15 and 0.1 while the TT alone yields the $\mathrm{Nu}/\mathrm{Nu}_0$ around 1.56–1.90 and 1.49–1.82 for $Y = 4$ and 5, respectively. This indicates that the heat transfer rate for the combined twisted-tape and V-winglet is around 40–44% higher than that for the TT alone. It is noted that the $\mathrm{Nu}/\mathrm{Nu}_0$ value for the combination of the $Y = 4$ twisted-tape and the $R_P = 2$ V-winglet with $R_B = 0.2$ is maximum around 5.9% and 12.2% above that with $R_B = 0.15$ and 0.1 while is about 3.9% higher than that of the $Y = 5$ twisted-tape and the $R_P = 2.5$ one. This can be attributed to the use of taller V-winglet with narrower pitch leading to stronger vortex strength of the flow and thus promoting high levels of mixing over the others. All the experimental data of $\mathrm{Nu}/\mathrm{Nu}_0$ are contained in Table 1 for comparison.

4.4. Effect of R_B and R_P on friction loss

The plot of friction factor ratio, f/f_0 against Reynolds number and R_B is, respectively, exhibited in Fig. 7a and b for various R_P values. It can be

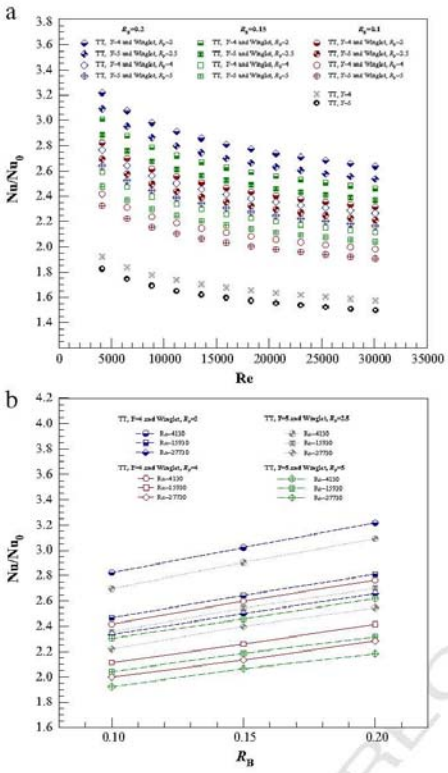

Fig. 6. Relationship of Nu/Nu_0 with (a) Re and (b) R_B.

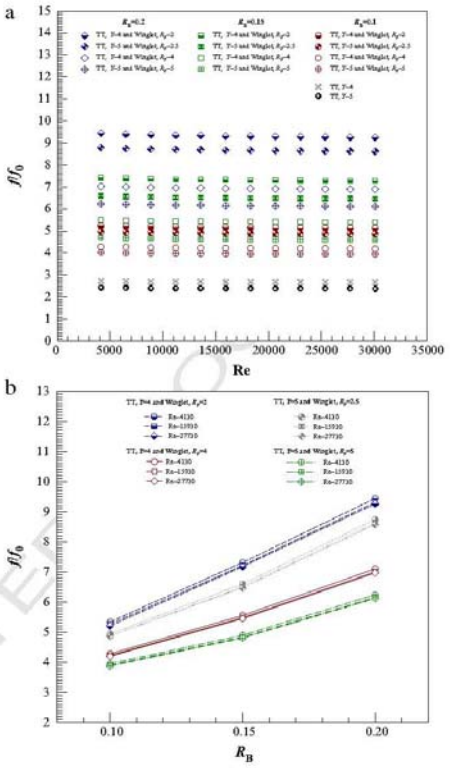

Fig. 7. Relationship of f/f_0 with (a) Re and (b) R_B.

observed in the figure that the f/f_0 for the inserted duct tends to increase considerably with rising R_B but with reducing R_P. However, the f/f_0 is found to slightly decrease with increasing Reynolds number or to be nearly independent of Reynolds number. The inserted duct at $R_B = 0.2$, $R_P = 2$ and $Y = 4$ provides the highest f/f_0 and the f/f_0 of the $R_B = 0.15$ is higher than that of the $R_B = 0.1$ at similar operating condition. This is because the use of $R_B = 0.2$, $R_P = 2$ and $Y = 4$, caused higher flow resistance, larger surface area and the reverse flow, leading to the substantial increase in pressure drop.

The f/f_0 for the combination of the $Y = 4$ twisted-tape and V-winglet is in the range of 6.11–9.44, 4.80–7.31 and 3.94–5.34 for $R_B = 0.2$, 0.15 and 0.1 while that for the TT alone at $Y = 4$ and 5 is about 2.57–2.62 and

Table 1
Experimental data for various vortex generators.

Vortex generators		Nu/Nu_0	f/f_0	η
Type 1: Twisted tape (TT) alone	$Y = 4$	1.56–1.90	2.57–2.62	1.13–1.38
	$Y = 5$	1.49–1.82	2.44–2.48	1.11–1.35
Type 2: Combined twisted tape and V-winglet on two walls (2 W), P = y	$R_P = Y = 4$, $R_B = 0.1$	1.98–2.42	4.20–4.28	1.23–1.49
	$R_P = Y = 4$, $R_B = 0.15$	2.10–2.58	5.26–5.37	1.21–1.47
	$R_P = Y = 4$, $R_B = 0.2$	2.27–2.76	6.96–7.10	1.19–1.44
	$R_P = Y = 5$, $R_B = 0.1$	1.91–2.33	3.94–4.02	1.21–1.46
	$R_P = Y = 5$, $R_B = 0.15$	2.01–2.44	4.80–4.90	1.20–1.45
	$R_P = Y = 5$, $R_B = 0.2$	2.16–2.64	6.11–6.24	1.18–1.43
Type 3: Combined twisted tape and V-winglet on four walls (4 W), P = y/2	$R_P = 2$, $Y = 4$, $R_B = 0.1$	2.32–2.82	5.23–5.34	1.33–1.62
	$R_P = 2$, $Y = 4$, $R_B = 0.15$	2.48–3.03	7.16–7.31	1.28–1.55
	$R_P = 2$, $Y = 4$, $R_B = 0.2$	2.64–3.22	9.25–9.44	1.26–1.52
	$R_P = 2.5$, $Y = 5$, $R_B = 0.1$	2.21–2.70	4.87–4.97	1.30–1.58
	$R_P = 2.5$, $Y = 5$, $R_B = 0.15$	2.37–2.88	6.47–6.60	1.27–1.54
	$R_P = 2.5$, $Y = 5$, $R_B = 0.2$	2.53–3.09	8.62–8.79	1.24–1.50

2.44–2.48, respectively. This means that the f/f_0 for the combined devices is about 2–4 times above that for the TT alone. It is noted that for the combined devices, the f/f_0 at $Y = 4$, $R_P = 2$ and $R_B = 0.2$ is around 22.5% and 43.4% above that at $Y = 4$, $R_P = 2$, $R_B = 0.15$ and 0.1, respectively and is about 6.9% higher than that at $Y = 5$, $R_P = 2.5$ and $R_B = 0.2$. Since the inserted duct with $Y = 4$, $R_P = 2$ and $R_B = 0.2$ has more the number of V-winglets than the others or the largest surface area, this gives rise to higher resistance of flow in duct. The experimental data of f/f_0 for all cases studied are also provided in Table 1.

4.5. Effect of R_B and R_P on thermal performance

Fig. 8 presents the influence of R_B and R_P values on thermal enhancement factor (η) for using the combined devices. The η value was obtained from comparison of the Nusselt number and friction factor ratios at similar blowing power as defined in Eq. (9). It is interesting to note in the figure that the η shows the downtrend pattern with the increment in Reynolds number for all cases investigated. The use of the newly designed vortex generator leads to much higher η than that of the TT alone for all cases indicating the advantage of the compound vortex-flow devices over the single one. The experimental data of the η values are also summarized in Table 1. It is seen that the maximum η is achieved for using the combined twisted-tape with $Y = 4$ and V-winglet at $R_B = 0.1$ and $R_P = 2$, and this case of Y, R_P and R_B values is considered to be the best operating condition in this investigation. The highest η is about 1.62 at the lowest Reynolds number and higher than the other cases around 2–17% depending on R_P and R_B values.

The Nu and f values obtained from the combined twisted-tape and V-winglet inserts correlated as functions of Re, Pr, R_B, R_P and Y are given in Table 2. These correlations of Nu and f for both the devices are valid for $R_B = 0.1$, 0.15 and 0.2; $R_P = 2$, 2.5, 4 and 5; and $Y = 4$ and 5 in the Re range from 4000 to 30,000.

The plots of Nusselt number and friction factor for the combined twisted-tape and V-winglet predicted by the equations given in Table 2 and measured data are portrayed in Fig. 9a and b, respectively. In the figure, the majority of both the data is within ±5% deviation for the Nu and f.

5. Conclusions

An experimental investigation on heat transfer and flow friction characteristics in a uniform heat-fluxed square duct with the combined twisted-tape and V-winglet inserts at different R_B and R_P for turbulent air flow, Reynolds number from 4000 to 30,000 has been conducted. The combined twisted-tape and V-winglet insert provides a significant effect on the change of flow direction in the duct leading to the considerable increase in both heat transfer and pressure drop. It is found that the maximum heat transfer rate and pressure drop from the combined devices are found at the largest R_B but at the smallest R_P and Y. The combined twisted-tape and V-winglet at $R_B = 0.2$, $R_P = 2$ and $Y = 4$,

Table 2
Correlations for various vortex generators.

Vortex generator types	Correlations
Type 1: Twisted tape (TT) alone	$Nu = 0.1368\ Re^{0.6976}\ Pr^{0.4}\ Y^{-0.2237}$
	$f = 1.6585Re^{-0.2860}Y^{-0.2423}$
Type 2: Combined twisted-tape and V-winglet on two walls (2 W), P = y	$Nu = 0.2691Re^{0.6976}\ Pr^{0.4}\ Y^{-0.2310}R_B^{0.1851}$
	$f = 16.3586Re^{-0.2860}Y^{-0.4263}R_B^{0.6710}$
Type 3: Combined twisted-tape and V-winglet on four walls (4 W), P = y/2	$Nu = 0.3084Re^{0.6976}\ Pr^{0.4}\ Y^{-0.2101}R_B^{0.1920}$
	$f = 26.1677Re^{-0.2860}Y^{-0.3661}R_B^{0.8168}$

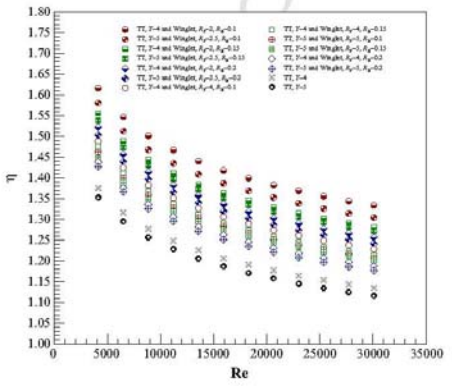

Fig. 8. Influence of combined twisted-tape and V-winglet on η.

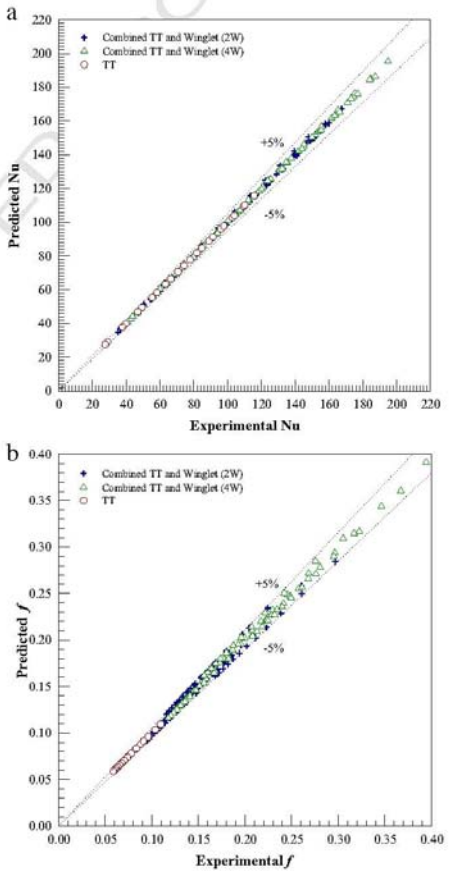

Fig. 9. Predicted data of (a) Nu and (b) f versus experimental data.

Please cite this article as: P. Promvonge, et al., Experimental study on heat transfer in square duct with combined twisted-tape and winglet vortex generators, Int. Commun. Heat Mass Transf. (2014), http://dx.doi.org/10.1016/j.icheatmasstransfer.2014.10.005

provides much higher Nu and f than the others. In thermal performance comparison, the $Y = 4$ twisted tape in conjunction with the V-winglet at $R_B = 0.1$ and $R_P = 2$ yields the highest thermal enhancement factor around 1.62 or about 17% above the twisted tape alone. Thus, the combined twisted-tape and V-winglet is a promising enhancement device to increase heat transfer in ducts with higher thermal performance.

Acknowledgment

The funding of this research is supported by the faculty of engineering, King Mongkut's Institute of Technology Ladkrabang (KMITL), Thailand.

References

[1] P. Promvonge, S. Skullong, S. Kwankaomeng, C. Thianpong, Heat transfer in square duct fitted diagonally with angle-finned tape—part 1: experimental study, Int. Commun. Heat Mass Transfer 39 (2012) 617–624.
[2] P. Promvonge, S. Skullong, S. Kwankaomeng, C. Thianpong, Heat transfer in square duct fitted diagonally with angle-finned tape—part 2: numerical study, Int. Commun. Heat Mass Transfer 39 (2012) 625–633.
[3] S. Eiamsa-ard, N. Koolnapadol, P. Promvonge, Heat transfer behavior in a square duct with tandem wire coil element insert, Chin. J. Chem. Eng. 20 (5) (2012) 863–869.
[4] P. Promvonge, W. Changcharoen, S. Kwankaomeng, C. Thianpong, Numerical heat transfer study of turbulent square-duct flow through inline V-shaped discrete ribs, Int. Commun. Heat Mass Transfer 38 (2011) 1392–1399.
[5] T. Chompookham, C. Thianpong, S. Kwankaomeng, P. Promvonge, Heat transfer augmentation in a wedge-ribbed channel using winglet vortex generators, Int. Commun. Heat Mass Transfer 37 (2010) 163–169.
[6] V. Sri Harsha, S.V. Prabhu, R.P. Vedula, Influence of rib height on the local heat transfer distribution and pressure drop in a square channel with 90° continuous and 60° V-broken ribs, Appl. Therm. Eng. 29 (11–12) (2009) 2444–2459.
[7] A. Gupta, V. SriHarsha, S.V. Prabhu, R.P. Vedula, Local heat transfer distribution in a square channel with 90° continuous, 90° saw tooth profiled and 60° broken ribs, Exp. Thermal Fluid Sci. 32 (2008) 997–1010.
[8] G. Tanda, Heat transfer in rectangular channels with transverse and V-shaped broken ribs, Int. J. Heat Mass Transf. 47 (2004) 229–243.
[9] P.R. Chandra, C.R. Alexander, J.C. Han, Heat transfer and friction behaviors in rectangular channels with varying number of ribbed walls, Int. J. Heat Mass Transf. 46 (2003) 481–495.
[10] A. Murata, S. Mochizuki, Comparison between laminar and turbulent heat transfer in a stationary square duct with transverse or angled rib turbulators, Int. J. Heat Mass Transf. 44 (2001) 1127–1141.
[11] J.C. Han, Y.M. Zhang, C.P. Lee, Influence of surface heat flux ratio on heat transfer augmentation in square channels with parallel, crossed, and V-shaped angled ribs, ASME J. Turbomach. 114 (1992) 872–880.
[12] J.C. Han, Y.M. Zhang, C.P. Lee, Augmented heat transfer in square channels with parallel, crossed and V-shaped angled ribs, J. Heat Transf. ASME DC 113 (1991) 590–596.
[13] S.C. Lau, R.T. Kukreja, R.D. McMillin, Effects of V-shaped rib arrays on turbulent heat transfer and friction of fully developed flow in a square channel, Int. J. Heat Mass Transf. 34 (7) (1991) 1605–1616.
[14] K. Nanan, C. Thianpong, P. Promvonge, S. Eiamsa-ard, Investigation of heat transfer enhancement by perforated helical twisted-tapes, Int. Commun. Heat Mass Transfer 52 (2014) 106–112.
[15] S. Eiamsa-ard, K. Yongsiri, K. Nanan, C. Thianpong, Heat transfer augmentation by helically twisted tapes as swirl and turbulence promoters, Chem. Eng. Process. 60 (2012) 42–48.
[16] C. Thianpong, K. Yongsiri, K. Nanan, S. Eiamsa-ard, Thermal performance evaluation of heat exchangers fitted with twisted-ring turbulators, Int. Commun. Heat Mass Transfer 39 (2012) 861–868.
[17] S. Eiamsa-ard, P. Seemawute, Decaying swirl flow in round tubes with short-length twisted tapes, Int. Commun. Heat Mass Transfer 39 (2012) 649–656.
[18] K. Wongcharee, S. Eiamsa-ard, Heat transfer enhancement by twisted tapes with alternate-axes and triangular, rectangular and trapezoidal wings, Chem. Eng. Process. 50 (2011) 211–219.
[19] S. Eiamsa-ard, Study on thermal and fluid flow characteristics in turbulent channel flows with multiple twisted tape vortex generators, Int. Commun. Heat Mass Transfer 31 (2010) 644–651.
[20] S. Eiamsa-ard, C. Thianpong, P. Eiamsa-ard, P. Promvonge, Convective heat transfer in a circular tube with short-length twisted tape insert, Int. Commun. Heat Mass Transfer 36 (2009) 365–371.
[21] S. Eiamsa-ard, K. Wongcharee, P. Eiamsa-ard, C. Thianpong, Heat transfer enhancement in a tube using delta-winglet twisted tape inserts, Appl. Therm. Eng. 30 (2010) 310–318.
[22] S. Eiamsa-ard, P. Seemawute, K. Wongcharee, Influences of peripherally-cut twisted tape insert on heat transfer and thermal performance characteristics in a laminar and turbulent tube flows, Exp. Thermal Fluid Sci. 34 (2010) 711–719.
[23] M. Rahimi, S.R. Shabanian, A.A. Alsairafi, Experimental and CFD studies on heat transfer and friction factor characteristics of a tube equipped with modified twisted tape inserts, Chem. Eng. Process. 48 (2009) 762–770.
[24] S.W. Chang, Y.J. Jan, J.S. Liou, Turbulent heat transfer and pressure drop in tube fitted with serrated twisted tape, Int. J. Therm. Sci. 46 (5) (2007) 506–518.
[25] S.W. Chang, T.L. Yang, J.S. Liou, Heat transfer and pressure drop in tube with broken twisted tape insert, Exp. Thermal Fluid Sci. 32 (2) (2007) 489–501.
[26] S. Eiamsa-ard, P. Promvonge, Thermal characteristics in round tube fitted with serrated twisted tape, Appl. Therm. Eng. 30 (2010) 1673–1682.
[27] P. Promvonge, S. Pethkool, M. Pimsarn, C. Thianpong, Heat transfer augmentation in a helical-ribbed tube with double twisted tape inserts, Int. Commun. Heat Mass Transfer 39 (2012) 953–959.
[28] S. Eiamsa-ard, P. Nivesrangsan, S. Chokphoemphun, P. Promvonge, Influence of combined non-uniform wire coil and twisted tape inserts on thermal performance characteristics, Int. Commun. Heat Mass Transfer 37 (2010) 850–856.
[29] P. Promvonge, S. Eiamsa-ard, Heat transfer behaviors in a tube with combined conical-ring and twisted-tape insert, Int. Commun. Heat Mass Transfer 34 (2007) 849–859.
[30] P. Bharadwaj, A.D. Khondge, A.W. Date, Heat transfer and pressure drop in a spirally grooved tube with twisted tape insert, Int. J. Heat Mass Transf. 52 (2009) 1938–1944.
[31] S. Ray, A.W. Date, Friction and heat transfer characteristics of flow through square duct with twisted tape insert, Int. J. Heat Mass Transf. 46 (2003) 889–902.
[32] ANSI/ASME, Measurement Uncertainty, PTC 19. 1–1985, Part I, USA, 1986.
[33] R.L. Webb, Performance evaluation criteria for use of enhanced heat transfer surfaces in heat exchanger design, Int. J. Heat Mass Transf. 24 (1981) 715–726.
[34] F.P. Incropera, P.D. Dewitt, T.L. Bergman, A.S. Lavine, Fundamental of Heat and Mass Transfer, John-Wiley & Sons Inc., 2006.

Please cite this article as: P. Promvonge, et al., Experimental study on heat transfer in square duct with combined twisted-tape and winglet vortex generators, Int. Commun. Heat Mass Transf. (2014), http://dx.doi.org/10.1016/j.icheatmasstransfer.2014.10.005

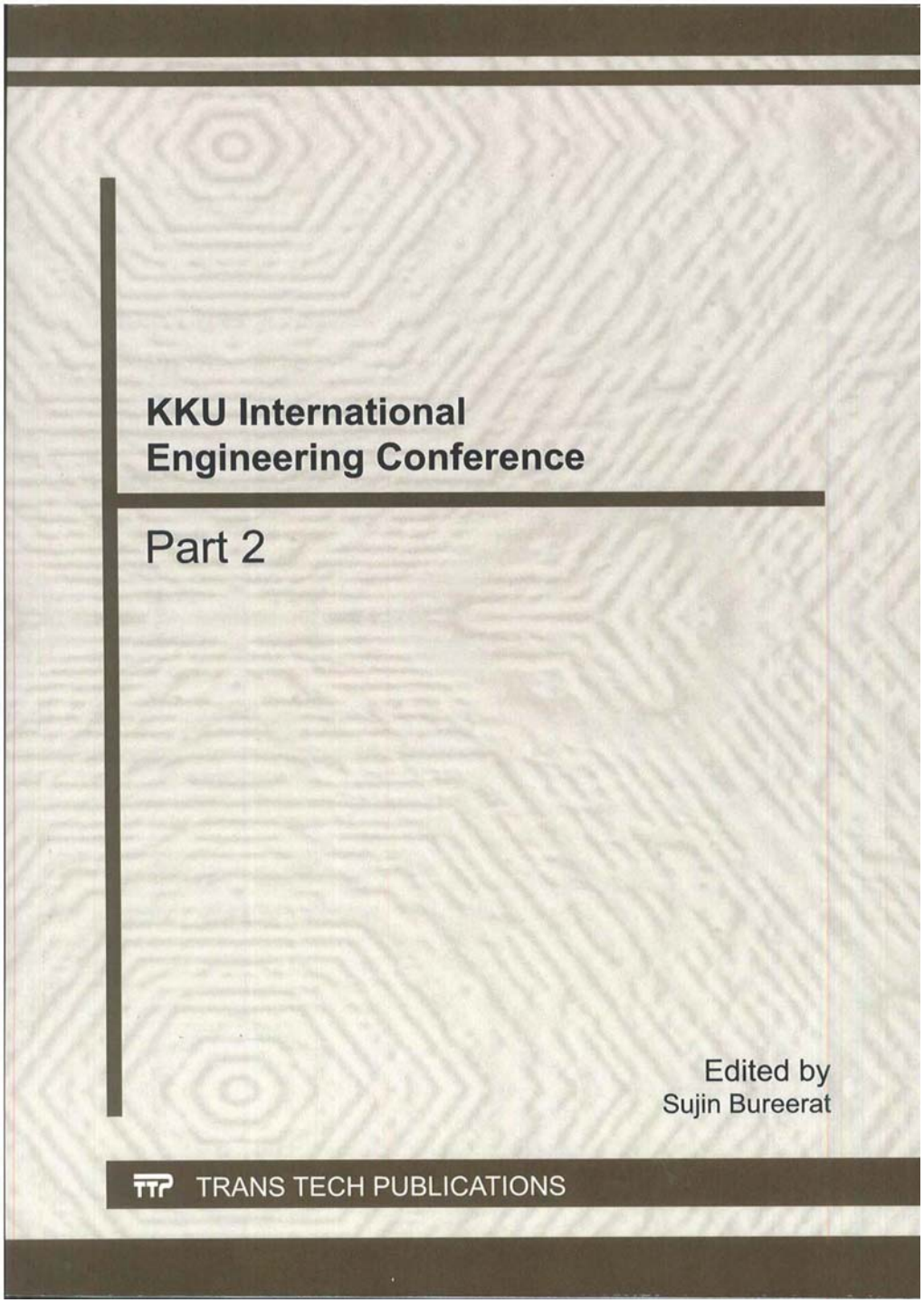
KKU International
Engineering Conference
Part 2
Edited by
Sujin Bureerat
TRANS TECH PUBLICATIONS

Advanced Materials Research Vols. 931-932 (2014) pp 1183-1187
Online available since 2014/May/09 at www.scientific.net

doi:10.4028/www.scientific.net/AMR.931-932.1183

Experimental Study on Flow Friction and Heat Transfer in a Square-Duct Heat Exchanger with Winglet Turbulators

Supattarachai Suwannapan[1], Panuwat Hoonpong[2],
Pongjet Promvonge[1,*] Sirisawat Juengjaroennirachon[2]
and Monsak Pimsarn[1]

[1]Department of Mechanical Engineering, Faculty of Engineering,
King Mongkut's Institute of Technology Ladkrabang, Bangkok, 10520, Thailand

[2]Department of Mechanical Technology, Faculty of Industrial Technology,
Thepsatri Rajabhat University, 321 Naraimaharat Road, Talaychubsorn, Lopburi, 15000, Thailand

* Corresponding author, E-mail address: kppongje@kmitl.ac.th

Keywords: Heat transfer, Friction factor, Square-duct heat exchanger, Winglet turbulators

Abstract. The paper presents an experimental study on airflow friction and heat transfer behaviors in a heat exchanger square-duct fitted with winglet turbulators. The experiments are carried out by varying the airflow rate in terms of Reynolds number from 4000 to 25,000. The winglets were mounted in tandem with three attack angles (α=30°, 45° and 60°), two winglet-pitch to duct-height ratios, (called pitch ratio, PR=P/H=1.0 and 1.5) and a single winglet-to duct-height ratio, (called blockage ratio, BR=e/H=0.2). Effects of the winglet parameters on heat transfer and pressure loss in terms of Nusselt number and friction factor are investigated. The experimental result reveals that the application of the winglets provides considerably higher heat transfer and pressure loss values than the smooth duct alone. The winglet at α=60° and PR=1 gives the maximum heat transfer and pressure loss but the one at α = 30° and PR=1.5 yields the highest thermal enhancement factor of about 1.49 at the lowest Reynolds number.

Introduction

Turbulators have been applied in high-performance thermal systems and they completely result in the change of the flow field and hence the variation of the local convective heat transfer coefficient. Several investigations have been conducted to study the effect of turbulators on heat transfer and pressure loss in the heat exchanger ducts such as ribs/fins/baffles [1-3], winglets [4], coiled wires [5] and helical/twisted tapes [6,7]. Most turbulators such as coil wire/helical tape/twisted tape are effectively applied to circular tubes while the ribs/baffles/fins and winglets are suitably employed for the channels or flat surface ducts. In the present work, the investigation on heat transfer and pressure loss behaviors for turbulent flow over the winglet turbulators placed on the central core has been conducted. The main aim of this work is to study the changes in the flow pattern and heat transfer performance in the duct.

Experimental Setup

A schematic diagram of the experimental apparatus is presented in Figure 1. The AC power supply was the source of power for the plate-type heater, used for heating all walls of the test section in order to maintain a uniform surface heat-flux. Air as the tested fluid was directed into the systems by a 1.45 kW high-pressure blower. The pressure drop across the orifice was measured using inclined manometer to indicate the airflow rate. In order to measure temperature distributions on the upper, lower and side walls, twenty-eight thermocouples K-type were fitted to the walls. To measure the inlet and outlet bulk temperatures, two thermocouples were positioned upstream and downstream of the test duct. The thermocouple voltage outputs were fed into a data acquisition system and then recorded via a personal computer. The pressure drops across the test section was measured by a digital differential pressure.

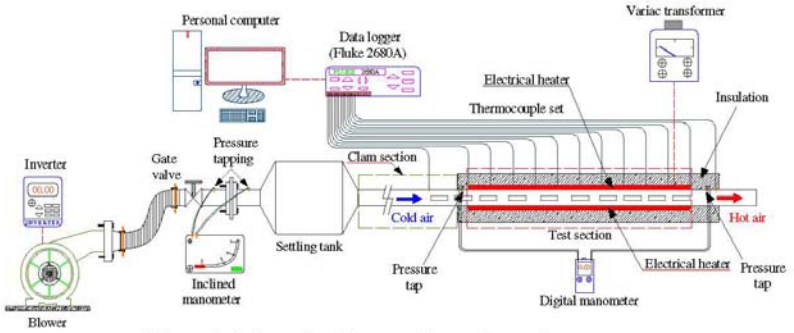

Figure 1. Schematic diagram of experimental apparatus.

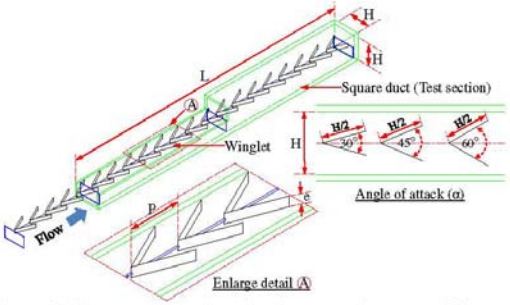

Figure 2. Test section with winglet turbulators.

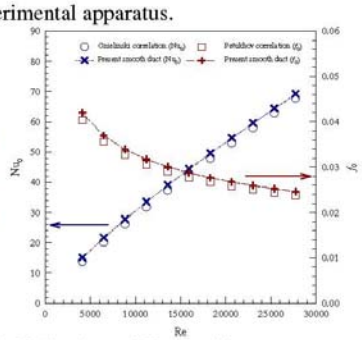

Figure 3. Validation of Nu and *f* for smooth duct.

The detail of winglets inserted into the heat exchanger square-duct is depicted in Figure 2. The tested duct made of 3 mm thick aluminum plates has a height of 45 mm (H) and a length of 1000 mm (L) while the winglets have the pitch (P) of 1.0H and 1.5H, the height (e) of 0.2H and 0.3 mm thickness with the attack angles (α) of 30°, 45° and 60°.

The uncertainty in the data calculation was based on Ref. [8]. The maximum uncertainties of non–dimensional parameters were ±5% for Reynolds number, ±7% for Nusselt number and ±9% for friction. The uncertainty in the axial velocity measurement was estimated to be less than ±7%, and pressure has a corresponding estimated uncertainty of ±5%, whereas the uncertainty in temperature measurement at the duct wall was about ±0.5%.

Data Reduction

The average heat transfer coefficients are evaluated from the measured temperatures and heat inputs, with heat added uniformly to fluid (Q_{air}) and the temperature difference of surface and fluid ($\tilde{T}_s - T_b$), average heat transfer coefficient will be evaluated by:

$$Q_{air} = Q_{conv} = \dot{m}C_p(T_o - T_i) \quad \Rightarrow \quad h = Q_{conv}/\left(A(\tilde{T}_s - T_b)\right) \tag{1}$$

in which, $T_b = (T_o + T_i)/2$ and $\tilde{T}_s = \sum T_s/28$ (2)

The term A is the convective heat transfer area of the heated wall whereas $\tilde{T}_s$ is the average surface temperature. Then, average Nusselt number based on the duct hydraulic diameter is written as:

$$Nu = hD_h/k \tag{3}$$

The friction factor is evaluated by:

$$f = 2\Delta P/\left((L/D_h)\rho U^2\right) \tag{4}$$

where ΔP is the pressure drop across the test section and U is the mean air velocity in the duct. The thermal enhancement factor (TEF) defined as the ratio of h of an augmented surface to that of a smooth surface, h_0, at a constant pumping power, Ref. [9], is written as:

$$\text{TEF} = h/h_0\big|_{pp} = Nu/Nu_0\big|_{pp} = \left(Nu/Nu_0\right)\left(f/f_0\right)^{-1/3} \tag{5}$$

Result and Discussion

Verification of Smooth Duct

The present experimental results on heat transfer and friction characteristics in a smooth duct are first validated in terms of Nusselt number (Nu) and friction factor (*f*). The Nu and *f* obtained from the present smooth duct are, respectively, compared with those from the correlations of Gnielinski and Petukhov found in the open literature, Ref. [10] for turbulent flow in ducts.

Correlation of Gnielinski

$$Nu = \left((f/8)(Re-1000)Pr\right)/\left(1+12.7(f/8)^{1/2}\left(Pr^{2/3}-1\right)\right) \quad \text{for} \quad 3000 < Re < 5 \times 10^6 \tag{6}$$

Correlation of Petukhov

$$f = \left(0.79\ln Re - 1.64\right)^{-2} \quad \text{for} \quad 3000 < Re < 5 \times 10^6 \tag{7}$$

Figure 3 shows a comparison of Nusselt number and friction factor obtained from the present work with those from correlations of Eqs. (6) and (7). It is observed that the present results reasonably agree well within ±5% for both the correlations.

Heat Transfer

The effect of various winglet parameters on heat transfer is presented in the form of Nusselt number ratio, Nu/Nu_0, defined as a ratio of the augmented Nu to Nu_0 of smooth duct. Figure 4a and b, respectively, displays the variation of Nu/Nu_0 with Re and α. It can be observed in the figure that the winglets provide a considerable Nu/Nu_0 increase with reducing PR, but with rising α. The Nu/Nu_0 shows a slightly decrease with the rise of Re. The winglet at PR=1 and α=60° provides the maximum heat transfer rate because of highly interrupting the flow and promoting higher levels of vortex strength. The winglet with PR=1.0 yields the Nu/Nu_0 of 2.01-2.35 times and 1.5-5.9% higher than the one with PR=1.5 for all α values. At a given PR, the winglet at α=60° gives the Nu/Nu_0 of 2.17-2.35 times and of 8.6-12.6% and 4.5-8.2% higher than the one at α=30° and 45°, respectively.

Pressure Loss

The friction factor ratio, f/f_0, plotted against the Re and α is depicted in Figure 5a and b, respectively. In the figure, it is visible that the f/f_0 tends to increase with the increment of Re and α values but with reducing the PR. The winglet at PR=1 and α=60° provides the highest f/f_0 because of higher flow blockage and larger surface area. The winglet with PR=1.0 yields the f/f_0 at about 2.89-6.89 times and 15-20% higher than the one with PR=1.5 for all α values. The α=60° winglet provides the f/f_0 of about 4.60-6.89 times and respectively, 46.29-49.74% and 27.50-32.70% higher than the α=30° and 45° ones for all PR values.

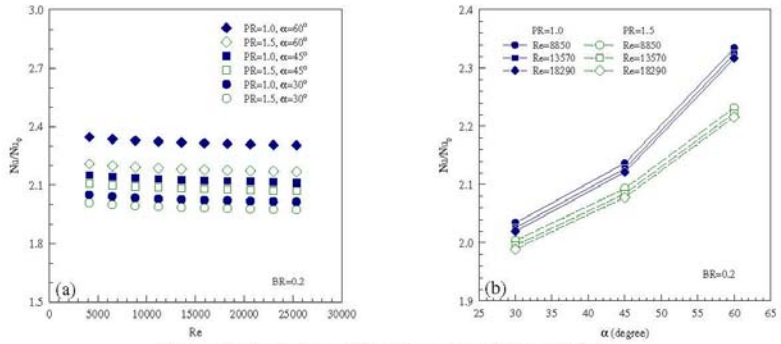

Figure 4. Variation of Nu/Nu_0 with (a) Re and (b) α.

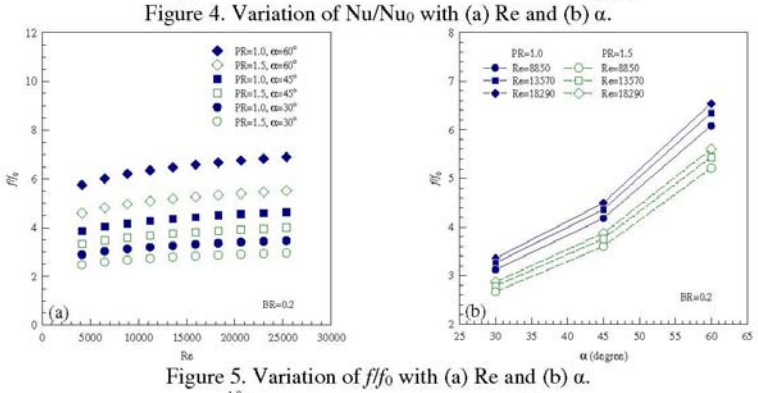

Figure 5. Variation of f/f_0 with (a) Re and (b) α.

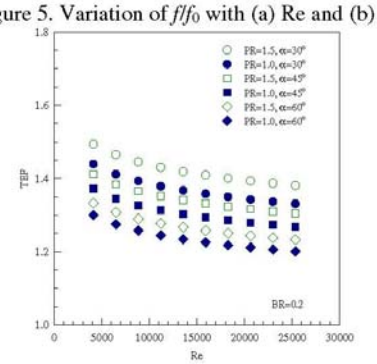

Figure 6. Variation of TEF with Re.

Thermal Enhancement factor (TEF)

Figure 6 shows the variation of the TEF with Re. For all, the data of Nu/Nu_0 and f/f_0 are compared at similar pumping power conditions. In the figure, the TEF tends to decrease with the rise of Re and α. It is seen that the winglet with PR=1.5 provides the TEF higher than the one with PR=1.0 for all cases at a similar attack angle. The optimum parameter of the present work are as PR=1.5 and α =30° because at this point yields high value of Nu/Nu_0 while shows the lowest of f/f_0 value thus, provides the highest TEF of about 1.49 at the lowest Re and gives 3.63-12.30% higher than the others.

Conclusion

An experimental study has been carried out to examine airflow friction and heat transfer characteristics in a uniform heat-fluxed square-duct fitted with winglet turbulators for the turbulent regime, Re from 4000-25,000. The use of winglets can induce vortex flows throughout the tested duct and provides better flow mixing than the smooth duct. The winglet turbulators yield a considerable increase in pressure drop and heat transfer over the smooth duct. The heat transfer rate and the flow friction increase with the increment of α and with decreasing the PR. The winglet at PR= 1.0 and $\alpha = 60^{o}$ gives the highest heat transfer rate and pressure loss. Respectively, the Nu/Nu_0 and f/f_0 values for the winglets are found to be about 1.98-2.35 and 2.47-6.89 times over the smooth duct for all cases while the best operating regime is found at PR=1.5 and $\alpha = 30^{o}$ which yields the maximum TEF of 1.49 at the lowest Re.

Acknowledgments

The funding of this research is supported by the Energy Policy and Planning Office (EPPO), Ministry of Energy, Thailand.

References

[1] P. Promvonge, S. Skullong, S. Kwankaomeng, C. Thiangpong, Heat transfer in square duct fitted diagonally with angle-finned tape–Part 1: Experimental study, Int. Commun. Heat and Mass Transfer. 39 (2012) 617-624.

[2] P.R. Chandra, C.R. Alexander, J.C. Han, Heat transfer and friction behaviour in rectangular channels with varying number of ribbed walls, Int. J. Heat Mass Transfer. 46 (2003) 481–495.

[3] J.C. Han, Y.M. Zhang, C.P. Lee, Augmented heat transfer in square channels with parallel, crossed and V-shaped angled ribs, ASME. Heat Transfer. 113 (1991) 590–596.

[4] T. Chompookham, C. Thianpong, S. Kwankaomeng, P. Promvonge, Heat transfer augmentation in a wedge-ribbed channel using winglet vortex generators, Int. Commun. in Heat and Mass Transfer. 37 (2010) 163–169.

[5] P. Promvonge, Thermal performance in circular tube fitted with coiled square wires, Energy Convers. Manage. 49 (2008) 980–987.

[6] S. Eiamsa-ard, C. Thianponge, P. Eiamsa-ard, P. Promvonge, Convective heat transfer in a circular tube with short-length twisted tape insert, Int. Commun. in Heat and Mass Transfer. 36 (2009) 365–371.

[7] S. Eiamsa-ard, P. Promvonge, Heat transfer characteristics in a tube fitted with helical screw-tape with/without core-rod inserts, Int. Commun. in Heat and Mass Transfer. 34 (2007) 176–185.

[8] ANSI/ASME, Measurement Uncertainty, PTC 19. 1–1985, Part I, USA (1986).

[9] R.L. Webb, Principles of Enhanced Heat Transfer, John Wiley & Sons, New York, 1992.

[10] F.P. Incropera, P.D. Dewitt, T.L. Bergman, A.S. Lavine, Introduction to heat transfer, fifth ed., John Wiley & Sons, 2006

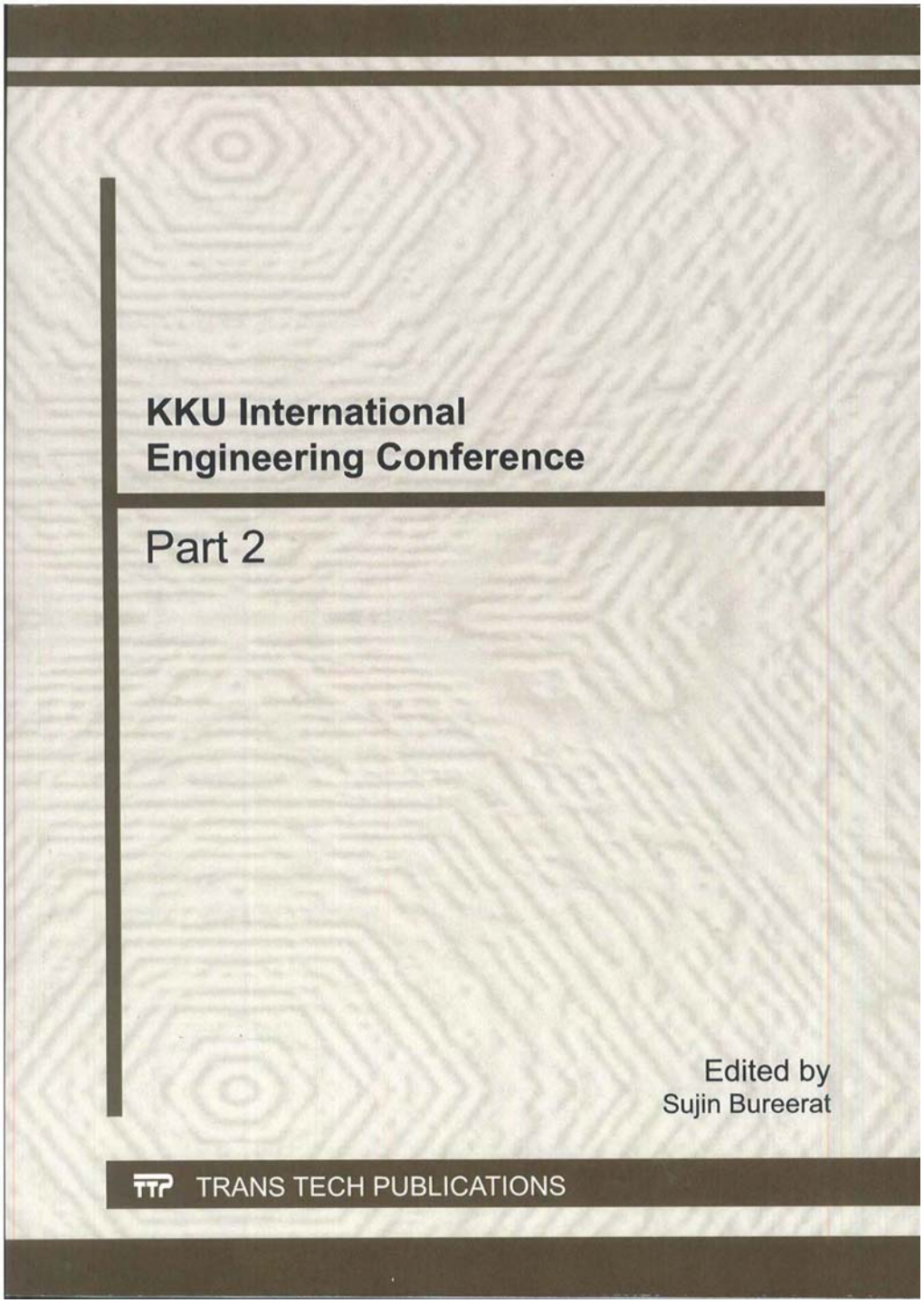
KKU International
Engineering Conference
Part 2
Edited by
Sujin Bureerat
TRANS TECH PUBLICATIONS

Advanced Materials Research Vols. 931-932 (2014) pp 1144-1148
Online available since 2014/May/09 at www.scientific.net

doi:10.4028/www.scientific.net/AMR.931-932.1144

Heat Transfer Improvement in a Square Duct with Diagonal Inclined Ribs

Supattarachai Suwannapan, Ratsak Poomsalood, Pongjet Promvonge*,
Withada Jedsadaratanachai and Thitipat Limkul

Department of Mechanical Engineering, Faculty of Engineering, King Mongkut's Institute of Technology Ladkrabang, Bangkok 10520, Thailand

*Corresponding Author: E-mail: kppongje@kmitl.ac.th Tel: 0-2329-8350, Fax: 0-2329-8352

Keywords: square duct, diagonal inclined rib, heat transfer, friction factor.

Abstract. This research presents a numerical study of turbulent periodic flow and heat transfer in three–dimensional isothermal–fluxed square duct with diagonal inclined rib inserted. The fluid flow and heat transfer characteristics are presented for Reynolds numbers in the range of 4000 to 20,000. The computations based on the finite volume method, and the SIMPLE algorithm has been implemented. Effects of rib pitch ratios (0.5 to 2) at a single blockage ratio of 0.2 and attack angle of 60° on heat transfer and friction factor in the duct are examined and their results of the inclined rib are also compared with those of the smooth duct. It is found that the inclined rib provides higher heat transfer rate and friction factor than the smooth duct for all cases. In addition, the decreasing of the pitch ratio leads to the rise in the Nusselt number and friction factor.

Introduction

The heat transfer enhancement technique is very important and needed in engineering thermal processes in order to reduce the cost and energy consumption in thermal systems. For decades, turbulators such as ribs, fins, grooves, and baffles have been extensively employed in many applied engineering works due to their high thermal loads and decreased dimensions. The cooling or heating fluid is supplied into the ducts mostly mounted with several ribs to increase the degree of cooling or heating levels and this configuration is often used in the design of heat exchangers. Therefore, rib spacing, angle of attack and height are among the most important parameters in the design of duct heat exchangers.

The concept of periodically fully developed flow was first introduced by Patankar et al. [1] to investigate numerically the heat transfer and flow characteristics in a duct. Since then, the periodically fully developed flow condition has been widely used to study thermal characteristics in ribbed ducts with different rib heights and pitch spacing lengths [2, 3].

A numerical investigation of laminar forced convection in a three-dimensional channel fitted with baffles for periodically fully developed flow and with a uniform heat flux in the top and bottom walls was conducted by Lopez et al. [4].

Most of the previous investigations have considered the laminar periodic flow and heat transfer characteristics for the angled baffle in square duct only. Therefore, the turbulent periodic flow in the square duct has rarely been reported. In the present work, the numerical computations for three dimensional turbulent periodic duct flows over a 60° diagonal inclined rib inserted in a square duct are conducted to examine the changes in the flow structure and its thermal performance. And comparison between experimental and simulation results is interested to obtain the correct data.

Mathematical foundation

The numerical model for fluid flow and heat transfer in the square duct was developed under the following assumptions: steady three-dimensional, turbulent and incompressible fluid flow by ignoring body forces, viscous dissipation and radiation heat transfer. Based on the assumptions

above, the duct flow is governed by the continuity, the Navier-Stokes equations and the energy equation. In the Cartesian tensor system, these equations can be written as follows:

Continuity equation:

$$\frac{\partial \rho}{\partial t}+\nabla\cdot(\rho\vec{v})=0 \tag{1}$$

Momentum equation:

$$\frac{\partial(\rho\vec{v})}{\partial t}+\nabla\cdot(\rho\vec{v}\vec{v})=\rho g-\nabla p-\nabla\cdot(\bar{\bar{\tau}}) \tag{2}$$

Energy equation:

$$\frac{\partial(\rho E)}{\partial t}+\nabla\cdot(\vec{v}(\rho E+p))=\nabla\cdot\left(k_{eff}\nabla T+(\bar{\bar{\tau}}_{eff}\cdot\vec{v})\right) \tag{3}$$

When

$$\bar{\bar{\tau}}=\mu\left(\left(\nabla\vec{v}+\nabla\vec{v}^{T}\right)-\frac{2}{3}\nabla\cdot\vec{v}I\right)$$

$$E=h-\frac{p}{\rho}+\frac{v^2}{2}$$

Realizable k - ε equations:

$$\frac{\partial(\rho k)}{\partial t}+\frac{\partial}{\partial x_i}(\rho k v_i)=\frac{\partial}{\partial x_j}\left(\alpha_k\mu_{eff}\frac{\partial k}{\partial x_j}\right)+G_k+G_b-\rho\varepsilon-Y_M \tag{4}$$

$$\frac{\partial(\rho\varepsilon)}{\partial t}+\frac{\partial}{\partial x_i}(\rho\varepsilon v_i)=\frac{\partial}{\partial x_j}\left(\alpha_\varepsilon\mu_{eff}\frac{\partial\varepsilon}{\partial x_j}\right)+C_{1\varepsilon}\frac{\varepsilon}{k}(G_k+C_{3\varepsilon}G_b)$$
$$-C_{2\varepsilon}\rho\frac{\varepsilon^2}{k}-R_\varepsilon+S_\varepsilon \tag{5}$$

All the governing equations were discretized by the QUICK differencing scheme while the velocity-pressure coupling in the equations is handled by the SIMPLE algorithm and solved using a finite volume approach [5]. The solutions were considered to be converged when the normalized residual values were less than 10^{-5} for all variables but less than 10^{-9} only for the energy equation.

Four parameters of interest in the present work are the Reynolds number (Re), friction factor (f), Nusselt number (Nu) and thermal enhancement factor (TEF). The Reynolds number is defined as

$$\mathrm{Re}=\rho\bar{u}D_H/\mu \tag{6}$$

The friction factor, f is computed by pressure drop, Δp across the periodic tube length, L as

$$f=\frac{(\Delta p/L)D_H}{\frac{1}{2}\rho\bar{u}^2} \tag{7}$$

The heat transfer is measured by local Nusselt number which can be written as

$$Nu_x=\frac{h_x D_H}{k} \tag{8}$$

The average Nusselt number can be obtained by

$$Nu=\frac{1}{A}\int Nu_x\partial A \tag{9}$$

The thermal enhancement factor (TEF) is defined as the ratio of the heat transfer coefficient of an augmented duct, h to that of a smooth duct, h_0, at similar pumping power and given by

$$\mathrm{TEF} = \left.\frac{h}{h_0}\right|_{pp} = \left.\frac{Nu}{Nu_0}\right|_{pp} = (Nu/Nu_0)/(f/f_0)^{1/3} \tag{10}$$

Where Nu_0 and f_0 stand for Nusselt number and friction factor for the smooth duct, respectively

Flow configuration

Diagonal inclined rib geometry and arrangement

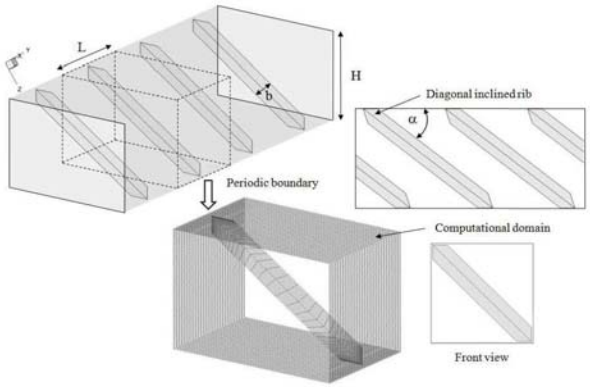

Figure 1. Square duct and computational domain of periodic flow module

The system of interest is a square duct with 60° diagonal inclined rib inserted into the square duct as shown in Fig. 1. The flow under consideration is expected to attain a periodic flow condition in which the velocity field repeats itself from one cell to another. The concept of periodically fully developed flow and its solution procedure has been described in Ref. [1]. The air enters the duct at an inlet temperature, T_{in}, and flows through the inclined rib where b is the size of the rib, H set to 0.05 m is hydraulic diameter of the duct and b/H is known as the blockage ratio, BR = 0.2. The axial pitch, L or distance between the rib cell is set to L = 0.5H to 2H in which L/H is defined as the pitch ratio, PR = 0.5 to 2.

Boundary conditions

Periodic boundaries are used for the inlet and outlet of the flow domain. Constant mass flow rate of air with 300K (Pr = 0.7) is assumed in the flow direction rather than constant pressure drop due to periodic flow conditions. The inlet and outlet profiles for the velocities must be identical. The physical properties of the air have been assumed to remain constant at average bulk temperature. Impermeable boundary and no-slip wall conditions have been implemented over the duct walls as well as the rib. The constant heat flux of the duct walls is maintained at 600 W/m^2 while the rib plate is assumed to be adiabatic wall conditions.

Verification of the smooth duct

Verification of the heat transfer and friction factor of the smooth square duct with no rib is performed by comparing with the Dittus–Boelter and Blasius correlations as shown in Fig. 2. The present smooth duct result is found to be in excellent agreement with data obtained from Dittus–Boelter and Blasius correlations found in the open literature [6] for both the Nusselt number and the friction factor, less than 5.1 and 3.2 % deviation, respectively.

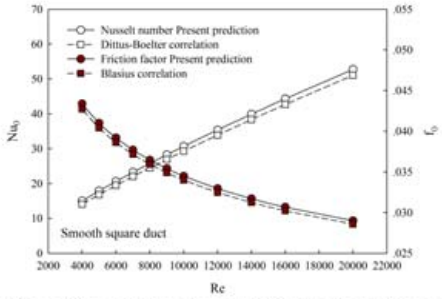

Figure 2. Verification of Nusselt number and friction factor for smooth square duct

Results and discussion

Fig. 3 exhibits the longitudinal streamline flow in the square duct. The diagonal inclined rib can create a secondary flow in the duct that leads to the drastic increase in heat transfer.

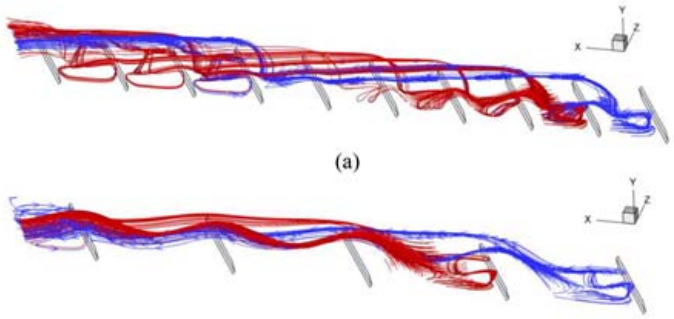

(a)

(b)

Figure 3. Longitudinal streamline flow in the square duct with inclined rib
(a) PR = 1, (b) PR = 2 at Re = 8000

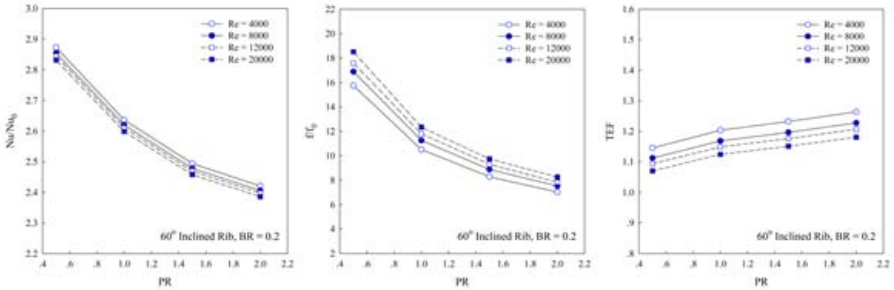

(a) (b) (c)

Figure 4 Variation of (a) Nu/Nu_0, (b) f/f_0 and (c) TEF with PRs at various Re

The variation of the Nusselt number ratio, Nu/Nu_0 ratio with PR at different Res is displayed in Fig. 4a. It is worth noting that the Nu/Nu_0 tends to decrease with the increment in PR. The higher Re value leads to the decrease in the Nu/Nu_0. The inclined rib in this work yields the heat transfer rate of about 2.39 – 2.87 times higher than the smooth duct alone.

Fig. 4b presents the variation of the friction factor ratio, f/f_0 with PR for various Res. In the figure, it is noted that the f/f_0 tends to decrease considerably with the rise of PR. The use of the inclined rib leads to considerable increase in friction factor in comparison with the smooth duct with no rib. The increasing the Re gives the higher friction factor. The f/f_0 for the inclined rib is found to be about 7.1 – 18.5 times depending on the PR and Re values.

Fig. 4c exhibits the variation of thermal enhancement factor (TEF) with PR for various Res. It is visible that the TEF trend is increased with the rise in PR. The TEF for using the inclined rib at all PRs is found in a range of 1.07 – 1.27, depending on the PR and Re values. The maximum TEF is about 1.27 for using the inclined rib at PR = 2 and Re = 4000.

To obtain the absolutely correct data, the comparison between experimental and simulation results is interested. Fig. 5 shows the comparison between experimental and simulation results of the inclined rib. It is found to be in good agreement with data obtained for the both Nu/Nu_0 and f/f_0, less than 4.1 and 6.2 % deviation, respectively.

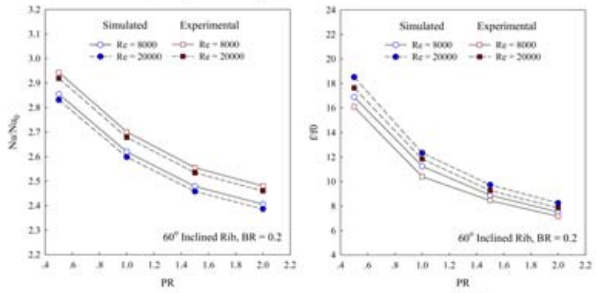

Figure 5. Comparison of (a) Nu/Nu_0 and (b) f/f_0 between experimental and simulation results

Conclusion

A numerical investigation has been conducted to examine both of turbulent periodic flow and heat transfer characteristics in a square duct inserted with 60° diagonal inclined rib. The counter-vortex flows created by the inclined rib exist and help to induce impingement flows. The order of enhancement is about 2.39 – 2.87 times. However the heat transfer augmentation is associated with the enlarged pressure loss ranging from 7.1 to 18.5 times. The highest thermal enhancement factor for the inclined rib with PR = 2 is found to be about 1.27 at the lowest Re.

Acknowledgments

The funding of this research is supported by the Energy Policy and Planning Office (EPPO), Ministry of Energy, Thailand.

References

[1] Patankar S.V, Liu C.H. and Sparrow E.M. ASME J. Heat Transf. 1977; 99: 180-186.

[2] Webb B.W. and Ramadhyani S. Int. J. Heat Mass Transf.1985; 28: 1679–1687.

[3] Kelkar K.M. and Patankar S.V. ASME J. Heat Transf. 1987; 109: 25–30.

[4] Lopez J.R., Anand N.K. and Fletcher L.S. Numer.l Heat Transf. A: Appl. 1996; 30: 189–205.

[5] Patankar S.V. Numerical heat transfer and fluid flow. McGraw-Hill. New York. 1980.

[6] Incropera F. and Dewitt P.D, Introduction to heat transfer 5rd edition, John Wiley & Sons Inc. 2006.

AUTHOR BIOGRAPHY

Name: Mr.Supattarachai Suwannapan
Date of birth: 11 September 1980
Place of birth: Maha Sarakham, Thailand
Education: - B.Eng (Mechanical), Khon Kaen University, 2003
- M.Eng (Mechanical), King Mongkut's Institute of Technology Ladkrabang, 2009
Experience: - Design engineer, LG Electronics Thailand Co.,Ltd., Rayong, Thailand, 2003-2005
- Senior quality control engineer, Sugino Press Thailand Co.,Ltd., Rayong, Thailand, 2006-2007

List of Publications

International Journal

1. Pongjet Promvonge, **Supattarachai Suwannapan**, Monsak Pimsarn, Chinaruk Thianpong, "Experimental Study on Heat Transfer in Square Duct with Combined Twisted-Tape and Winglet Vortex Generators", accepted by International Communications in Heat and Mass Transfer, 2014.
2. **Supattarachai Suwannapan**, Watcharin Noothong, Chinaruk Thianpong, Pongjet Promvonge, "Enhanced Heat Transfer in a Heat Exchanger Square–Duct with Discrete V–Finned Tape Inserts", accepted by Chinese Journal of Chemical Engineering, 2014.
3. **Supattarachai Suwannapan**, Panuwat Hoonpong, Pongjet Promvonge, Sirisawat Juengjaroennirachon, Monsak Pimsarn, "Experimental Study on Flow Friction and Heat Transfer in a Square-Duct Heat Exchanger with Winglet Turbulators", Advanced Materials Research, Vols. 931-932, 2014, pp. 1183-1187.
4. **Supattarachai Suwannapan**, Ratsak Poomsalood, Pongjet Promvonge, Withada Jedsadaratanachai, Thitipat Limkul, "Heat Transfer Improvement in a Square Duct with Diagonal Inclined Ribs", Advanced Materials Research, Vols. 931-932, 2014, pp. 1144-1148.
5. **Supattarachai Suwannapan**, Sompol Skullong, Teerapat Chompookham, Pongjet Promvonge, Chinaruk Thianpong, "Heat Transfer Characteristics in Square Duct with Winglet Inserts", The Journal of Interdisciplinary Networks: Special Issue on Interdisciplinary Research and Development in ASEAN Universities. Vol. 2, 2013, pp. 32-38.

International Conferences

6. Sombat Tamna, **Supattarachai Suwannapan**, Pongjet Promvonge, Chinaruk Thianpong and Sompol Skullong, “Numerical Investigation of Laminar Flow and Heat Transfer in a Square Channel with Oblique Baffles”, International Conference on Engineering, Applied Sciences, and Technology (ICEAST), 21-24 August, 2013, Bangkok, Thailand.
7. Chayodom Hinthao, **Supattarachai Suwannapan**, Sirisawat Juengjaroennirachon, Sompol Skullong, Teerapat Chompookham, Pongjet Promvonge, “Thermal Behaviors in a Square Duct with Inclined-Baffle Inserts”, The 4th International Conference on Mechanical Engineering (TSME-ICoME), 16-18 October 2013, Pattaya, Chonburi, Thailand.
8. **Supattarachai Suwannapan**, Sompol Skullong, Teerapat Chompookham, Sutapat Kwankaomeng, Pongjet Promvonge, “Heat Transfer Behaviors in a Square Channel with Different Turbulators Insert”, The 3rd TSME International Conference on Mechanical Engineering (TSME-ICoME), 24-27 October 2012, Chiang Rai, Thailand.
9. **Supattarachai Suwannapan**, Teerapat Chompookham, Sombat Tamna, Sompol Skullong, Chinaruk Thianpong, Pongjet Promvonge, “Augmented Heat Transfer in Square Channel with 45° Inline Baffles”, International Conference on Green and Sustainable Innovation 2012 (ICGSI), 24-26 May 2012, Chiang Mai, Thailand.
10. **Supattarachai Suwannapan**, Sompol Skullong, Pongjet Promvonge, “Thermal Behavior in a Square Channel with 45° Cross Baffle”, The 1st International Symposium on Technology for Sustainability (ISTS), 26-29 January, 2012, Bangkok, Thailand.